SEDIMENTOLOGY, STRUCTURE, AND GEOCHEMISTRY OF THE GALICE FORMATION: SEDIMENT FILL OF A BACK-ARC BASIN AND ISLAND ARC IN THE WESTERN KLAMATH MOUNTAINS

A thesis presented to the Faculty

of the State University of New York

at Albany

in partial fulfillment of the requirements

for the degree of

Master of Science

School of Science and Mathematics

Department of Geological Sciences

Rosann Park-Jones

1988

SEDIMENTOLOGY, STRUCTURE, AND GEOCHEMISTRY OF THE GALICE FORMATION: SEDIMENT FILL OF A BACK-ARC BASIN AND ISLAND ARC IN THE WESTERN KLAMATH MOUNTAINS

Abstract of

a thesis presented to the Faculty

of the State University of New York

at Albany

in partial fulfillment of the requirements

for the degree of

Master of Science

School of Science and Mathematics

Department of Geological Sciences

Rosann Park-Jones

1988

ABSTRACT

The western Jurassic belt of the Klamath Mountains is an ideal locale for the study of ophiolite genesis, island arc development, and study of flysch deposition from a nearby eroding island arc and continental margin. Closure and imbrication of an inferred back-arc basin coincided with the Late Jurassic Nevadan orogeny (ca 150 Ma).

The Galice Formation is the youngest formation involved in the Nevadan orogeny (Lanphere *et al.*, 1968). In the type section in southwestern Oregon, the Galice structurally overlies the Rogue Formation volcaniclastics. The Rogue Formation has been previously interpreted as an island arc assemblage (Garcia, 1979). The type Galice consists of thin-bedded, dark grey to black slaty shales with a prominent cleavage. Chert-pebble conglomerate is found locally and most probably represents the basal Galice. Coarse-grained pebbly sandstone beds with large shale rip-up clasts are interpreted as representing water-cut channels. Paleoflow data were calculated from measurements of flute casts, parting lineation, grooves, and longitudinal ridges found across from the town of Galice and along Grave Creek. Paleoflow was found to be dominantly towards the west (Grave Creek section) and north (Galice type section) after corrections for local folding and overturned bedding.

The Galice is dated as late middle Oxfordian to middle Kimmeridgian on the basis of *Buchia concentrica* (Sowerby) (Imlay, 1980). Plant fragments consisting of carbonaceous broken stems and possible leafy material are preserved in Galice shales. Apparent trace fossils are found parallel to sub-parallel to bedding.

The Galice Formation contains minor interbedded volcaniclastics which appear indistinguishable from the Rogue Formation volcanics. Flattened shale clasts were observed locally in the tuffaceous units within the Galice.

The Rogue and Galice Formations generally strike N to NE and dip to the SE. The Rogue-Galice contact is a probable high-angle fault whose exact displacement and times

of displacement are uncertain.

Nevadan folds are found throughout the study area cut by an axial-planar cleavage. Post-Nevadan folds are defined as those folds that have refolded the axial-planar cleavage. Bedding-cleavage intersection lineations were used to describe the trend and plunge of Nevadan fold axes. An asymmetric Nevadan fold overturned to the NW was identified across from the town of Galice. The Grave Creek section reveals tight to isoclinal Nevadan folds and fold vergence alternates in a systematic way from NE to SW. Proposed F_3 or post-Nevadan folds trend NW-SE and account for the dispersal of Nevadan fold axes.

The Nevadan axial plane AP_1 strikes 022° and dips 060°SE. The orientation of the post-Nevadan axial plane AP_3 is $119^{\circ}/080^{\circ}$NE. F_1 and F_2 fold axes have similar orientations as they both trend SSW and plunge gently SW at $4\text{-}10^{\circ}$. The F_1 and F_2 fold axes are interpreted as Nevadan fold axes with F_2 representing a late-stage Nevadan folding episode. The mean F_2 fold axis trends 303° and plunges 14°NW. The fold interference pattern is transitional between types I and II of Ramsay (1967).

XRF and INAA analyses show differences exist between the type Galice and "Galice" shales that overlie the Josephine ophiolite to the south. The type Galice and "Galice" shales have higher V, Cr, and Ni abundances than the standard SCo-1, which is thought to represent an arc volcaniclastic component or ophiolitic component. Differences were noted in the mean values of the type Galice and "Galice" in the abundance of Mn, Mg, Na, K, Sr, and Rb, but these differences are not significant at the 2σ level. Comparison of immobile elements showed differences in geochemical behavior between the type Galice and "Galice" shales in the plots of Zr versus Al_2O_3, K_2O versus TiO_2, K_2O versus Al_2O_3, Y versus Al_2O_3, and K_2O versus V. These differences in geochemical behavior are presented as preliminary, general findings worthy of more detailed study to more accurately characterize the similarities and differences between the type Galice and "Galice" shales.

ACKNOWLEDGEMENTS

My sincere thanks go to all the people who have helped me with this thesis. First, I am grateful for all the time my advisor, Greg Harper, has expended towards this project. He initially suggested its potential and has advised me through subsequent stages. In the field, I was ably assisted by Eric Wetzstein, who helped maneuver and paddle our river raft, and he drove a rented truck that had very poor brakes on steep, winding, four-wheel drive logging roads in otherwise inaccessible parts of my field area.

I would like to thank my committe members, Greg Harper, Bill Kidd, and John Delano for all of their thoughtful comments and constructive criticisms of the initial drafts. Discussions about Klamath geology with Len Ramp, Monty Elliott, Bill Purdom, John Griffin, and Nan Lindsley-Griffin were also helpful. Assistance in logistics was given by Ruth Pavlat of the Oregon Department of Geology and Mineral Industries' office in Grants Pass, Oregon and Bonnie Clark of the U.S. Forest Service office in Grants Pass.

X-ray fluorescence analyses of Galice rock powders were performed by Dr. S. T. Ahmedali of McGill University's Geochemical Laboratory. INAA work was done at Ward Laboratory and Snee Hall at Cornell University through the generousity of many people, including Jack Bird and Howard Adderhold. Many thanks go to Karl Wirth for all his patience and help during the counting sessions. Matthias Ohr instructed me on the ND-NOVA and was a patient instructor on the fine art of making good funnels for sample preparation before irradiation. I am indebted to Karl Wirth, his housemates and fellow graduate students at Cornell who provided many good meals and a place to stay during the counting sessions.

Financial assistance from GSA Penrose Grant No. 3478-85, a Sigma Xi Grant-In-Aid, SUNY Benevolent Association Research Grant, and funds from T. Mark Harrison

made this project possible, along with a research assistantship from John Delano and Greg Harper.

Finally, I would like to thank my family and friends for their morale support and kindnesses shown to me over the years. A special word of thanks go to my husband, Ross, and to Tabitha, who have made this past year the best of times.

TABLE OF CONTENTS

LIST OF FIGURES

(localities in parentheses)

LIST OF TABLES

CHAPTER 1: INTRODUCTION

The study of ancient orogenic and magmatic terranes has been aided in the past few decades by the development of plate tectonic concepts and the study of modern analogs in continental-margin arcs and island arcs. The age-old questions concerning the genesis of ancient orogenic terranes are now being answered by careful petrological and structural studies and by use of highly refined geochemical techniques.

The Western Jurassic belt of the Klamath Mountains, located in southwestern Oregon and northwestern California, presents an ideal locale for the study of ophiolite genesis, island arc development, and deposition of flysch derived from an arc and continental margin into an inferred back-arc basin (Harper and Wright, 1984). The basin most likely opened along an active volcanic arc, a line of weakness (Karig, 1974), and received volcanogenic debris from the arc and eroding craton. The opening of the basin, emplacement of the ophiolite, and subsequent closure and imbrication of the active arc, overlying flysch, ophiolite, and remnant arc terranes occurred in a well-dated, relatively short time span from 164-150 Ma (Saleeby *et al.*, 1982; Wright and Wyld, 1986; Wyld and Wright, 1988). The closure and imbrication of the basin coincided with the Late Jurassic Nevadan orogeny (ca 150 Ma). This series of events is consistent with prevailing theories on marginal basin development and closure, as marginal basins tend to have a limited lifespan, due to their location at destructive plate margins (Tarney and Windley, 1981).

The Galice Formation consists of slaty shales and volcanic-rich greywackes that overlie both the Josephine ophiolite in northwestern California (Harper, 1983) and the Rogue Formation (Wells and Walker, 1953), part of a late Jurassic arc complex (Garcia, 1979), in southwestern Oregon. It outcrops in a belt 16-48 km wide that extends for about 300 km along the western margin of the Klamath Mountains (Imlay, 1980).

Recently, these limits were expanded southward of the Klamath Mountains, as slivers of Galice blocks 1/2 to 4 km long were found 5-60 km south of its previously reported southern limit; these slivers are surrounded by sheared serpentinite and serpentinized ultramafic rock (Jayko and Blake, 1986).

The thickness of the Galice Formation can not be measured accurately due to the intense folding, faulting, and intrusions. Irwin (1960) estimated the thickness of the Galice Formation to be on the order of 3,050 to 9,140 m. Evidence presented in this thesis suggests a minimum thickness of 1510 meters (4963') at the type locality, which takes into account the large-scale isoclinal folds.

The Galice Formation in southwestern Oregon has never been carefully studied in detail at its type locality. It has only been described in a regional context, with most of the work done between 1900-1955, when mining of gold, silver, lead, and copper was important in this region. The advent of plate tectonic concepts and detailed studies of ophiolite complexes in the last two decades have changed the focus of geologic studies. The proposed model of Harper and Wright (1984) of development of an active back-arc basin along the continental margin during the late Jurassic needs further regional work to support or refute this model. The structures and sedimentologic features contained in the Galice have the potential of yielding important evidence about the source area and depositional environment of the flysch, which later was deformed by folding, faulting, and the development of a Nevadan-age cleavage.

1.1 Methods

The intent of this thesis is to present the results from study of the Galice Formation where it crops out at the type locality in southwestern Oregon, near Galice Creek and the hamlet of Galice. Sedimentologic and structural data were collected in the field over one field season, June-July, 1985. Compilation of these data and examination of representative samples in thin-section, and aerial photo interpretation followed in the

ensuing months at SUNY-Albany. Geochemical analyses of shales and sandstones from the type locality were completed at McGill University and at Cornell University.

The development of the field of sedimentary geochemistry has the potential for adding to our knowledge of source provenance and the conditions under which the shale and greywacke were deposited. Discriminant parameters using major and trace element concentrations are being developed at the present time. It is hoped that the geochemical data presented in this thesis will add to our current knowledge of the relationships between geochemistry and the corresponding tectonic regime or source area.

1.2 Geographic Setting

The study area consists of approximately 58 square kilometers located near the hamlet of Galice, Oregon, approximately 25 kilometers northwest of Grants Pass, Oregon. The study area is bounded on the south and west by the Rogue River, by Grave Creek to the north, and on the east by a north-trending imaginery line from Hell's Gate Canyon.

The terrain in this area has been interpreted as the remnants of a dissected peneplain by J. S. Diller (1902), one of the earliest geologists who studied this region of southwestern Oregon. According to Diller, this erosional surface was once formed near sea level and was then uplifted unevenly in late Cenozoic time, such that it sloped westward towards the coast. Presently, this surface slopes from about 1220 meters in the interior of the province to about 610 meters elevation above sea level near the coast.

The Rogue River drains a large portion of southwestern Oregon, from the western slopes of the Cascade Mountains through the Klamath Mountains and Coast Range, to the Pacific Ocean. The Rogue River had established its course across southwestern Oregon prior to uplift of the broad plateau. It possesses sufficient discharge and downcutting power to create the steep-walled canyons where it flows through resistant volcanic and metamorphic rocks.

The study area's topography is rugged and mountainous, with considerable relief, and is typified by a mixed conifer, mixed evergreen, madrone, and oak woodland forests. Due to the remote nature of the area, it is sparsely populated, with the exception of mining claims and some settlements found dotted along the Rogue River and its tributaries.

The earliest encounter between white men and the local tribes was hostile, and by 1841 these Indians and their territory were known as "Rogue" (Purdom, 1977). This region was populated by Indians of the Takelma and Tututni groups, which included the Shasta Costa and Galice Indians. The discovery of gold on Josephine Creek in 1850 and at Jacksonville in 1851 attracted thousands of prospectors and settlers to the area. This influx of people escalated the violent nature of the conflicts between the white men and the native Indians. The Rogue River Indian War of 1855-1856 is described in Purdom (1977). After this war, the surviving Indians were transported to reservations in northwestern Oregon. Mining activities resumed and flourished, with over 21 million dollars' worth of gold, silver, and copper being produced in Josephine County between 1852 and 1979 (Ramp and Peterson, 1979).

The "Wild and Scenic River Act," Public Law 90-542, was passed in 1968 to preserve the primitive nature of many of the nation's waterways. Portions of the Rogue River are classified under this law as wild, scenic, and recreational. The wild and scenic portion of the river begins at the confluence of Grave Creek with the Rogue, and extends westward for 67 km. Over this portion of the river, the U. S. Forest Service controls the number of people who raft the river by issuing permits.

In the study area, the Rogue River is classified as recreational, meaning that it is readily accessible and may be used by everyone. Access can be gained to the study area by a paved road that extends from Merlin (10 km east of the study area) to approximately 2.5 km east of Grave Creek Bridge. Dirt roads and unimproved logging roads are present where the land is under the jurisdiction of the Bureau of Land

Management. Excellent exposures are found along the Rogue River, accessible by raft and by walking up its tributaries.

1.3 Previous Work

The Klamath Mountains have been the focal point of geologic study since they were first described by Lawson (1893) and Diller (1893). Powell (1895) officially named the Klamath Mountains. Diller (1902) and Louderback (1905) are credited with developing acceptable theories about the topographical development of the Klamath province.

The Galice Formation was first characterized and defined by Diller (1907). The type section is an exposure of shales, minor sandstone and conglomerate found along Galice Creek. Hershey (1911) mapped a long belt of Galice slate in northern California. Fossils collected from the Galice Formation are reported by Diller (1907, 1908), Taliaferro (1942), Imlay et al. (1959), and Imlay (1980).

Diller and Kay (1924) and Jones (1960) described the Cretaceous rocks that crop out along Grave Creek, northeast of the study area. Wells et al. (1949) issued a preliminary map and description of the Galice Formation to the south in the Kerby quadrangle. Areal mapping of the Galice quadrangle was done from 1945-1950, culminating in the publishing of a map by Wells and Walker (1953) of the U. S. Geological Survey. Modifications on the regional geologic map of western Oregon were made by Wells and Peck (1961) when they combined the volcanic rocks of the Galice and Rogue Formations as one mappable unit.

Geologic reports on the mineral resources of the study area were published by Diller (1914), Libbey (1967), and Ramp and Peterson (1979). Other geologic work in the area include: Kays (1967, 1968), Wise (1969), Baldwin (1969), Hotz (1971), Garcia (1979), a preliminary reconnaissance geologic map by Page and others (1977), a preliminary geologic map by Smith and others (1982), and Riley (1987).

1.4 Tectonic and Structural Relationships

The Klamath Mountain province in northern California and southern Oregon is an arcuate assemblage of Paleozoic and Mesozoic-age ophiolitic and ultramafic rocks, with associated marine arc-volcanic and sedimentary rocks. This assemblage consists of thrust packages of lithologically distinct, fault-bounded terranes that young from east to west. The four terranes include the Eastern Klamath belt, the Central Metamorphic belt, the Triassic and Paleozoic belt, and the Western Jurassic belt (Figure 1-1). Data and interpretations for the terranes east of the Western Jurassic belt include Lanphere et al. (1968), Hamiliton (1969, 1978), Irwin (1981), Lindsley-Griffin (1982, 1983), Miller (1983), Helper (1983, 1986), Gray (1985, 1986), Goodge (1986), Wallin et al. (1988), and Wright and Fahan (1988).

The youngest and westernmost terrane in the Klamath Mountain province is the Western Jurassic belt, bounded by regional north-trending eastward-dipping faults. On the eastern side of this belt, the Preston Peak (Snoke, 1977) or Orleans fault (Gray, 1985; Jachens et al. 1986) separates the Western Jurassic belt from the Triassic and Paleozoic belt to the east. The western boundary of the Western Jurassic belt marks the western limit of the Klamath Province and is delineated by the Coast Range fault (Garcia, 1979; Saleeby *et al.*, 1982) which juxtaposes latest Jurassic- and Cretaceous-age Franciscan rocks (Dothan Formation in Oregon) against the Western Jurassic belt.

The Western Jurassic belt contains oceanic crust and mantle (Josephine ophiolite), a dissected magmatic arc (Chetco complex, Rogue volcanics), a remnant arc (Western Hayfork terrane) and sediment fill (Galice Formation). Reviews of these topics except the latter can be found in Harper (1980a, 1980b, 1982a, 1982b, 1983, 1984), Harper and Wright (1984), Harper et al., (1985), Garcia (1979), Saleeby et al., (1982), Dick (1976), and Snoke (1977). The relationships between the study area and the Western Jurassic belt are shown in Figure 1-2. The study area consists of metasedimentary rocks of the Galice Formation and metavolcanic rocks of the Rogue Formation, shown by the area

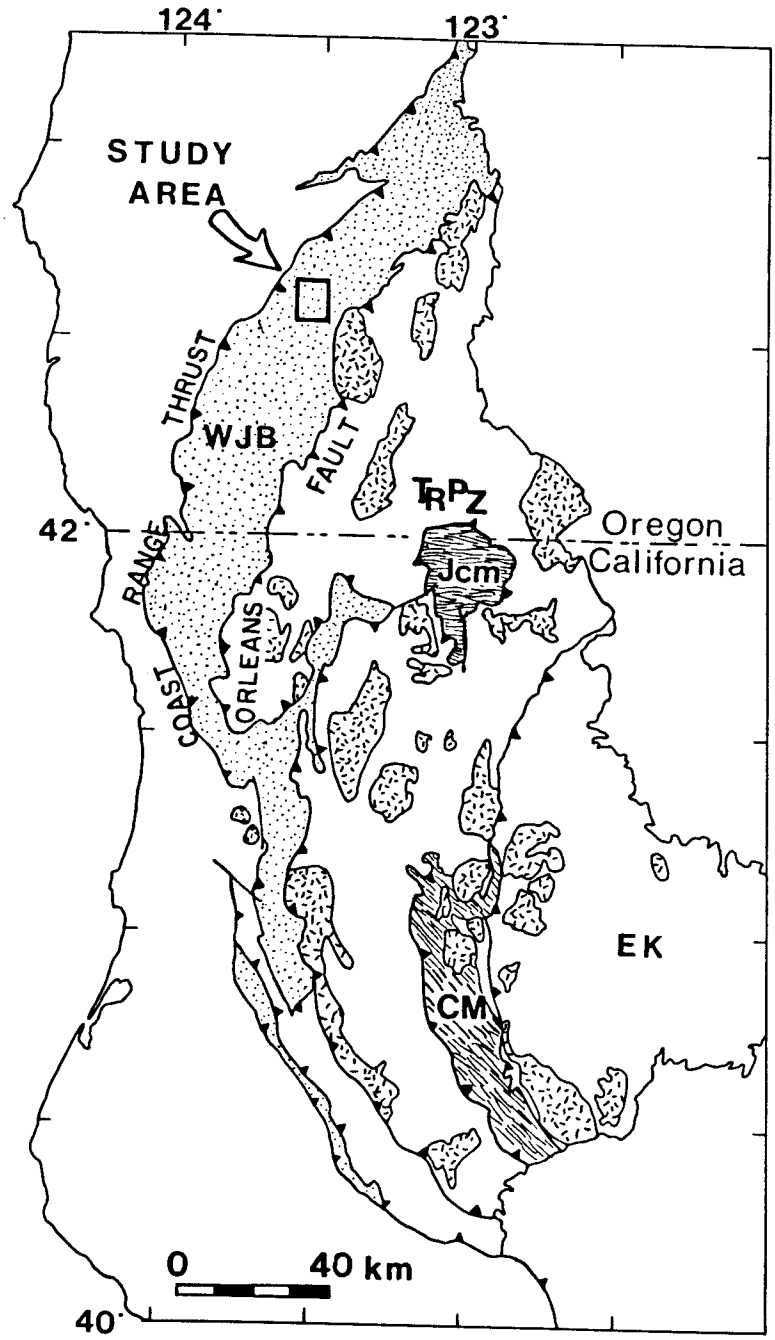

Figure 1-1: Map of the Klamath Mountain tectonic terranes. From east to west (oldest to youngest): (1) the Eastern Klamath belt, (2) Central Metamorphic belt, (3) Triassic and Paleozoic belt, and (4) Western Jurassic belt. After Irwin (1981) and Jachens and others (1986).

Figure 1-2: Map illustrating the position of the study area relative to (1) the Western Jurassic belt lithologies, and (2) the surrounding Franciscan Complex and the Triassic and Paleozoic belt. This map is modified after Harding (1987), Irwin (1981), Jachens et al. (1986), Ramp and Peterson (1979), Saleeby et al. (1982), and Snoke (1977).

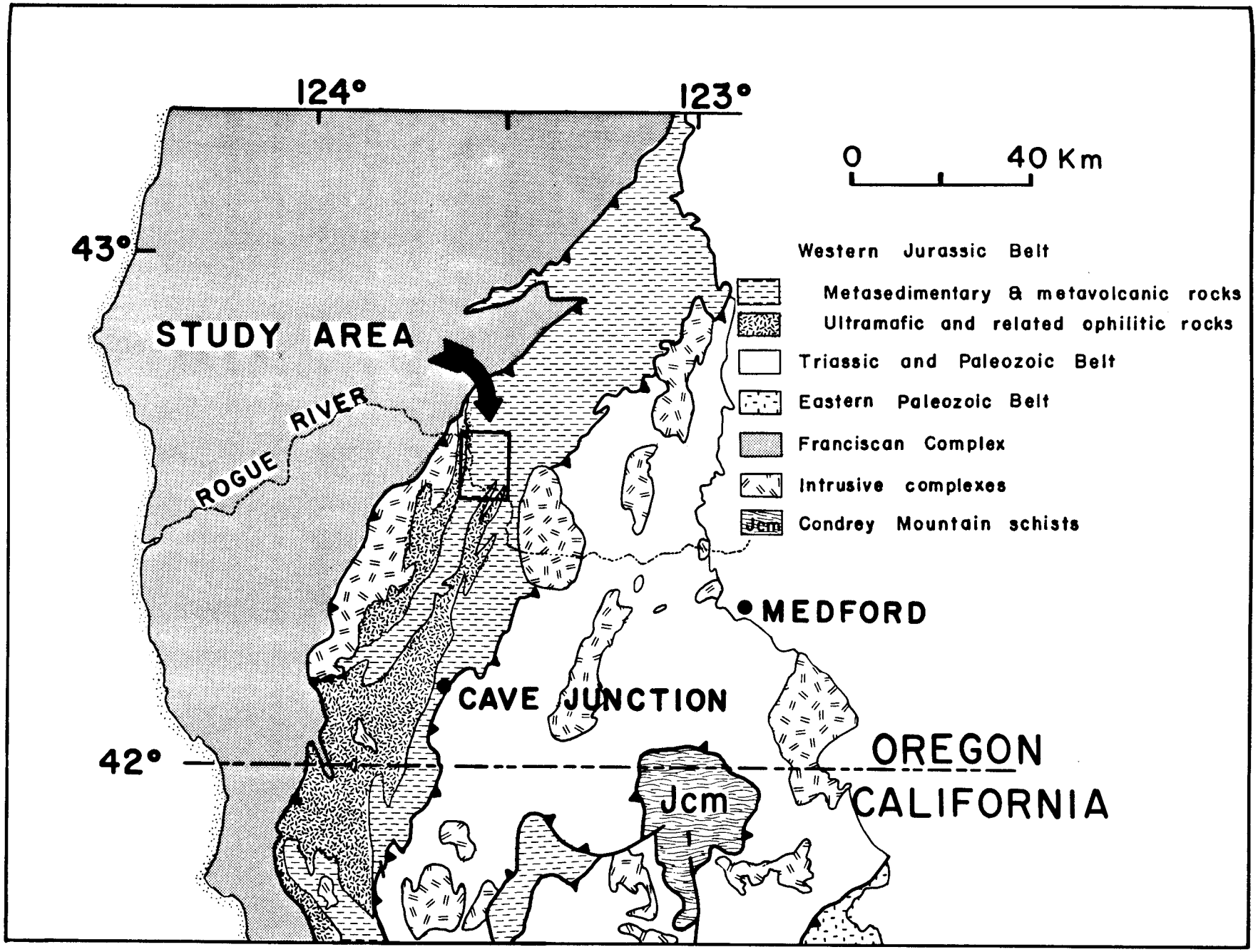
124°
123°
43°
42°
0
40 Km
STUDY AREA
ROGUE RIVER
MEDFORD
CAVE JUNCTION
OREGON
CALIFORNIA
Jcm
Western Jurassic Belt
Metasedimentary & metavolcanic rocks
Ultramafic and related ophilitic rocks
Triassic and Paleozoic Belt
Eastern Paleozoic Belt
Franciscan Complex
Intrusive complexes
Jcm
Condrey Mountain schists

shaded by the horizontal dashed pattern. Additionally, slivers of serpentinized ultramafic and related ophiolitic rocks extend into the southern part of the study area and are most probably genetically related to the Josephine ophiolite and peridotite that lie to the south.

1.5 Paleomagnetism and Paleogeography

Accretion of exotic Mesozoic terranes is an important aspect of North American Cordilleran tectonic history, as much of the margin is composed of lithologically distinct, fault-bounded terranes that contain faunal evidence of more southerly origins (Coney et al., 1980). The areas north and south of the Klamath and Sierran Mountains are thought to be accretionary (Davis *et al.*, 1978), but the origin of the western Klamaths has been debated. Davis et al. (1978) thought the Klamaths and Sierran region were part of a single arc complex. Hamilton (1969, 1978) believed that the Jurassic rocks of the western Klamath Mountains were exotic to the margin, having been carried there atop a Pacific Ocean lithospheric plate. Others since that time have argued for in-situ development of the western Klamaths along the continental margin (Harper and Wright, 1984), also termed a "native" terrane by Gray (1985, 1986).

The argument about the "exotic" or "native" origin of the different components of the western Klamath Mountains rests on paleomagnetic and paleontological evidence that could show pronounced differences between neighboring terranes. The following section reports on two aspects of paleomagnetism: (1) a summary of the published paleomagnetic studies on the Klamaths, and (2) a summary of Late Jurassic paleogeography of North America.

1.6 Klamath Paleomagnetic Studies

The published paleomagnetic studies dealing with the Klamath Mountains have concentrated on rocks from the Eastern Klamath belt. Mankinen and others (1984) reported clockwise rotations of 100^{o} on Permian through Jurassic rocks, and clockwise rotations of 60^{o} from Jurassic-age rocks they studied. They deduced that this movement was accomplished by a rigid block rotation, not the result of oroclinal bending. Similarly, Fagin and Gose (1983) found evidence for a rigid body rotation of the Eastern Klamath belt but no evidence for north-south displacement. They theorized that this rotation occurred in conjunction with Cenozoic rotations of the Oregon Coast Range, as the Klamath province was coupled to the underlying and rotating Franciscan Complex. The findings of Mankinen and Irwin (1982) do not support Fagin and Gose's theory of a rotation of the Klamath province after early Cretaceous time. Mankinen and Irwin (1982) studied Upper Cretaceous and Tertiary-age rocks, including the Cretaceous Hornbrook Formation that depositionally overlies the Ashland pluton in the Eastern Klamath belt.

In contrast to the concept of rigid block rotations, Renne et al. (1986b, 1988) refuted this idea by finding no significant rotation or latitudinal translation with respect to cratonic North America since the Permian. They based their study on six sample sites in the ash flow tuffs and tuffaceous sedimentary rocks of the Upper Permian Nosoni Formation, located in the Eastern Klamath belt. Renne et al. (1988) suggest that other paleomagnetic results from the Redding Section may be domain-specific, that is, they appear to correlate with the observed structural trends. Variable, structural-domain specific rotations of the eastern Klamaths are attributed to vertical-axis oroclinal deformation by Renne et al. (1986b, 1988). Furthermore, variable rotations are found in the western Klamaths (Renne and Scott, 1986).

Schultz and Levi (1983) sampled five calc-alkaline plutons of the Triassic and Paleozoic terrane. The ages of these plutons are Jurassic except for the Grants Pass

pluton, which is early Cretaceous age. For these plutons, Schultz and Levi (1983) ascertained clockwise rotations of 50-78^{o} for the Grants Pass, Slinkard, and Wooley Creek plutons, 111 ± 22^{o} for the Greyback pluton, and they deduced a counterclockwise rotation of 14 ± 22^{o} for the Ashland pluton. Notwithstanding the widely variable ranges and the sizeable errors associated with their findings, Schultz and Levi (1983) suggest that their data substantiate the hypothesis that parts of the Klamaths have had some clockwise rotation on the order of 50-100^{o}. They acknowledge that post-emplacement tilting of the plutons they studied would alter their results considerably. Tilting of plutons of up to 40^{o} is reported in the Klamaths (Barnes et al., 1986), although many plutons lack paleohorizontal indicators. According to Barnes et al., (1986), tilting of the Ashland pluton and Wooley Creek batholith are due to thrusting of the plutons and surrounding country rock over the western Jurassic belt and later doming of the buried rocks of the underthrust terrane, now known as the Condrey Mountain Schist (see Figure 1-2).

Recently, the Western Jurassic belt has been studied for possible rotations using paleomagnetism. In the study area, Bogen (1986) reports that the type Galice section was rotated 100^{o} clockwise since the late Jurassic. His findings are based on samples of metatuff contained within the Galice Formation. Bogen infers that the magnetizations are secondary and post-date late Jurassic folding. The likely times of remagnetization, according to Bogen, are either (1) during low-grade metamorphism of the Late Jurassic Nevadan orogeny (ca 150 Ma), or (2) during intrustion of the Grants Pass pluton in early Cretaceous time (ca 139 Ma).

Critical reviews by Renne and Scott (1986) and Harper and Park (1986) point out the following problems with Bogen's study: (1) Bogen does not substantiate whether the magnetism is primary or metamorphic, (2) a weathering overprint appears likely from the data, which would produce a larger apparent clockwise rotation, (3) Bogen did not adequately document the structural complexity of the region as overturned bedding is

common, and he did not take into consideration the presence of moderate to steeply-plunging fold axes, and (4) Bogen's study lacks evidence of paleohorizontal indicators, yet he rules out the effects of post-Nevadan tilting. Tilted Cretaceous sediments unconformably overlie the Galice to the north and south of the study area (Ramp and Peterson, 1979; Page *et al.*, 1977; Smith *et al.*, 1982). Evidence for more than one phase of folding in the type Galice is presented in Chapter 3.

In summary, many paleomagnetic studies of volcanic rocks in the Klamaths suggest variable, clockwise rotations on the order of $50\text{-}100^{o}$. These reported rotations have been used to support theories of rigid block rotations of the terranes (e.g., suturing of accreted "exotic" terranes) and more recently, to support the idea of vertical-axis oroclinal bending. Since the amounts of observed rotations vary from site to site within one terrane, it seems most likely that these variations correlate with observed structural trends. In the study area, Bogen's finding of 100^{o} clockwise rotation of the type Galice after the late Jurassic may be conceptually correct; problems associated with his techniques, however, shed some doubt as to the exact magnitude of this rotation. A clockwise rotation of this magnitude is consistent with the observed bending of structural trends in the Klamaths.

1.7 Late Jurassic Paleogeography of North America

Rapid apparent polar wander paths have been calculated for the Jurassic (Mankinen *et al.*, 1984) as the Jurassic represents the age at which the largest deviations occur (Harrison and Lindh, 1982). Information about the relative movement of the North American continent with respect to Africa comes from paleomagnetic studies on rocks of late Jurassic age from the Colorado Plateau, a relatively stable interior province. Kocurek and Dott (1983) report the use of the following formations from western North America of Oxfordian to Kimmeridgian age in paleomagnetic studies: Stump, Morrison,

Curtis, Summerville, Ralston, Todilto, Junction, Bluff, and Cow Springs. According to Steiner (1983), rapid apparent polar wander paths are found from study of the Summerville strata (ca 150 Ma) that continue until early Cretaceous time (Steiner, 1983). Data from the Colorado Plateau indicate a change in paleolatitude from 5-10^{o} to about 33-38^{o}N latitude during this time interval (Steiner, 1983).

Recently it has been shown that the Colorado Plateau has experienced a clockwise rotation on the order of 3-5^{o} with respect to cratonic rocks east of the Rocky Mountains and Rio Grande Rift (Hamilton, 1981; Cordell, 1982). Bryan and Gordon (1985) calculated the magnitude of this rotation as 3.8^{o} ± 2.9^{o}. As a result, May and Butler (1986) constructed a revised Triassic-Early Cretaceous North American APW path (Figure 1-3) based on eight reliable Jurassic paleomagnetic poles listed in Table 1-1. This APW path (Figure 1-3) is corrected for a 3.8^{o} clockwise rotation of Colorado Plateau poles and is significantly different than older compilations (*e.g.*, Harrison and Lindh, 1982; Irving and Irving, 1982).

Paleomagnetic Euler pole (PEP) analysis by May and Butler (1986) on nine reliable Jurassic and Early Cretaceous poles reveals two cusps, J1 and J2, in the Triassic-Early Cretaceous APW path of North America (Figure 1-4). The apex of the J1 cusp is defined by the Wingate Formation pole and the J2 cusp is defined by the lower Morrison Formation pole. According to May and Butler (1986), each of these cusps represents a change in the direction and velocity of North American plate motion. May and Butler (1986) suggest that J1 and J2 correspond to the syn-rift phase of Atlantic spreading history and to the Nevadan orogeny in western North America, respectively. The angular velocity diagram of May and Butler (1986) is shown in Figure 1-5 and it evaluates the angular progression of poles along the two Jurassic APW paths. The slope of the J1-J2 line defines an angular velocity of 0.6^{o}/m.y. or about 5 cm/yr linear velocity from a reference point, San Francisco, California. The second segment, J2-K, shows a much higher angular velocity of 2.8^{o}/m.y. during the Tithonian, which suggests

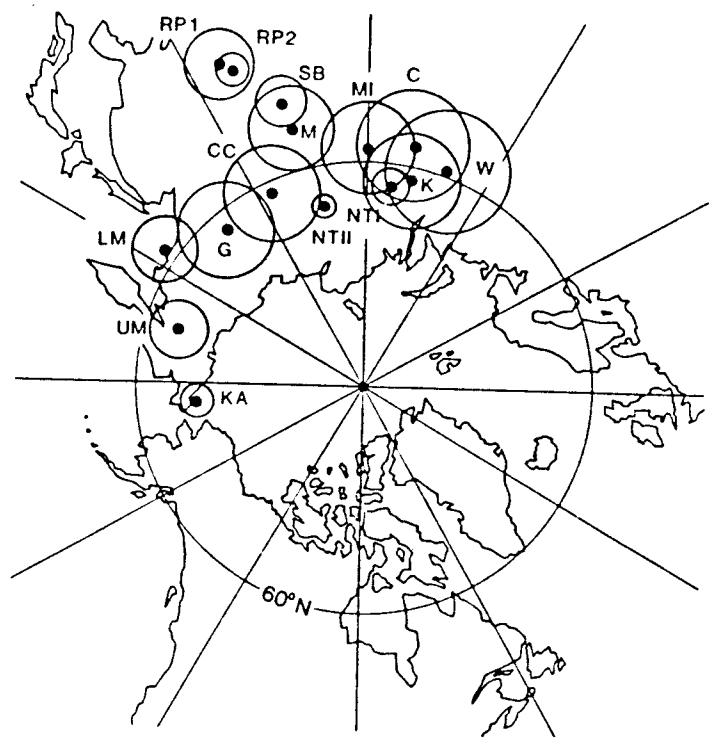

Figure 1-3: Stereographic north polar projection of the Triassic-Early Cretaceous North American APW path, from May and Butler (1986). Mean pole locations are shown by solid circles and associated A_{95} confidence regions. Poles from the Colorado Plateau that are corrected for 3.8^{o} clockwise rotation include: UM, LM, K, W, and M. Symbols for Jurassic poles are W, Wingate Formation; K, Kayenta Formation; NTI, Neward Trend Group I; NTII, Neward Trend Group II; CC, Corral Canyon; G, Glance Conglomerate (Canelo Hills); LM, lower Morrison Formation; UM, upper Morrison Formation. Other poles include RP, Red Peak Formation of Chugwater Group (2 poles); SB, State Bridge Formation; M, Moenkopi Formation; MI, Manicouagan Impact Structure; C, Chinle Formation; and KA, Cretaceous average pole of Mankinen (1978).

North American Jurassic Reference Poles

Pole	Symbol	Age (Ma)	Pole Latitude degrees N	Pole Longitude degrees E	A-95 degrees	Reference
Upper Morrison Fm	UM	145	67.6	161.9	3.9	Steiner and Helsley (1975)
Lower Morrison Fm	LM	149	61.4	142.3	4.2	Steiner and Helsley (1975)
Glance Conglomerate	G	151 ± 2	62.7	131.5	6.3	Kluth and others (1982)
Corral Canyon Rocks	CC	172 ± 5.8	61.8	116.0	6.2	May and others (1986)
Newark Trend Group II	NTII	179 ± 3	65.3	103.2	1.4	Smith and Noltimier (1979)
Newark Trend Group I	NTI	195 ± 4	63.0	83.2	2.3	Smith and Noltimier (1979)
Kayenta Fm	K	194-200	62.1	70.2	6.3	Steiner and Helsley (1975)
Wingate Fm	W	200-206	59.0	63.0	8.0	Reeve (1975) from Gordon and others (1984)

Table 1-1: North American Jurassic reference poles from May and Butler (1986).

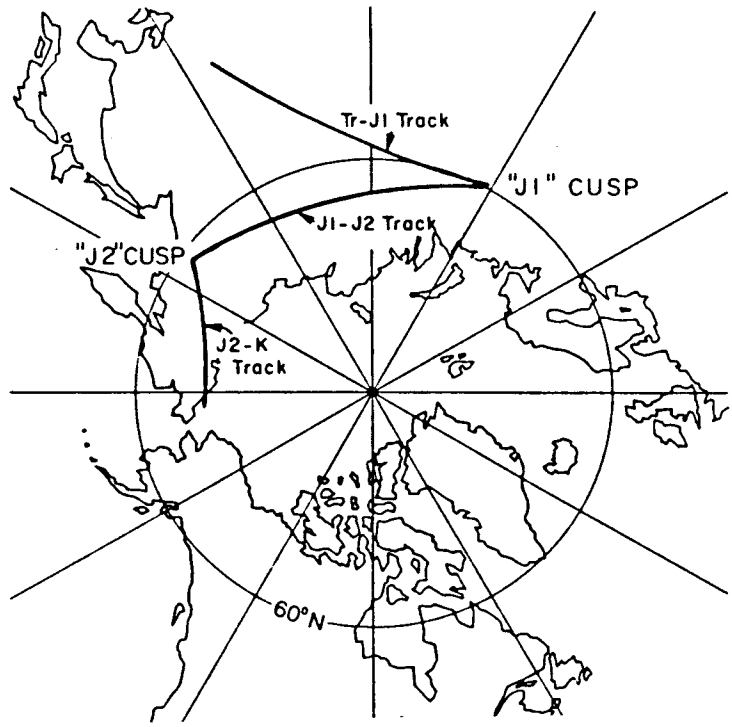

Figure 1-4: Paleomagnetic Euler pole model applied to the North American Triassic-Early Cretaceous APW path of May and Butler (1986). Two cusps are present within the Jurassic APW path, an older cusp "J1" and a younger cusp "J2". The apex of J1 is defined by the Wingate Formation pole, and the J2 cusp is defined by the lower Morrison Formation pole.

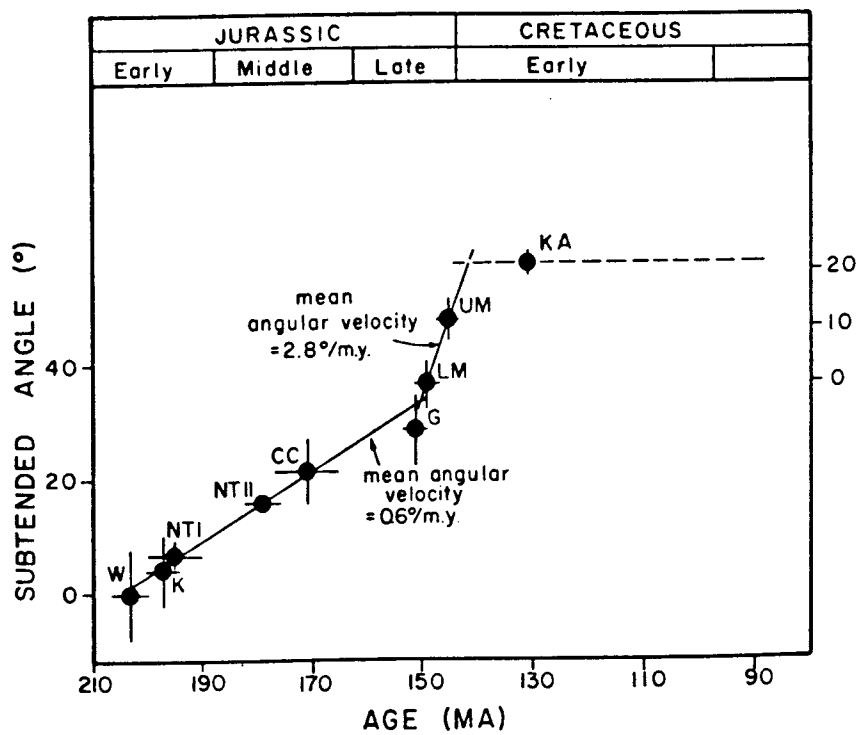

Figure 1-5: Angular velocity diagram for the Jurassic APW path with corrected Colorado Plateau poles from May and Butler (1986).

increased plate velocity rates (ca 50 cm/yr) or a large error due to the small data set used to constrain this time interval.

Changes in relative sea level occurred during the Jurassic (Brenner, 1983). This effect was produced by the reordering of spreading centers, the change in global spreading rates, and the change in the volume of the oceans (Vail *et al.*, 1977; Miall, 1986). A major world-wide Jurassic marine transgression caused sea level to rise during the Oxfordian, reaching a peak during the Kimmeridgian (Haq *et al.*, 1987). Marine deposition occurred from Alaska to southern California during this transgression (Brenner, 1983). During the Oxfordian and early Kimmeridgian, dark clay, silt, and fine volcanic material were deposited along the western North American margin, as the sea covered much of California west of the crest of the Sierra Nevada, extending northwestward into Oregon and Washington (Imlay, 1980).

At the same time as this transgression, a large epeiric sea existed on North America adjacent to the Cordillera that had limited exchange with arc-trench basins along the continental margin (Brenner, 1983). The uplift of the western edge of the craton during the Kimmeridgian-Tithonian by magmatic arc growth and tectonic activities provided a large abundance of fluvial siliciclastics into the epeiric sea and emerging Cordillera foreland thrust belt (Porter *et al.*, 1982; Brenner, 1983). Thus, the late Jurassic sediments of the Colorado Plateau record changes in: (1) sedimentation, from chemical precipitation to dominantly siliciclastic sedimentation, (2) climate, from an arid tropical environment to a more humid and temperate climate, and (3) paleolatitude, as North America changed its relative movement with respect to Africa.

A reconstruction of the paleogeography of North America during the late Jurassic is shown in Figure 1-6. This map shows the positions of paleolatitudes (Brenner, 1983) as well as the position of land (Imlay, 1980) and the location of late middle Oxfordian to early Kimmeridgian ammonites and *Buchia* (Figure 10 of Imlay, 1980). *Buchia* are of northern derivation (Imlay, 1965, p. 1034), and ages of *Buchia*-bearing strata from

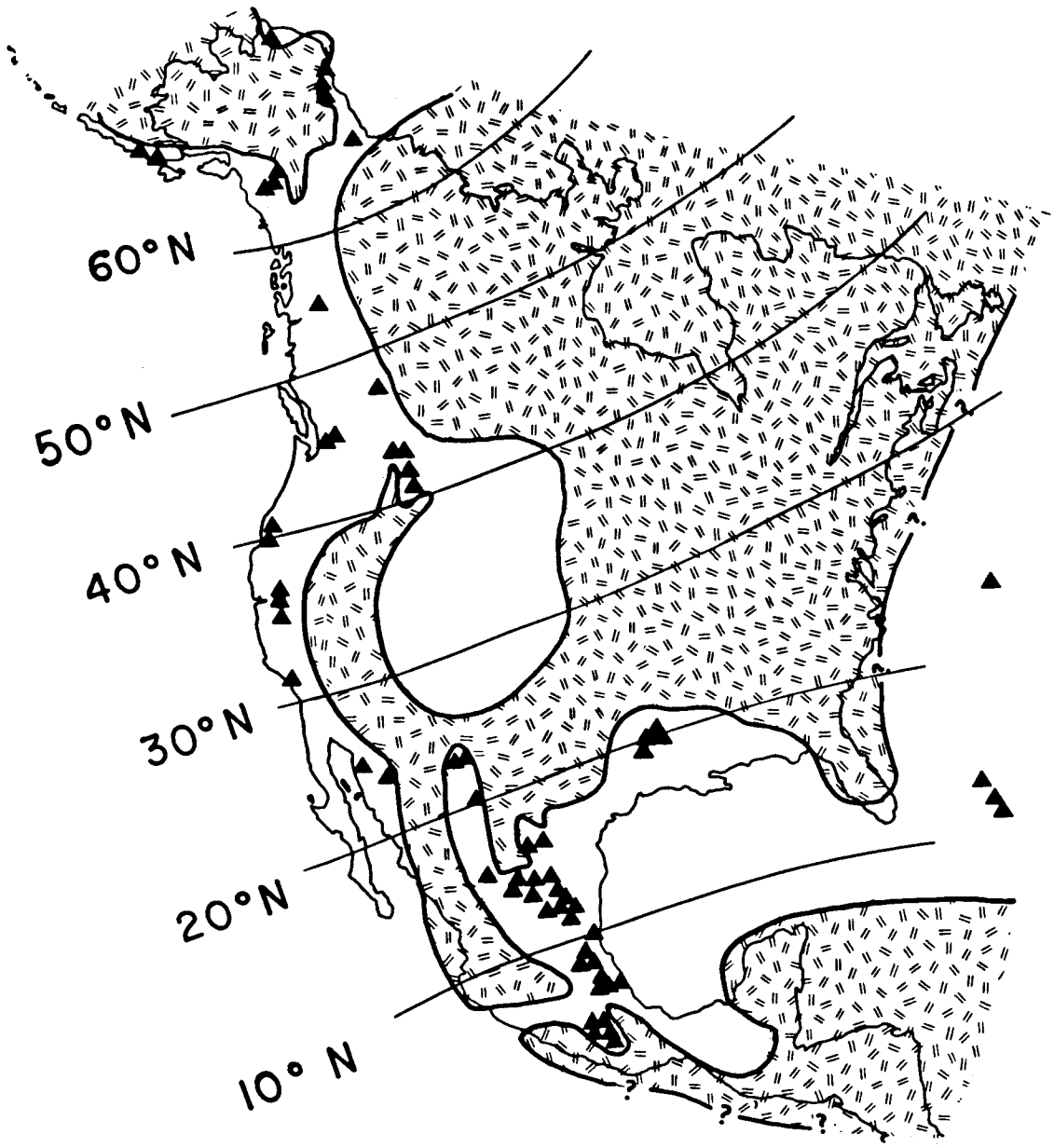

Figure 1-6: Paleogeographic map of North America during the late Jurassic showing paleolatitudes, position of land (shaded area) and sea, and the distribution of late middle Oxfordian to early Kimmeridgian ammonites and *Buchia* (solid triangles). The configuration of North America and the Gulf of Mexico are both shown in a schematic sense (*see* Pindell, 1985). From Brenner (1983) and Imlay (1980).

northwestern California and southwestern Oregon were determined on the basis of the ammonites present (Imlay and Jones, 1970). In California, *Buchia concentrica* (Sowerby) is found in conjunction with the lower Kimmeridgian boreal ammonite *Amoeboceras* (Amoebites) and the nonboreal ammonites *Subdichotomoceras*? and *Idoceras* (Imlay, 1980).

Imlay (1980) summarized his work on Jurassic rocks from California and Oregon. He concluded that during the late Bajocian until the end of the Jurassic, differentiation of ammonite faunas occurred from north to south. As mentioned above, he found both boreal- and Tethyan-affinity genera in rocks from California and Oregon. This same pattern of Tethyan- and boreal-affinity genera is reported from radiolarian assemblages from the Coast Range Ophiolite and the Izee terrane from east-central Oregon (Pessagno and Blome, in press). Pessagno and Blome (in press) report that they found a progressive change up section in rocks from these terranes, namely, Central Tethyan → Northern Tethyan → Southern Boreal. Thus, it seems conclusive from faunal and paleomagnetic data that there was a significant change in paleolatitude for the Northern Californian part of the North American continent from middle Jurassic to early Cretaceous time.

CHAPTER 2: LITHOLOGY AND CONTACT RELATIONSHIPS

Five lithologies are found in the Galice, Oregon vicinity: (1) slaty shales and greywackes of the Galice Formation, (2) lithic tuffs, breccias, and lava flows of andesitic to dacitic composition, ascribed to the Rogue Formation, (3) hornblende diorite porphyry dikes, (4) massive amygdaloidal basalt rocks, and (5) highly sheared, serpentinized ultramafic rocks. This suite of rocks illustrates the complexity and activity of an active magmatic arc setting. Each of these units is fully described in the following sections, with interpretations provided in chapter six. Following the lithologic descriptions is a section describing the depositional and fault contacts in the study area.

2.1 Rogue Formation

The Rogue Formation consists of greenish-grey lava flows, lithic tuffs, and breccia, all of andesitic to dacitic composition. Wells and Walker (1953) defined the Rogue Formation as Upper Jurassic metavolcanic rocks and related intrusive rocks exposed from Whiskey Creek to Almeda mine, as well as in the lower reaches of Grave Creek and Reuben Creek. The type section is the exposure of metavolcanic rocks along the Rogue River. Pb/U zircon ages for the type Rogue tuff-breccia are 157 ± 2 Ma (Saleeby, 1984).

The flows are massive and commonly show spaced joints parallel to the contact. Excellent examples of flows are found west of Indian Mary Campground along the north side of the Rogue River, at stations 1-4. The massive lithic tuff breccia units are composed of poorly-sorted, fragmental volcanic and volcaniclastic rocks. The volcanic rocks are composed of sodic plagioclase, actinolitic amphibole, epidote, and chlorite, with original textures and structures generally preserved (Hotz, 1971). Figure 2-1 shows the texture of the poorly-sorted lithic tuffs from locality 6.

Figure 2-1: Photo illustrating the texture of the poorly-sorted lithic tuff breccia (Rogue Formation). This water-polished section shows lithic clasts that range from angular to well-rounded. Photo taken at locality 6 along the Rogue River.

More recent work on the Rogue was completed by Riley (1987) who examined the type Rogue from Almeda Mine to Rainie Falls, and along Grave Creek up to the Galice Formation contact. Riley (1987) deduced a stratigraphic order in the section he studied. He came up with the following order (oldest to youngest): (1) andesitic matrix-supported flow breccias, (2) crystal-lithic volcaniclastic turbidites, (3) volcanic ash tuffs, and (4) volcanic flows and intrusions. In his conclusions, Riley (1987) stated that multiple magma chambers were most probably present, and that the Rogue extrusives represented a relatively young island arc with a tholeiitic parent magma, based on his study of clinopyroxene compositions of Rogue basalts and basic andesites.

The Rogue volcanics strike north-northeast and dip at steep to shallow angles to the southeast (Diller, 1907). At the type locality, Wells and Walker (1953) estimated a thickness on the order of 4600 m. Riley (1987) estimated the Rogue to have a minimum thickness of 3.4 km (2.125 mi), an estimate which Riley asserted takes into account the structural repetition due to large-scale isoclinal folds.

The Rogue volcanics exhibit folds, as can be seen on the map by Wells and Walker (1953) in the vicinity of Mouse Creek, southwest of the Grave Creek Bridge. Wells and Walker (1953) described the sedimentary and volcanic rocks as "closely folded" with steep easterly dips. They describe "drag folds" in the volcanics that range in size from microscopic laminar structures to folds that have amplitudes of 60 meters or more. More recent studies on the Rogue have shown that the metavolcanic rocks of the Rogue display tight to isoclinal folds that are reclined to the southeast and generally plunge north (Kays, 1967). Riley (1987) inferred isoclinal folds up to 800 meters in wavelength from the overturned, graded volcaniclastic beds that he studied.

Wells and Walker (1953) noted that the volcanic rocks locally show pillow structures, and sometimes show vesicular and amygdaloidal structures. Dismembered pillow lavas were found in the study area near the confluence of Grave Creek and the Rogue River, just east of the bridge. Kays (1968, Plate 2B) documents highly disrupted

and "sheared" Rogue metavolcanics that occur along the Rogue River near the Grave Creek Bridge. Riley (1987) concurred with Kays (1968) that the pillow-like structures at this location were sheared volcanic ash tuffs.

Grey to grey-green cherts are found in conjunction with the Rogue lithic tuffs. Along the southwestern side of the Rogue River between Taylor and Galice Creek, the Rogue tuffs are interbedded with greenish-grey bedded cherts and minor shales. The alternating tuff-chert beds are extensive and outcrop for approximately 60 meters along the southwestern side of the paved road. The cherts at this locality contain radiolarians (Pessagno, personal communication, 1988) that are in a poor state of preservation. These beds are clearly overturned, as determined from graded beds seen in the tuffs at location 143. Figure 2-2 shows the appearance of these bedded tuffs and cherts. Another locality where cherts are a significant constituent in the lithic tuffs is an exposure in the Rogue River canyon walls about 800 meters west of the Almeda mine, where cherty tuffs overlie amygdaloidal lava (Wells and Walker, 1953).

Rhythmically bedded chert sequences are common in orogenic belts and are in many cases the result of deposition by turbidity currents (Ijima and others, 1985). The color of bedded cherts has been correlated on a first-order basis with the corresponding depositional environment. Bedded cherts deposited on a basaltic basement most likely are red or green, while bedded cherts in a continental margin environment are dark grey or black (Jones and Murchey, 1986). In particular, island-arc chert is commonly green to grey-green and is well-laminated, according to Jones and Murchey (1986). Thus, if the correlation by Jones and Murchey (1986) is universally valid, it would confirm the island arc origin of the cherts interbedded with Rogue volcaniclastic rocks.

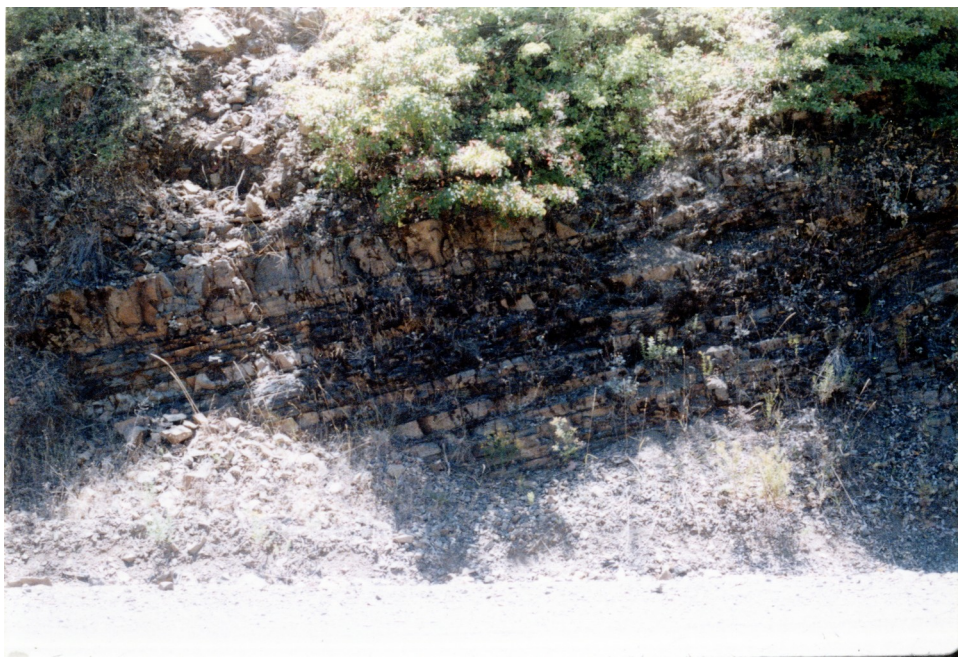

Figure 2-2: Photo of interbedded tuff and dark grey to greyish-green chert at locality 143. This site is located on the southwestern side of the Rogue River on the paved road between Taylor Creek and Galice Creek. The tuffs are inversely graded and reveal that the beds are overturned. Photo taken looking to the southwest.

2.2 Galice Formation

The Galice Formation consists of thin-bedded, dark grey to black shales that consistently show a prominent cleavage. Throughout this thesis, the term "shale" is used in describing the type Galice, even though an axial-plane cleavage is present. Slates are found in the "Galice" metasediments that overlie the Josephine ophiolite to the south. The slaty shales in the study area generally strike northeast with steep southeasterly dips. Poor exposures of shale are found along the dirt and logging roads, while better, water-polished exposures are found along the Rogue River and its tributaries. The shales are in beds typically between 2-25 cm thick with thin lenses of greywacke (Figure 2-3).

Coarse-grained sandstone and pebble conglomerate are locally found along the banks of the Rogue River across from the town of Galice at localities 11 and 14. Coarse-grained sandstone beds were also found along Grave Creek at localities 102 and 133. These coarse pebbly sandstone beds consist of well-rounded grains and are conspicuous by the presence of large, elliptical shale rip-up clasts that are up to 12 cm in diameter (see Figure 2-4). The bases of the pebbly sandstone beds appear irregular and scoured. These beds are interpreted as occupying water-cut channels, due to the presence of (1) poor sorting of clasts, (2) coarse grain size, and (3) lack of imbrication, grading, or water-escape structures (Leeder, 1982, p. 81).

Chert-rich pebble conglomerate beds occur at one locality in the study area, along Galice Creek, southwest of the hamlet of Galice (location 148). The conglomerate is grain-supported with a sandy and silicic volcanic matrix. The pebbles are subrounded to well-rounded, poorly-sorted in the textural sense, and they are lithologically diverse. The pebbles range from less than 2 mm up to 7 cm. They consist of bluish-grey chert, black mudstone, reddish foliated sandstone pebbles with shale rims, silicic volcanic tuff, quartzite, and minor basalt clasts. The pebbles appear to have a poorly-developed fabric produced by imbrication. Figure 2-5 shows a large piece of the chert-rich pebble conglomerate.

Figure 2-3: Photo of Galice bedded shales with greywacke lenses. Shale beds are typically 2-25 cm thick and have a prominent cleavage. Sandstone lenses have faint ripple structures with an amplitude of 1 cm. Locality 50.

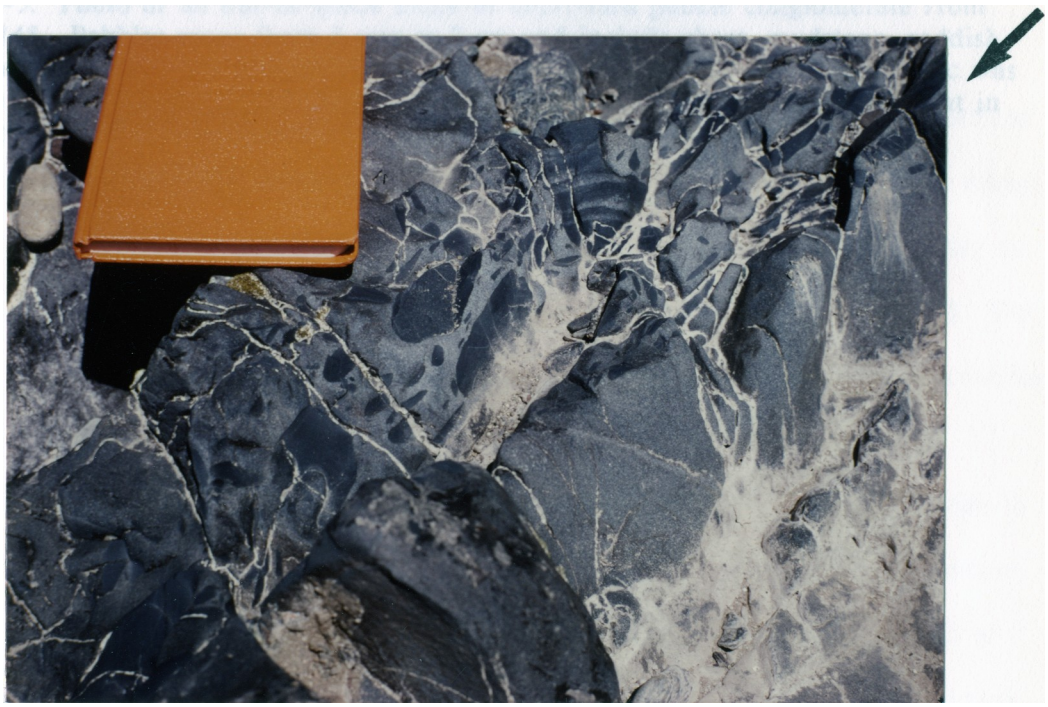

Figure 2-4: Coarse-grained sandstone bed at locality 11 that has large, elliptical rip-up clasts of shale. Shale clasts range up to 12 cm in diameter. Arrow shows scoured base of this bed.

Figure 2-5: Photo of an out-of-place block of chert-rich pebble conglomerate from locality 148. Pebbles range from 2 mm to 7 cm and include chert, mudstone, reddish sandstone with shale rims, volcanic tuff, quartzite, and minor basalt clasts. Fabric was most probably produced by imbrication, such that paleoflow was from left to right in this photo.

Chert is the major constituent of these conglomerates. A pebble count of 344 pebbles from the Galice Creek locality indicated that chert accounted for 82% of the total clasts, and mudstone made up 9% (Seiders and Blome, 1988, supplemental data 8803).

The presence of well-rounded to subrounded pebbles of diverse sizes and lithology is interpreted as a quickly deposited conglomerate, with clasts from multiple sources. The preponderance of grey chert and black mudstone clasts imply exposure of a basement pelagic sequence. Other clasts, such as volcanic tuff and basalt indicate an arc source, while reddish sandstone clasts with shale rims and the white quartzite clasts signify a continental margin source.

The Galice Formation is dated as Late Jurassic on the basis of *Buchia concentrica* (Sowerby) found at a few locations in the study area. The first locality is about 30 meters east of the Almeda mine, at locality 24, as was reported by Diller (1907). This site consists of shales interbedded with minor sandy lenses, and is located east of the Galice-Rogue contact.

The second locality is located about 1 km south of Grave Creek, between McKnobe and Butte Creeks, at locality 100, where casts of *Buchia concentrica* (Sowerby) are found in rusty weathered shales (Figure 2-6). This location represents a new fossil locality as the casts were positively identified by D. L. Jones (personal communication, 1985). The black mudstone near the mouth of Rock Creek is the third location of *Buchia concentrica* (Sowerby) in the study area (Libbey, 1967, p. 3).

Buchia concentrica (Sowerby) is a bivalve that ranges from late middle Oxfordian to middle Kimmeridgian (Imlay, 1980, p. 24-25), previously referred to in older literature as *Aucella erringtoni* (Imlay, 1959; Imlay et al., 1959). It is the characteristic fossil of the Galice Formation (Diller, 1907, 1908; Taliaferro, 1942). Diller (1907) reported that it was found at "numerous sites" in the Galice Formation.

Figure 2-6: Casts of *Buchia concentrica* (Sowerby) in well-weathered Galice shales from new fossil locality 100. Positive identification by D.L. Jones (personal communication, 1985).

Diller (1907) reported Dr. T. W. Stanton's observations on the fossils from the study area. At Almeda mine, *Buchia concentrica* (Sowerby) was found together with the ammonite *Perisphinctes. Trigonia, Amberleya,* and *Belemnites* and *B. concentrica* (Sowerby) were described in a conglomerate bed located at the mouth of Anderson Gulch (Diller, 1907, p. 404). Many years later, Taliaferro (1942) and Imlay (1961) concurred that the ammonite *Perisphinctes (Dichotomosphinctes)* and *Buchia concentrica* (Sowerby) were present in the Galice and its correlative unit in California, the Mariposa Formation, both units of middle Oxfordian to early Kimmeridgian age (Pessagno and Blome, in press). Pessagno and Blome (in press) concluded that the presence of *Dichotomosphinctes* and *Buchia concentrica* (Sowerby) in the basal section of the type Galice demonstrated that it was correlative with the SCHILLI Subzone (Tethyan Realm) and the ILOVAISKII Subzone (Boreal Realm). Furthermore, they assigned the basal Galice to the mid-middle Oxfordian, which they considered younger than 157 Ma. They reassigned the Oxfordian-Kimmeridgian boundary to 154 Ma from 157 Ma (of Harland et al., 1982) based on the use of Westermann's (1984) "scaled equal subzone method."

Wells and others (1949) reported that carbonaceous layers up to 10 cm thick were found in the Galice Formation at a few localities. These sooty layers commonly contain carbonized woody plant fragments. In the study area, plant fragments were found at *Buchia* locality 100. These plant fragments appear to be broken stems and possible leafy material. The stems range up to 2 cm long and 2 mm in diameter. The presence of these plant fragments indicates that the flysch detritus was organic-rich and quickly deposited. Organic carbon in the form of plant debris has been found to be a very important factor governing early diagenetic reactions in turbiditic sediments (deLange, 1986). A photo of these plant fragments from locality 100 is presented in Figure 2-7.

Apparent trace fossils in the Galice are best seen in thin-section or on bedding planes. In thin section, they appear as dark, organic-rich lenses in contrast to lighter-colored material. These sinuous structures are postulated as representing feeding and

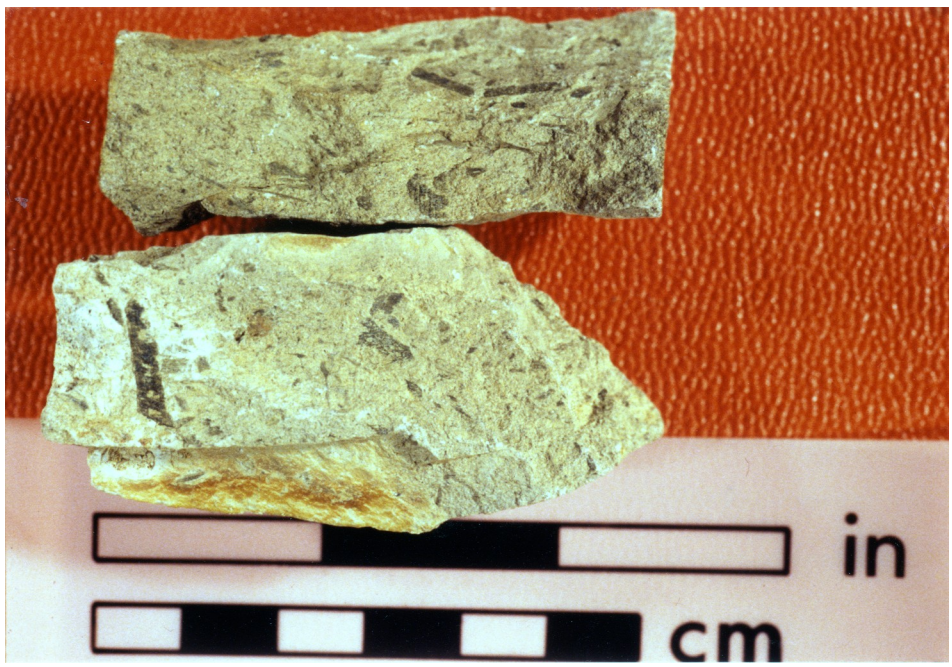

Figure 2-7: Carbonized plant fragments including broken stems and possible leafy material from locality 100 (Galice Formation).

grazing traces at the sediment-water interface. Figure 2-8 shows sketches of two thin-sections which illustrate these branching structures that are found parallel to the bedding plane. An alternative hypothesis is that these structures may have been burrows deformed by some combination of sedimentary compaction and shortening during cleavage formation (W.S.F. Kidd, personnal communication, 1988). Another hypothesis for these structures would suggest that these laminae illustrate "stratal disruption," such as is found in mudstone and silt laminae from DSDP site 181 in the Aleutian trench (e.g., Fig. 2 of Lundberg and Moore, 1986). Stratal disruption is defined by Lundberg and Moore (1986) as bedding discontinuities that are not attributed to primary deposition, bioturbation, or drilling deformation. Nonetheless, the evidence from these thin-sections (Figure 2-8) supports a biogenic origin for the following reasons: (1) the folded and distended lenses are dark and more organic-rich than the surrounding lighter-colored matrix, probably the result of biologic concentration, and (2) one section of these "burrows" on higher magnification reveals concave inner wall surfaces (Figure 2-9).

A. A. Ekdale identified deep water trace fossils *Cosmoraphe*, *Spirophycus*, and *Chondrites* from the Galice slate and fine-grained sandstone that overlies the Josephine ophiolite, to the south (Harper, 1983; Harper 1982a; Harper, 1980a). Positive identification of trace fossils from the type Galice is not possible because they are too deformed (E. Landing, personal communication, 1987). Nevertheless, the most logical supposition is that these traces were produced by one of the members of the *Chondrites-Nereites* "facies" assemblage (Seilacher, 1964; Simpson, 1975). These trace fossils are restricted to the muddy deep sea, characterized by quiet waters periodically interrupted by turbidity flows (Frey, 1975). Schematic diagrams of these members are shown in Figure 2-10.

The presence of intensely bioturbated shale horizons may indicate slow rates of sedimentation, as the organisms had time to graze and rework the sediment before

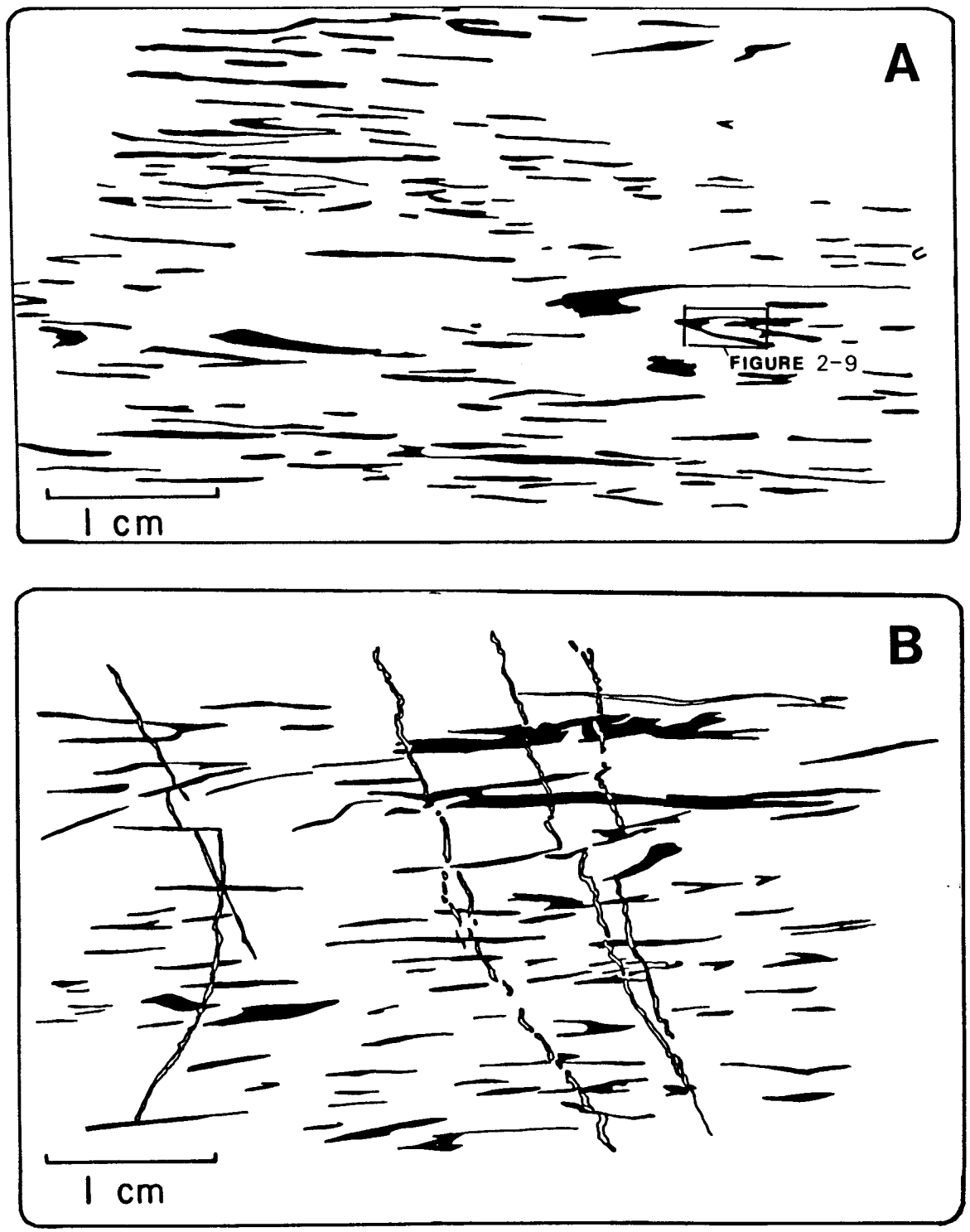

Figure 2-8: Sketches of two thin-sections of Galice shale cut normal to bedding that show dismembered organic-rich lenses. These lenses are thought to represent feeding and grazing traces. Both thin-sections are from locality 22. (a) Thin-section with apparent fold closures and section of detail shown in Figure 2-9. (b) Thin-section of shale cut by calcite veins, some of which are offset.

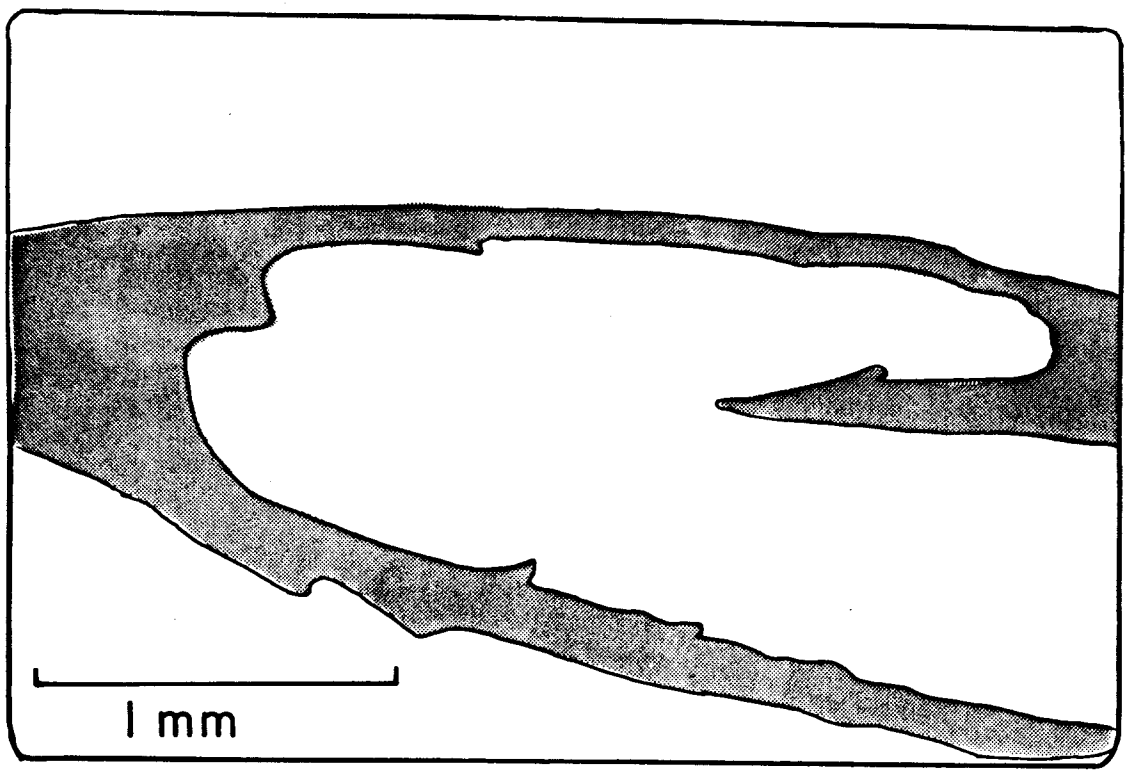

Figure 2-9: Sketch of a possible burrow structure from the thin-section shown in Figure 2-8a, but on higher magnification. Field of view is approximately 6 mm^2. Biogenic origin presumed due to the concavity of the inner wall surfaces.

Figure 2-10: Schematic diagrams of *Chondrites* and *Helminthoida* trace fossil types from Frey (1975). *Chondrites* is characterized by an intricate array of branches while *Helminthoida* grazes efficiently across the sediment-water interface making 180^{o} turns.

another laminae of mud was deposited. Trace fossils were found at stations 22, 24, and 58. Station 24 is located about 30 m east of the Rogue-Galice contact, and is thought to represent basal or lowermost Galice. Stations 22 and 58 are both located approximately 1/2 km east of the contact; station 22 is southeast of Almeda mine, while station 58 is on the western side of Rock Creek, north of Grave Creek. Going eastward from the Rogue-Galice contact to stations 22 and 58, the Galice is composed exclusively of bedded black shales. The trace fossil evidence together with the fact that only shales appear to be deposited in the lowermost section of the Galice indicates that the basal Galice was dominated by quiescent, hemipelagic sedimentation.

2.3 Hornblende Porphyry Dikes

Intrusive dikes and irregular-shaped knoblike masses (Diller and Kay, 1924) of hornblende-rich diorite porphyry trend northeast, near or along the geological boundary between the Rogue and Galice Formations. Generally, these dikes are 6-12 m across and 30-100 m long. The largest mass is a sill-like intrusion (Hotz, 1971) exposed at Almeda mine that is 121 m wide and 3.2 km long (Libbey, 1967). The dikes have a vertical attitude and are characterized as dark-colored rock with phenocrysts of dark-green hornblende set in a felsitic matrix of feldspar (andesine, when not altered, according to Shenon, 1933) and minor quartz. These dikes have been previously labelled as "quartz porphyry or alaskite" by Diller (1914), "dacite porphyry" by Winchell (1914), "porphyritic dacite" by Shenon (1933) and Hotz (1971), "dacite porphyry" by Wells and Walker (1953), and "quartz diorite and related rock (i.e., hornblende diorite, granodiorite, dacite, and diabase dikes)" by Ramp and Peterson (1979). Zircons extracted from these dikes that cut the upper Rogue give an age of 150 ± 2 Ma (Saleeby, 1984).

In this study, these dikes have been classified as hornblende diorite porphyry dikes for the following reasons: (1) the texture of the rock is porphyritic with a felsitic groundmass, and is composed of more than 50% phenocrysts, (2) quartz is rare, while

feldspar is present in significant amounts, and (3) hornblende makes up the largest portion of this rock in the form of euhedral, interlocking dark-green phenocrysts.

At Almeda mine, a large sill-like intrusion is found near the contact between the Rogue and Galice Formations. This zone is mineralized with significant amounts of pyrite, bornite, chalcopyrite, barite, calcite (Libbey, 1967), native gold, native copper, and molybdenite associated with the diorite dike (Ramp and Peterson, 1979). All of the tunnels at the Almeda mine were driven northward to explore the contact between the Galice shale and the diorite porphyry (Libbey, 1967) (see also Section 2.6.2). Diller (1914) described the ore at this mine as occurring in "bunches", which meant that the longest direction is vertical, and that the ore is lenticular in form. Reports of ore containing more than 50% $BaSO_4$ were not uncommon (Libbey, 1967). Well-rounded clasts of barite were found at the mine and along the traverse up Grave Creek.

Dikes were found at the following stations in the study area (see locale map in back flap): stations 160, 24 (Almeda mine), 106, 107, and 51. Out-of-place boulders of hornblende diorite porphyry were found at site 108.

2.4 Ultramafic Rocks

Ultramafic rocks crop out in the southeastern portion of the study area in narrow, highly dissected, offset and sheared belts. The ultramafic rocks are serpentinized yet contain residual peridotite, including harzburgite, dunite, and pyroxene (Ramp and Peterson, 1979). These rocks occupy zones of major faulting, conjectured to be genetically related to the Josephine peridotite to the south (Harper, personal communication, 1985). The serpentinized ultramafic rocks are characteristically dark-green to black, glassy on fresh surfaces, highly sheared, with little or no vegetation growing on them. They weather to buff or rust, and are cut by 1-2 m wide rodingite dikes parallel to the trend of the serpentinite bodies (Figure 2-11). The absence or near absence of vegetation facilitates aerial photo interpretation of these serpentinite bodies,

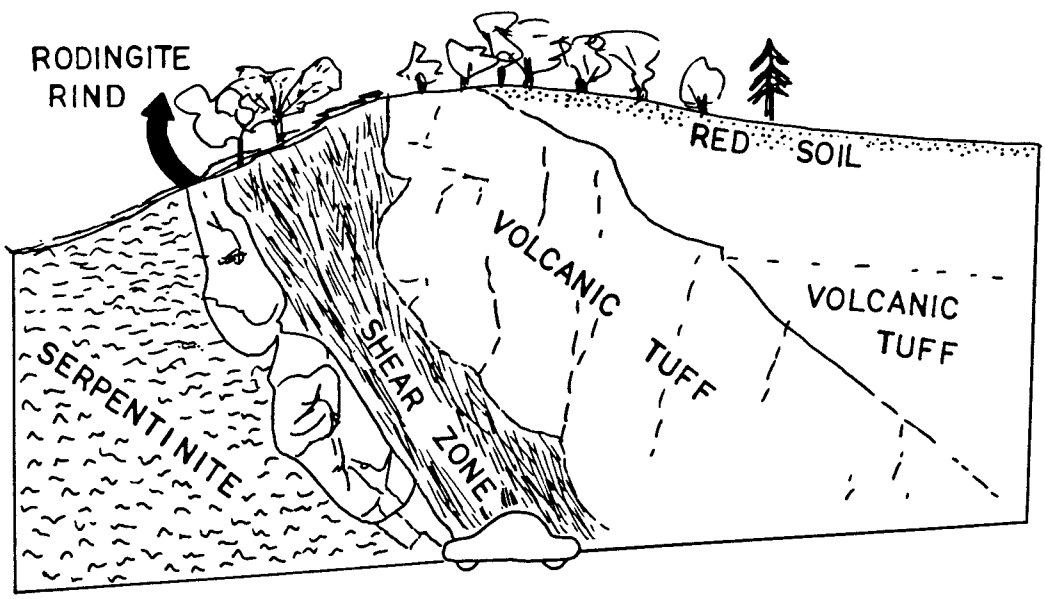

Figure 2-11: Serpentinized ultramafic rocks and volcanic tuff separated by a shear zone and rodingite rind at locality 165. Sketch below is taken directly from field notebook of a larger area from which a portion is shown in the above photo.

as their contacts and numerous offsets are easily detected.

In describing the ultramafic rocks, Diller (1914) noted that the gold-bearing veins are often found near the serpentine, and that the veins are cut off "sharply at the contact" and do not continue into the serpentine. Thus, the serpentine is highly dissected and many high angle reverse faults are found along these bodies, e.g., west of Hellgate (Wells and Walker, 1953).

The belts of ultramafic rocks are in contact with Rogue volcanic lithic tuffs and flows, and appear to extend northward as far as 0.6 km south of stations 33 and 34. The existence of a zone of north-northeast trending faults that bring ultramafic rocks into contact with volcanic rocks to the east and shales to the west, is seen in the crenulated, disrupted shales at locations 87, 88, and 89. The importance of this fault and the development of crenulation cleavage will be brought out more fully in the structural section 3.3.3.

2.5 Basalt

Basalt flows are found east of Stratton Creek, along logging roads. The basalt is dark greenish-grey to black, amygdaloidal with vesicles filled with calcite, probable zeolite minerals, and biotite. Many small veins of calcite cross-cut the basalt. The basalt weathers to buff to a dull reddish color. The basalt has been quarried as road metal, and crops out in the quarry at stations 32 and 35 where it is at least 100 meters thick.

2.6 Contact Relationships

2.6.1 Interbedded Shale and Metatuff

The black shales of the Galice Formation are interbedded with, or overlain by, volcanic rocks at a few localities in the study area. On the geologic map (Plate 1, back flap), the localities of these interbedded shales and volcaniclastics are indicated by Ji. Irwin (1981) calls these minor volcanics and volcaniclastics "pyroclastic interlayers." These volcanic rocks consist of andesitic flows and flow breccias that grade upwards into more siliceous tuffs, tuff breccias, and thin flows (Ramp and Peterson, 1979, p. 7). These tuffs and flows appear indistinguishable from the Rogue Formation volcanics. The thin-bedded tuffs in the Galice contain Late Jurassic radiolarians (Irwin and others, 1978).

Flows are found interbedded with shale beds at localities 1-4. The shale-tuff contacts are undulant, and slaty cleavage is prominent in the shale beds at these localities. Siliceous tuffs are interbedded with shale at localities 26, 53, 136, 139, and 140.

A stratigraphic section of interbedded shales and volcanic tuffs was measured at station 26 across from the Indian Mary boat ramp, on the north side of the Rogue River. This 10.5 meter exposed section consists of alternating shale and tuff beds typically 30-60 cm thick, as shown in Figure 2-12. The base of the tuff beds is drawn as a solid line if the contact is sharp, and as a dashed line if the contact with the shales is gradational. Photos from this outcrop (Figures 2-13 and 2-14) show the interbedded shales and volcanic tuffs at two different scales. From a moderate distance, the beds appear as distinct packages of shale and volcanic tuff. A close-up view of the banded tuff reveals that flattened shale clasts are also present.

Other observed localities that exhibit interbedded shales and volcanic rocks are southwest of the Rogue River. At location 53, 8-9 m of black, fissile shale crops out

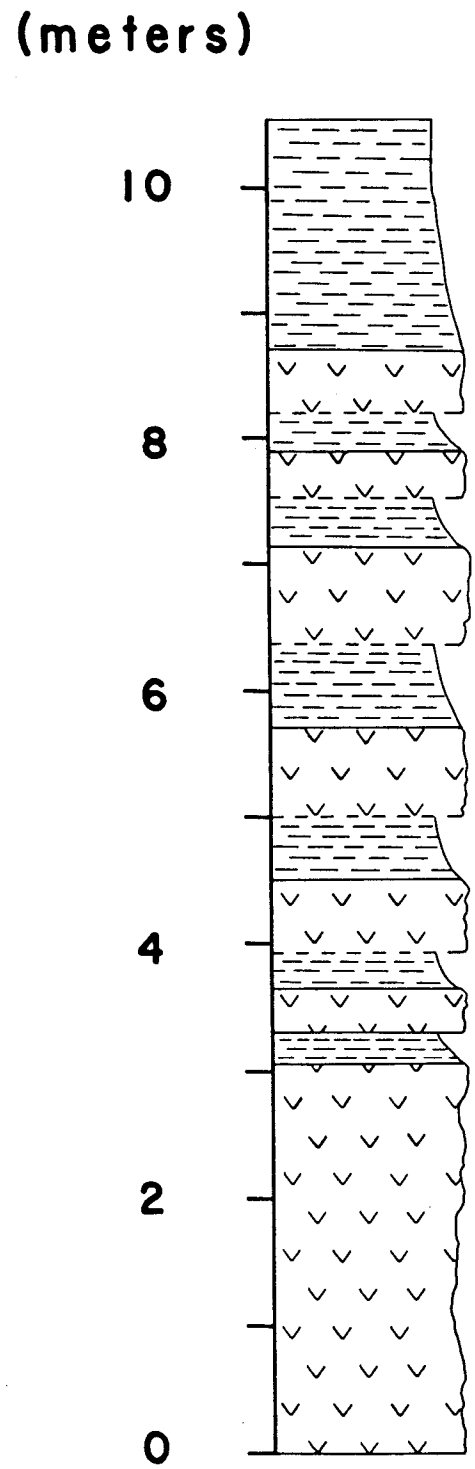

Figure 2-12: Measured section of alternating shale and tuff beds at locality 26. The volcanics are represented by V's and the shales are diagrammed by a horizontal dashed pattern. Gradational contacts are shown by a dashed line, while the sharp contacts have a solid line.

Figure 2-13: Photo of alternating shale and tuff beds. Field notebook lies on volcanic tuff section. Shales are black and thinly bedded.

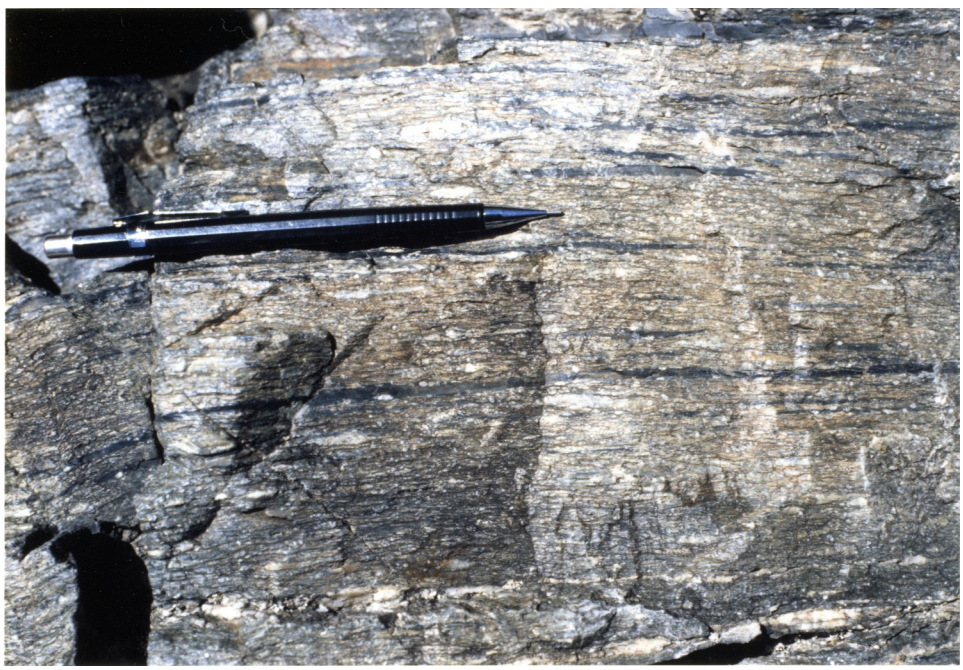

Figure 2-14: Close-up photo of volcanic tuff section just above the field notebook. Grains appear highly flattened parallel to bedding and include thin stringers of shale.

which is in turn overlain by greenish, rusty-weathering, thinly-bedded volcanic rocks. The volcanics are associated with a prominent reddish soil horizon. At site 136, shale beds overlie volcanic beds. The intersection of Taylor Creek Road with the highway at site 139 exposes blocks of shale, tuff breccia, and altered tuff breccia. Site 140 has blocks of tuff breccia that appear to be large, isolated blocks surrounded by uniformly-bedded shales.

Additional manifestations of Galice shale interbedded with tuffs are: (1) east of the Rogue-Galice contact at Almeda mine, a zone of tuffs and shales interbedded on the scale of a few centimeters crops out over a distance of a few meters (G. Harper, personal communication, 1987) (*see* Section 2.6.2), and (2) at Reuben Station near Cow Creek, just north of the study area, Galice shales are reported to be interbedded with volcanics (Taliaferro, 1942, p. 83). In the study area, these interbedded flows and tuffs appear to be a local feature which are not continuous or correlatable from outcrop to outcrop.

At this point, the enigmatic question is whether or not these volcanic rocks (Ji on Plate 1) should be classified as Rogue volcanics (implying a proximal arc source, or intercalation by multiple fault or fold contacts), or as a Galice "member". The preferred hypothesis is the latter, as these volcanics are interpreted to be the result of sporadic, contemporaneous submarine volcanism, deposited during quiescent deposition of black shales. An example of the presence of mudstone interbedded with volcaniclastic turbidites and tuff is documented at DSDP site 459B on the upper slope of the Mariana forearc (Lundberg and Moore, 1986), which indicates that this pattern can be found today in faulted basins (*see also* Mitchell, 1970).

In the past, Wells and Walker (1953) distinguished the Rogue Formation volcanics from the extensive band of volcanic rocks that crop out east of the type Rogue section by differentiating a Galice volcanic member (in this report indicated as Rogue Jvt on Plate 1). The interpretation by Wells and Walker (1953) was revised when Wells and

Peck (1961) combined the volcanic rocks from both formations under one heading. Page and others (1977) mapped the Wimer Quadrangle (just NE of the study area) according to lithology only, and did not describe the units in terms of the Rogue or Galice Formations.

2.6.2 Rogue-Galice Contact

The nature of the Rogue-Galice contact is significant in that it helps to delineate the nature of basin closure during the late Jurassic. Generally, both formations on a gross scale strike N to NE and dip steeply to the southeast at the type locality. The Galice structurally lies above the Rogue, and there exists evidence that this contact is a possible depositional contact faulted parallel to or nearly parallel to bedding.

Opinions that have stated that this contact is depositional include Garcia (1979), Harper et al. (1986), and Miller and Saleeby (1987). These authors have maintained that the contact is depositional, but they have not cited any direct evidence in these publications. Rather, regional and age relationships are used as justifications for these units sharing a depositional contact (Harper, personal communication, 1987). Other workers have stated that this contact is in "apparent conformity" (Baldwin, 1969), or that it is "approximately conformable" (Ramp and Peterson, 1979), although the latter authors note that Diller (1914) found evidence of Cenozoic movement along the contact. Diller (1914, p. 98-101) reported finding gravel terraces overlying Galice shale at the Rogue-Galice contact. The gravels and basement shales had been offset 9-12 meters by two parallel faults ($280^{o}/72^{o}$ SW) at Old Channel Mine in Rich Gulch.

Reports published by the U. S. Geological Survey since 1914 have supported the claim that the Rogue-Galice contact is a fault. Diller (1914) proposed that this contact is a fault that could be traced for over 32 km from Briggs Creek valley to Cow Creek at Reuben Spur. He acknowledged that the contact was irregular in the vicinity of the ore bodies. Diller (1914, p. 74) noted that faults are common in the Galice shales near

Almeda mine and he found two parallel faults ($015^{o}/50^{o}$ NW) that displaced a dike within the shales 1.2 meters to the northwest. Winchell (1914) and Shenon (1933) deduced that numerous faults cut the ore at Almeda mine while later, northwest-trending faults offset the ore bodies.

Examination of vertical cross-sections and plan view maps of the numerous portals and shafts of the Almeda mine reveals a complex set of cross-cutting faults (*e.g.*, vertical sections drawn by A. B. Yates in 1932, Figure 10 of Libbey, 1967). The lithologies encountered by the mining engineers are described as greenstone; altered and brecciated dacite or quartz porphyry with barite, calcite, and pyrite; red shale; slate; massive pyrite bands; altered shear zones; and fault gouge on the order of a meter or more wide (Libbey, 1967).

A plan view map of the exposed rocks along the Rogue River south of the mine entrance is diagrammed in Figure 2-15. This plan view map was drawn by C. F. Herbert in 1953 (Figure 20 of Libbey, 1967), and establishes that the Rogue-Galice contact is not sharp, but exhibits numerous small faults, sections of sheared-up rock, and covered sections. An extensive gossan up to 4.6 meters deep (Diller, 1914, p. 75) at the mine stains the rocks in the covered sections, and the rocks are yellowish-brown due to the presence of limonite.

No depositional contact was identified at Almeda mine during field work in 1985. It was concluded, after chipping away on the exposed stained rock along this section, and after repeated searches, that the contact was either a fault, or else that it was too concealed to assume that it was a depositional contact. Sheared rock was found on the order of a few meters, which suggests movement along and near this boundary did occur. Based on field work of 1985, Herbert's plan view map appears to be accurately drawn.

Harper (personal communication, 1987), along with Jim Wright, found a zone of interbedded tuffs and shales east of the contact at the Almeda mine during

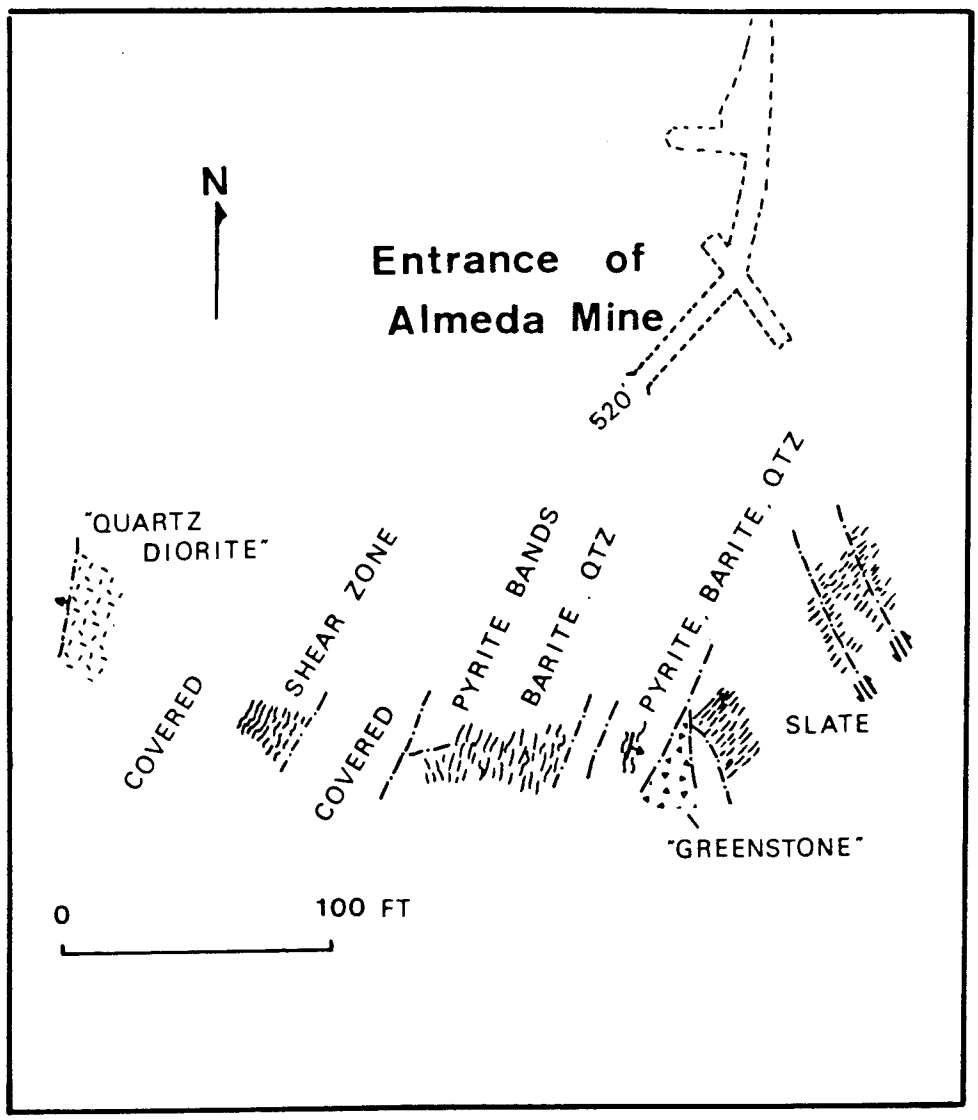

Figure 2-15: Plan view map of the exposed sections along the Rogue River just south of the Almeda Mine entrance (520' level), as drawn by C.F. Herbert in 1953 and later reported by Libbey (Figure 20, 1967).

reconnaissance work in summer, 1986. They found the tuffs and shales to be interbedded on the scale of a few centimeters, in a section that extended over many meters. The presence of interbedded tuffs and shales is not necessarily *prima facie* evidence of a depositional contact, as over 1 km of exposed outcrop north and west of the Indian Mary Campground shows interbedded tuffs, shales, and flows. It does, however, point to the fact that sporadic volcanism is recorded in the shales near the contact, and that the Rogue-Galice contact is obscure.

Other sites that show the contact between the Rogue volcanics and Galice shales were found in the study area by the author during field work of 1985. First, the Rogue-Galice contact at Grave Creek was presumed to be a high-angle fault because of the fact that the volcanics at station 45 were too poor to take any readings for 50-80 meters, yet this outcrop was sandwiched between bedded volcanics (locality 44) and uniformly bedded shales with good cleavage (station 46). Additionally, the beds dip steeply to the southeast on either side of this contact, as shown on the cross-section (*see* Figure 3-9[b]). A second locality was found just east of the Galice-Rogue contact at station 66, where it was noted that an outcrop of shales along a logging road showed "Almeda mine appearance" in that the shales were bedded yet strongly altered, warped, and had a very prominent brownish-red weathering overprint. This section is about 10 meters wide. A third locality that showed "Almeda mine appearance" was found in the shales at station 108. These shales had a thick, brownish-red alteration that was not limited to the exposed, weathered part of the rocks, but penetrated the entire rock. Thus, a sharp contact was not identified at these three sites; rather, only altered shales were found that had a similar appearance to the gossan found at Almeda mine.

Diller and Kay (1924) described the volcanic rocks along the Rogue-Galice contact as "profoundly sheared" such that schistose textures were produced. Taliaferro (1942) found "sheared rhyolite agglomerates" at the Rogue-Galice contact along Cow Creek (north of study area). Dole and Baldwin (1947), in reconnaissance work north of

Almeda mine, concluded that mineralization was not continuous along the fault contact. They found independent shear zones located in an "en-echelon arrangement."

Near the Grave Creek bridge, M. A. Kays (1968) documented what he thought was "cataclasized augen gneiss" derived from the shearing of metavolcanic rocks. Kays (1968) found other evidence of a shear zone when he examined the Rogue-Galice contact along the North Fork of Galice Creek (just southwest of the study area). There he found mylonitized blocks of sheared serpentinite, as well as isoclinally folded Galice mudstone close to the fault contact. These folds, according to Kays (1968), appeared to show a decrease in fold amplitude eastward of the contact. He postulated that the Galice shales had been plastically deformed aginst this contact.

Some serpentinite slivers along the Rogue-Galice contact in the vicinity of the North Fork of Galice Creek are shown on the map by Wells and Walker (1953). The serpentinite bodies must have come up from depth along a fault zone. Wells and Walker (1953) draw the Rogue-Galice contact on their map as a depositional boundary, yet in their report they suggest that the contact has angular discordances, as they state:

> "The Galice Formation lies to the east of the Rogue Formation...(and) is intensely folded along this contact and in places intersects the line of contact at a small angle, though elsewhere it is parallel..."

The most definitive report to date on the Rogue-Galice contact was written by P. E. Hotz (1971). He sampled four localities along the contact for major and trace element analysis. He unequivocally stated in his report that the Rogue-Galice contact is a fault (p. 64 of Hotz, 1971). His map on page 65 shows this fault contact along the creeks south of Almeda mine, at the mine, and north of the mine, as shown in Figure 2-16.

2.6.3 Mineralized Zone

The mineralized belt in the Galice district was referred to as the "Big Yank" zone by Diller (1914). This zone, according to Diller (1914), is approximately 8 km wide and 32 km long, trending north-northeast parallel to the regional strike of the strata. An

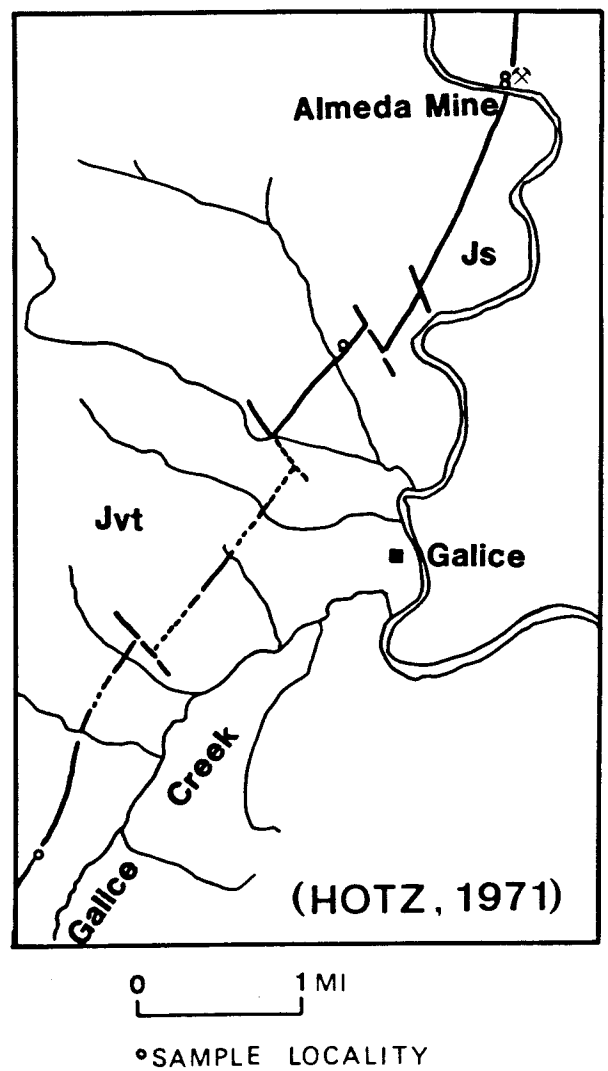

Figure 2-16: Map of four sample localities along the boundary between the Rogue and Galice Formations from Hotz (1971). These samples were analyzed for major and trace element distribution by the U.S.G.S. The Rogue-Galice contact is shown as a fault on this map in the Galice vicinity, and is stated as such in the report.

extensive gossan was exposed at the town of Galice (Libbey, 1967) and at the Almeda mine. This mineralized belt includes stratiform disseminated and massive sulfides along the contact and in the volcanic rocks of the Rogue Formation (Ramp and Peterson, 1979). The gold deposits throughout this area are localized along well-defined shear zones (Hotz, 1971) that have intrusions as well as secondary replacement and deposition of hydrothermal vein mineral assemblages. Gold is usually found associated with quartz, and the most productive gold-bearing veins trend east-west with high dips (Diller and Kay, 1924).

The significance of this mineralized belt or zone is that many major ore deposits have been shown to be related to lineaments that trace out major disturbance zones (*e.g.*, O'Driscoll, 1986). This gossan was probably produced as a result of sea-floor hydrothermal alteration, or perhaps later alteration, along this zone of disturbance. Additionally, the presence of northeast-trending sill-like intrusions and dikes points to the fact that this belt was a zone of weakness. Dike trends have been found to be better guides than fault trends in giving the directions of minimum stress, since fractures can also develop during emplacement (for example, Oman back-arc basin, Pearce et al., 1981). The Galice mineralized belt appears to verify these generalizations in the following ways: (1) the ore bodies are aligned parallel to the regional strike of the high-angle fault that separates the Galice from the Rogue, (2) internal shearing within these two formations is evident and suggests a fairly wide zone of disturbance, (3) the dike trends are approximately parallel to the fault contact, to the strike of the beds, and to the overall trend of Nevadan fold axes (presented in Chapter 3).

CHAPTER 3: NEVADAN DEFORMATION AND STRUCTURAL STYLES

3.1 Nevadan Orogeny

Early geologists, such as Whitney (1879), established that rocks of the Sierra Nevada were folded at the close of the Jurassic. This led Blackwelder (1914) to propose the term "Nevadan" for folds that appeared to him to extend from the west coast of North America to South America. Goranson (1924), in his studies of the Mariposa Formation of the Sierra Nevada, concluded that the Nevadan orogeny began in middle Jurassic and culminated in late Jurassic with batholithic intrusions in British Columbia and the Sierra Nevada. Later studies of the Mariposa showed it to be lithologically and faunally similar to the Galice (Taliaferro, 1942; Lanphere *et al.*, 1968) and that both areas were deformed by the Nevadan orogeny. Bateman and Clark (1974) redefined the Nevadan orogeny as a short-lived, intense deformation of Late Jurassic age.

The Nevadan deformation is characterized by the presence of tight to isoclinal folds, overturned beds, thrust faulting, slaty cleavage development in argillaceous strata, and prehnite-pumpellyite to lower greenschist facies metamorphism in Galice slates (Taliaferro, 1942; Kays, 1968; Saleeby *et al.*, 1982). An approximate timing for the Nevadan orogeny at 150 Ma is delineated by Saleeby and others (1982). Post-Nevadan deformation is characterized by open folding, kinking, and possible high-angle faulting (Saleeby *et al.*, 1982). Other possible post-Nevadan structures are epithermal veins (Kays, 1967). The youngest plutons in the Klamaths (Russian Peak, Deadman Peak, Caribou Mountain, Horseshoe Lake, and Shasta Bally) range in age from 140-127 Ma, and are associated with significant gold mineralization deposits (Lanphere *et al.*, 1968).

Wright and Miller (1986) document that the duration of Jurassic orogenesis along the Klamath continental margin was approximately 20 Ma. Examination of cross-cutting relationships and the results of isotopic geochronology show that this period of

orogenesis consisted of a pre-Nevadan (ca 168 Ma) compressive event, an intervening period of extension from 164-157 Ma, and a second compressive event (Nevadan orogeny) from 151-147 Ma (Wright and Miller, 1986).

These compressive events are inferred to have occurred in an active arc setting, above an eastward-dipping subduction zone. Mortimer (1986) believes the mid-Jurassic (ca 168 Ma) compressive deformation is the product of a collision between a western and an eastern belt. This period is characterized by pluton emplacement (169-160 Ma), a regional cleavage development, and greenschist- to amphibolite-grade metamorphism in east-central Nevada (Wright and Miller, 1986). Within the Klamath Mountains, the mid-Jurassic deformation is inferred from: (1) K-Ar ages (168-177 Ma) of the Hayfork Bally Meta-andesite, (Fahan, 1982), the age of regional metamorphism; and (2) U/Pb zircon ages of the Ironside Mountain Batholith (170 Ma) and the Wooley Creek Batholith (160-162 Ma), two plutons that cross-cut the thrust that separates the western Hayfork terrane from the Rattlesnake Creek terrane (Fahan and Wright, 1983; Wright and Miller, 1986; Wright and Fahan,1988, in press).

During the intervening extension period, rifting of the continental margin occurred, such that a small ocean basin opened. This ocean basin is represented by a belt of ophiolites that includes the Smartville, Josephine, and Coast Range ophiolites (Harper *et al.*, 1983, 1985). Dike swarms intruded older rocks flanking these ophiolites.

The Nevadan orogeny (151-147 Ma) is postulated to have been a dominantly westward-directed thrusting event (Davis, 1966; Snoke, 1977; Gray, 1983), or a dominantly strike-slip event (Saleeby, 1981). A schematic plate tectonic model that accounts for both of these components before deformation is shown in Figure 3-1.

This cycle, or coupling between extension and shortening, is a commonly recognized feature of other orogenies. The oceanic crust that develops during extension often floors a sedimentary basin which is subsequently shortened and uplifted during collision (Etheridge, 1986). In addition, the basin may act as a favorable site for ore deposits

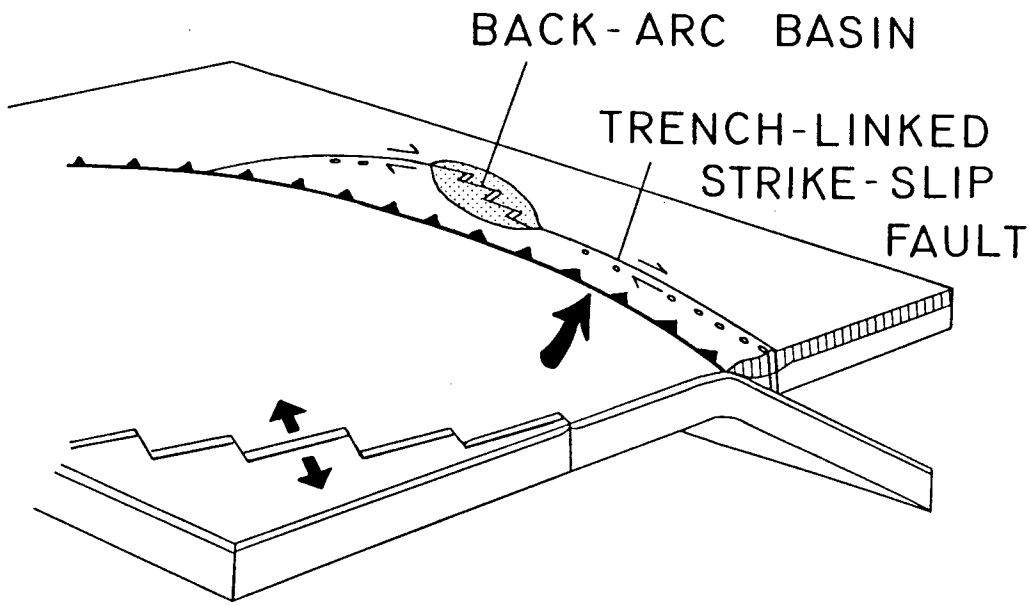

Figure 3-1: Schematic plate tectonic model that incorporates both convergent and strike-slip components in a back-arc setting. This model may be applicable to the late Jurassic back-arc basin of the western Klamath Mountains. From Woodcock (1986).

because of many factors that provide an ideal environment for mineral deposition. These factors include: (1) a highly-faulted oceanic crust that exists during back-arc spreading provides fault-bounded troughs, (2) low Eh values, and (3) restricted seawater circulation (Tarney and Windley, 1981).

Theoretical models proposed to account for the Nevadan orogeny involve either: (1) a collision of two arcs, (2) an intra-arc deformation, or (3) a volcanic arc emplaced by transform-related strike-slip movement. Schweickert and Cowan (1975) and Schweickert et al. (1984) conclude that the features produced by the Nevadan orogeny in the Sierra Nevada are the result of a collsion between an island arc (western side) and an andean-type arc (eastern side) along the continental margin of North America. Other models, such as the one offered by Harper and Wright (1984), state that the Nevadan orogeny was the result of intra-arc deformation due to the closure of a back-arc basin by imbrication of the arc, back-arc, and remnant arc. The third hypothetical model suggests that Nevadan structures were produced by strike-slip transport of a Jurassic arc fragment into the Sierra region, while later, early-Cretaceous regional extension by batholithic emplacement accounts for the tilting of beds and the development of tectonite fabrics (Tobisch and others, 1986).

The duration of the Nevadan orogeny is well-constrained by isotopic dating. Emplacement of the Josephine ophiolite was accomplished by widespread intrusion of calc-alkaline dikes, sills, and small plutons into the Josephine ophiolite and the overlying Galice Formation. The maximum age of Nevadan metamorphism and thrusting is 162 ± 1 Ma, determined by Pb/U zircon ages from the Josephine ophiolite (Saleeby, 1987, cited in Wyld and Wright, 1988), 157 ± 2 Ma for the Rogue Formation (Saleeby, 1984), and the assignment of *Buchia concentrica* (Sowerby) to the late middle Oxfordian to middle Kimmeridgian (Imlay, 1980). Dacitic dikes that cut both the Rogue and Galice are 150 ± 2 Ma (Saleeby, 1984). The minimum ages of Nevadan metamorphism are 150 ± 2 Ma and 146 ± 4 Ma, two Pb/U zircon ages from the Summit Valley and Pony Peak

plutons, respectively, which cut the thrust that places the Rattlesnake Creek terrane over the Galice Formation (Harper *et al.*, 1986).

A major effect of the Nevadan orogeny was easterly underthrusting of an assembled late Jurassic-age mafic-ultramafic terrane and overlying flysch along the Preston Peak fault (Hill, 1983). The Preston Peak fault has been renamed the Orleans fault by Jachens et al. (1986) as it includes other faults that also mark the base of the Western Paleozoic and Triassic belt where they are in fault contact with the Western Jurassic belt. The Orleans fault (see Figure 1-1) has been shown to be a thrust fault with a minimum throw of 40 km, based on gravity studies that indicate continuous outcrop (subsurface structure) of Western Jurassic belt rocks 40 km east of the fault (Jachens *et al.*, 1986). Use of gravity modeling and known density contrasts between sediments and ultramafic rocks gives 60 km additional offset, which suggests that the Orleans fault has had at least 100 km offset in an east-west direction, or a 40% shortening across the Klamath Mountains (Jachens *et al.*, 1986).

In the Klamath Mountains, the Galice Formation is considered the youngest formation involved in the Nevadan orogeny (Lanphere *et al.*, 1968). The Galice Formation represents sediments derived from a volcanic arc, the uplifted continental margin, and nonvolcanic material from the Western Paleozoic and Triassic belt (Saleeby *et al.*, 1982). These sediments were most probably deposited in a submarine fan complex due to their sedimentary structures indicating deposition by turbidity currents (Chapter 4). The type Galice was isoclinally folded and overturned to the northwest during the Nevadan orogeny, which will be described in the following section.

3.2 Descriptions of Structures

3.2.1 Folds

The Nevadan orogeny is manifested in the study area by tight to isoclinal folding and the development of a strong, axial planar cleavage. Broadly speaking, the Nevadan folds trend northeast with axial planes that dip steeply to the southeast. Post-Nevadan folds appear to be folds that trend NW-SE which warp the hingelines of F_1 folds (see Sections 3.3.1[ii] and 3.3.2). The difference between Nevadan and post-Nevadan folds is whether or not cleavage has been refolded or deformed.

Examples of Nevadan fold hinges are found at places where cleavage is normal to bedding. At station 118, a small-scale Nevadan fold is cut by axial planar cleavage, in beds of silty shale and greywacke (Figure 3-2). Another excellent example is located at the point bar along the Rogue River, northwest of station 21, where cleavage is approximately normal to bedding.

A second illustration of Nevadan folding occurs at station 121. At this locality, two fold limbs are truncated such that they are thought to represent Nevadan isoclinal folds that later experienced shear along adjacent fold limbs. Original bedding of the shales can be clearly seen, and graded beds give the younging direction as shown by the arrows in Figure 3-3. The direction of younging for both presumed isoclinal fold limbs is consistent with the hypothesis that these truncated fold limbs were originally isoclinal folds later sheared parallel to the pencil direction. Slight thickening in the hinge zone of these fold limbs is also apparent.

A larger-scale fold is found in folded layers of dark green volcanic tuff and porphyritic basalt at locality 80. The basalt has weathered to a buff-colored rock, and the volcanic tuff shows epidote alteration and dissection by numerous calcite veins. A photo of this fold (Figure 3-4) was taken looking NE (063^{o}). In all probability, this fold

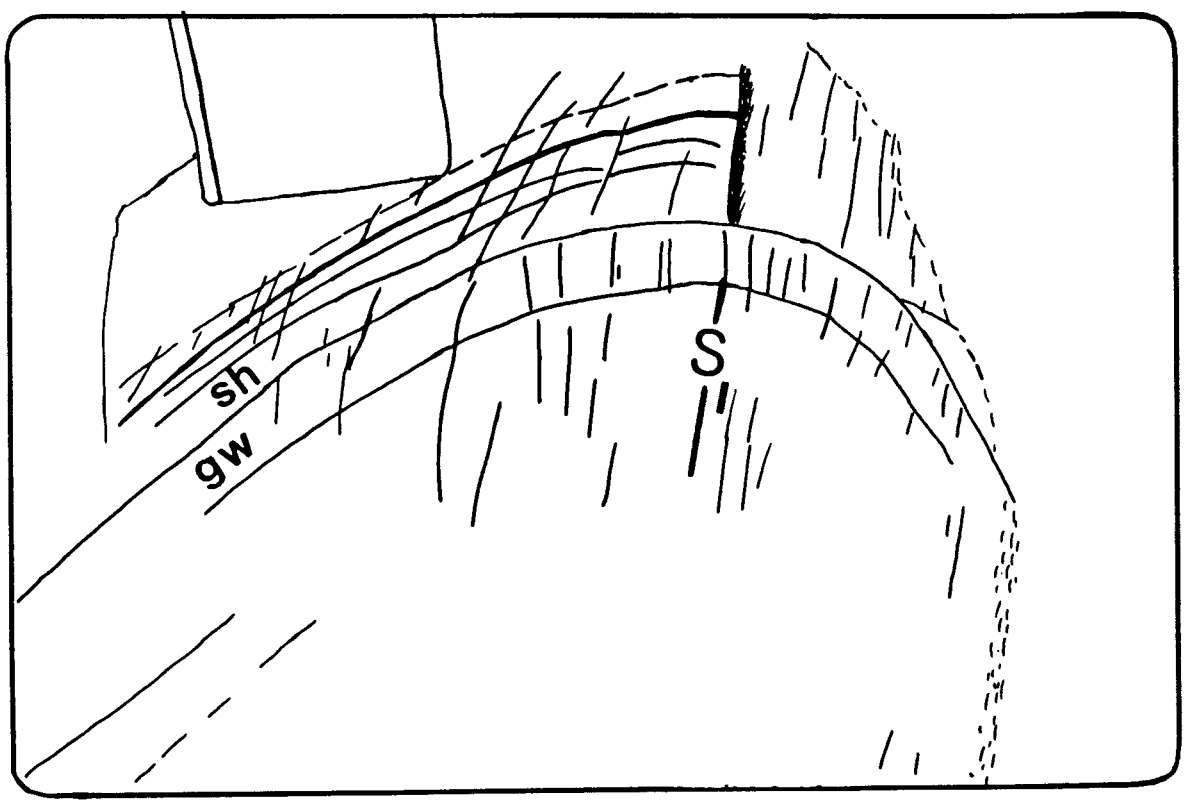

Figure 3-2: Photo and sketch of a small Nevadan fold cut by axial planar cleavage from locality 118. The beds consist of silty shale and greywacke. The lower edge of the field notebook is 12 cm.

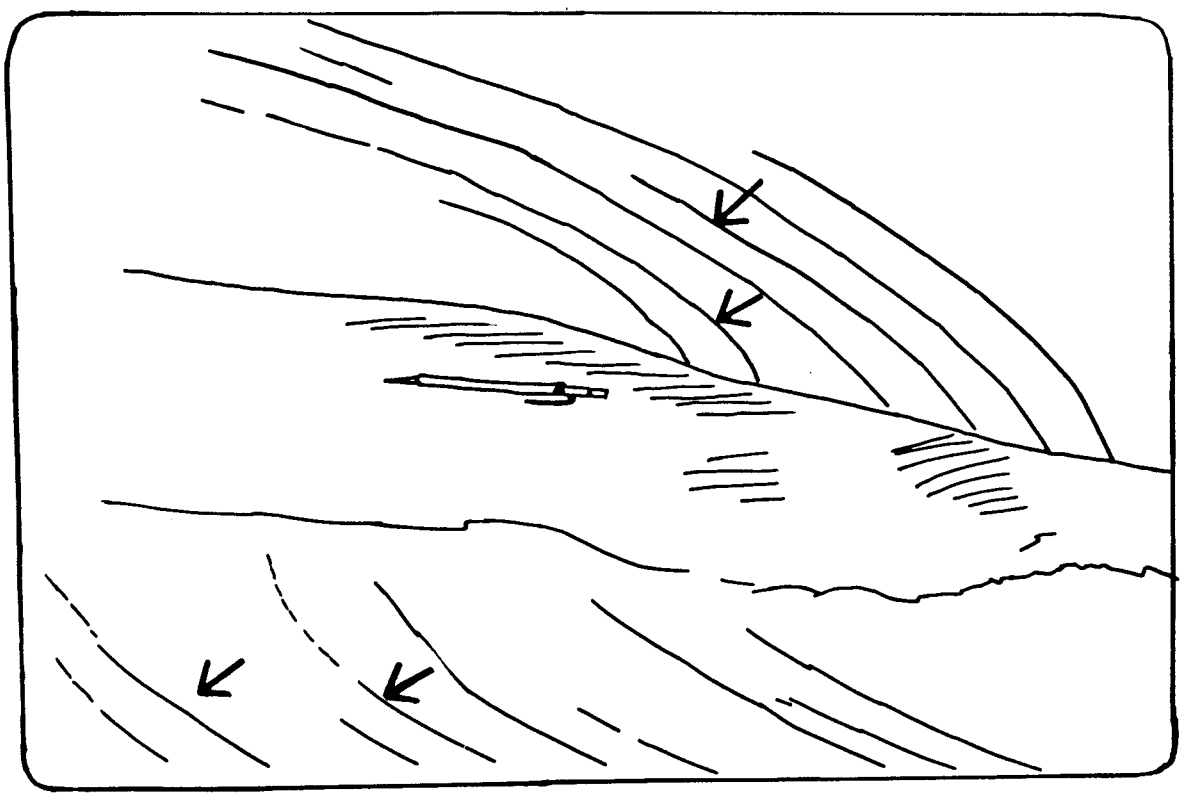

Figure 3-3: Photo and sketch of truncated fold limbs of a possible isoclinal Nevadan fold that later experienced shear along the fold limbs. Younging direction of the two presumed fold limbs is indicated by the arrows in the lower sketch. Photo taken looking down on a flat surface. The trace of cleavage is seen parallel to the pencil direction in the upper fold and in the section between the truncated fold limbs. Locality 121 along Grave Creek.

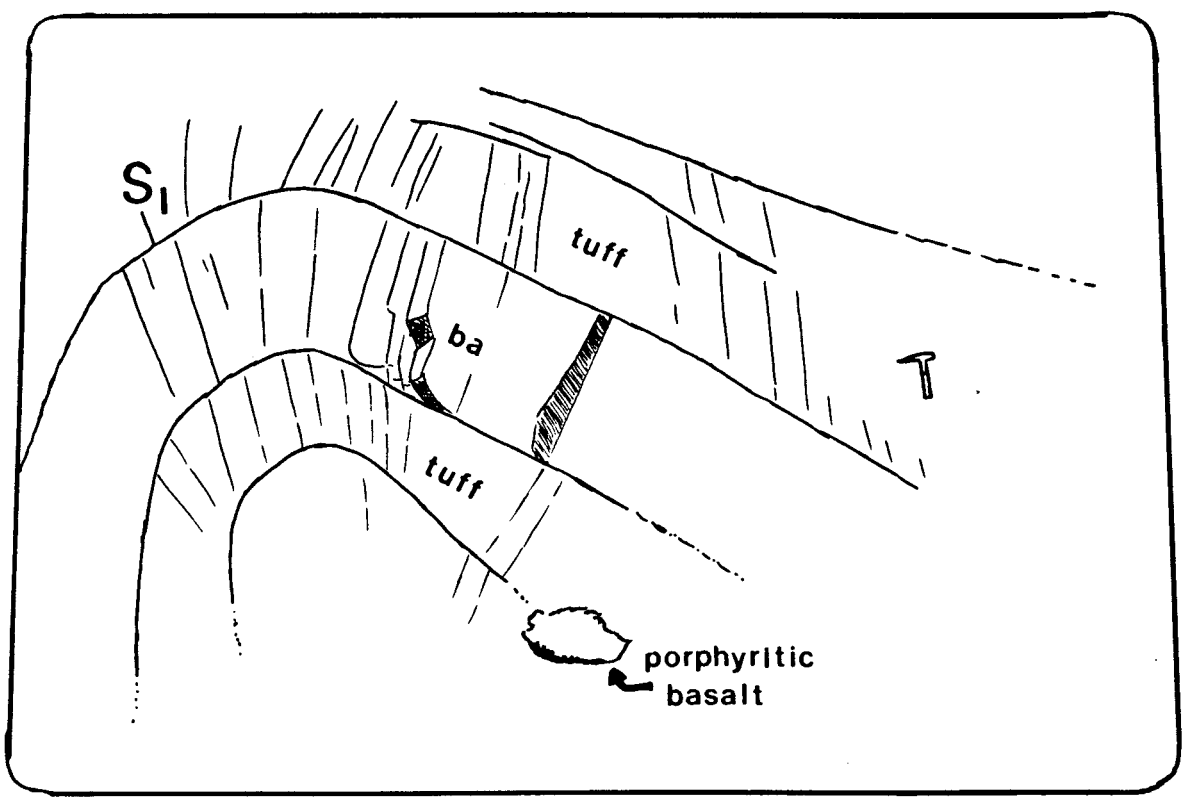

Figure 3-4: Photo and sketch of an asymmetric fold of dark volcanic tuff and lighter-colored, weathered porphyritic basalt, both ascribed to the Rogue Formation. A close inspection of the above photo reveals a regular, spaced cleavage, S_1, in both units that is roughly parallel to the axial plane of the fold and is diffracted at the lithologic boundaries.

is Nevadan as it is asymmetric, overturned to the NW, and has a regular spaced cleavage roughly parallel to the axial plane of this fold.

A post-Nevadan fold of Galice shale beds from locality 18 is shown in Figure 3-5. This fold is classified as post-Nevadan because of two factors: (1) a crenulation lineation is observed at the hinge zone crest, with a trend of 354^{o}, assumed to be produced by later folding of the Nevadan cleavage, and (2) the bedding-cleavage intersection lineation from this site trends 116^{o} with a 27^{o} easterly plunge, which falls close to the F_3 axial plane (*see* Figure 3-22).

In map view, the Nevadan and post-Nevadan folds have variously trending and plunging fold axes, depending on the direction of observation made along a fold axis (*e.g.*, Figure 4.9 of Hobbs *et al.*, 1976). This pattern of non-uniform trending and plunging fold axes was produced by the imposition of post-Nevadan folds onto asymmetric Nevadan folds, such that it warped the previously formed fold hinges. Examination of structural profiles made at two localities will make this relationship more clear. First, the folds at the town of Galice are described, followed by a discussion of the folding relationships seen along Grave Creek.

3.2.1[i] Galice Type Section

An example of the multiplicity of fold attitudes is observed at the type Galice section, Figure 3-6. On this map, a half-mile section of water-polished Galice shales and greywackes was measured and studied. The fold axes' trend and plunge were calculated by the intersection of bedding and cleavage planes. This intersection gives a point that describes a line parallel to the trend and plunge of the fold axis at that location. Four out of six calculated fold axes from this area show a northeasterly trend and plunges of 31-70^{o} SE. The other two fold axes have these orientations: (1) trend of 163^{o} and a plunge of 20^{o} SE (station 10), and (2) trend of 216^{o} with a 43^{o} SW plunge (station 15).

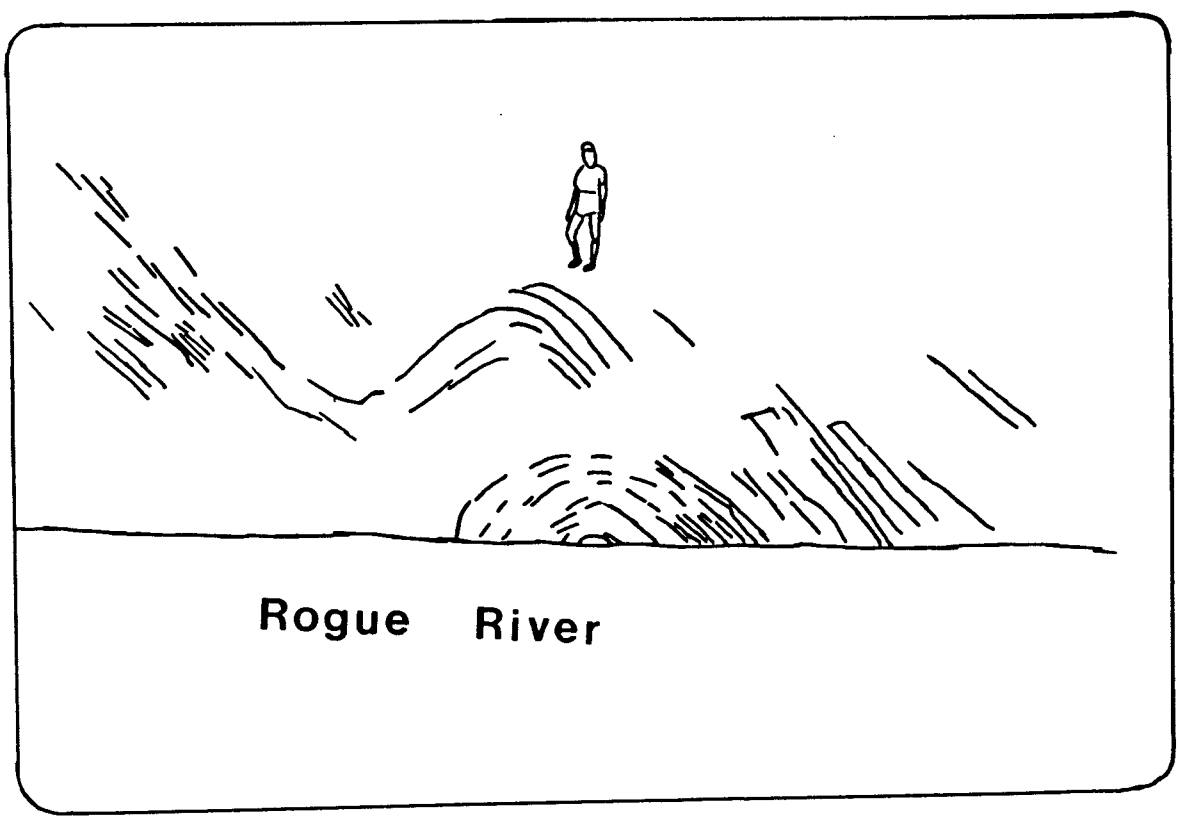

Figure 3-5: Photo and sketch of a post-Nevadan (F_3) fold from locality 18. Photo taken from raft looking NE. Bedding-cleavage intersection lineation from this locality is plotted in Figure 3-22 along with the F_1, F_2, and F_3 fold axes.

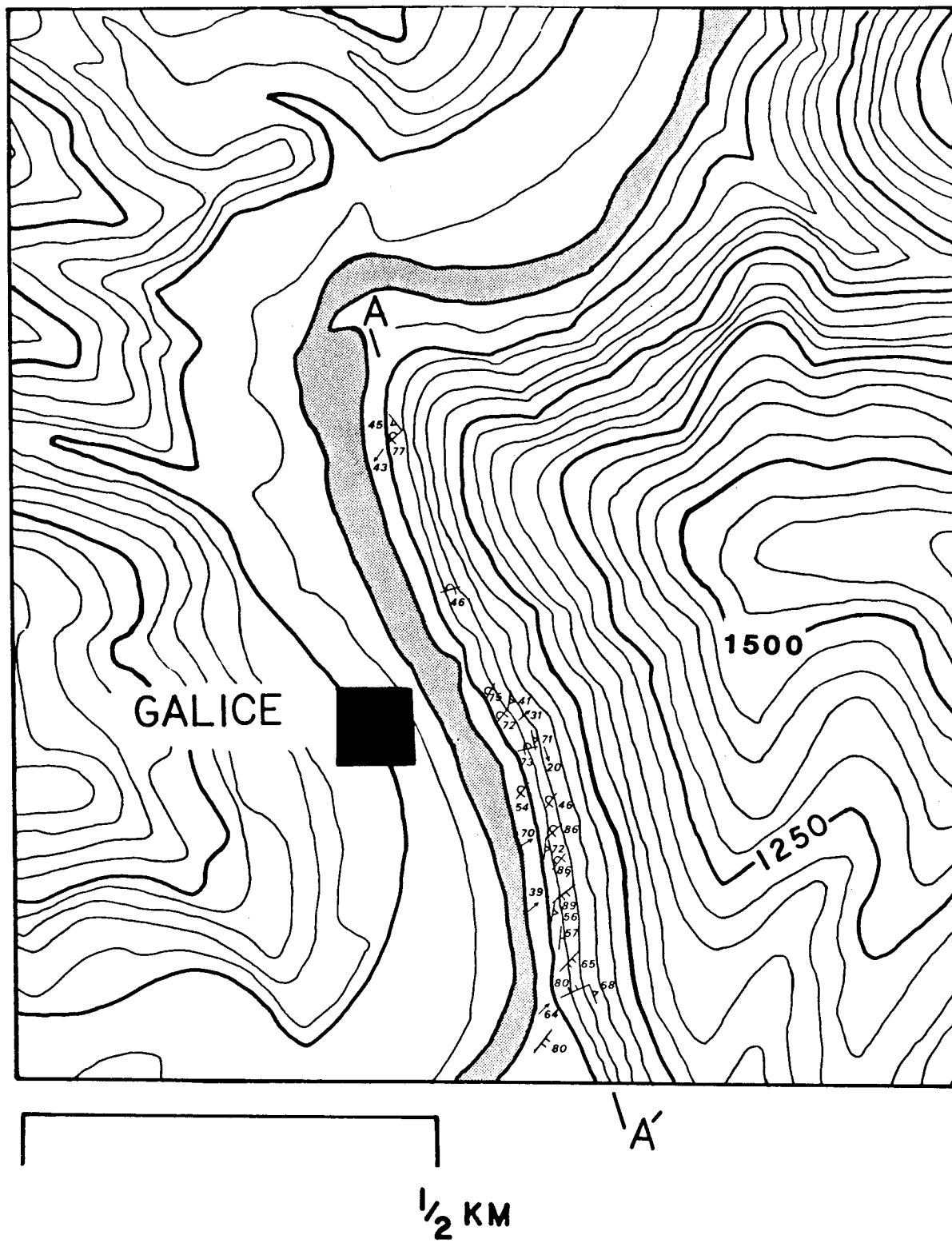

Figure 3-6: Map of the Galice vicinity showing bedding, cleavage, and calculated fold axes measurements (S_0 x S_1) on Galice flysch in the type section. Light grey stippled pattern represents the Rogue River. Area of cross section A-A' (Figure 3-7) shown.

A structural profile constructed from A to A' (Figure 3-7) uncovers a Nevadan fold overturned to the northwest that is on the order of 1/4 km across. Younging indicators are diagrammed above the profile, based on graded beds. Heavy lines that signify the apparent cleavage traces in this profile are also shown, and two sets of cleavage orientations are apparent. In all probability, a much larger overturned fold occurs to the NW, of which we see one overturned limb in this profile.

3.2.1[ii] Grave Creek Section

Fold axes with variously trending and plunging attitudes can be found along Grave Creek. The vergence of the folds alternates in a systematic way, such that they change from northeast to southwest, as can be seen in Figure 3-8 which shows a map of this area (*see also* Figure 3-20, Section 3.3.2). The proposed F_3 folds trending NW-SE (approximately $300^0/120^0$) would account for the dispersal of the fold axes in this manner, and the trend of F_3 is diagrammed on this map.

A structural profile cross-section B to B' (Figure 3-9) was drawn normal to the regional strike of bedding for beds along Grave Creek. This cross-section shows many tight to isoclinal folds, and one apparent isoclinal fold has been faulted out in the hinge region. The apparent Nevadan cleavage (S_1) is diagrammed by heavy lines, and younging indicators determined from graded greywacke beds are indicated. A northeast-trending dike cuts through the shales parallel to the contact.

3.2.2 Cleavage

The Galice Formation consistently shows a strong, axial planar cleavage development in shale, and a poorly-developed, local spaced cleavage in greywacke. The cleavage is assumed to be axial planar to macroscopic Nevadan folds, since it appears parallel to subparallel to the axial planes of mesoscopic folds seen in outcrop. It is generally accepted that cleavage is perpendicular or approximately perpendicular to the direction

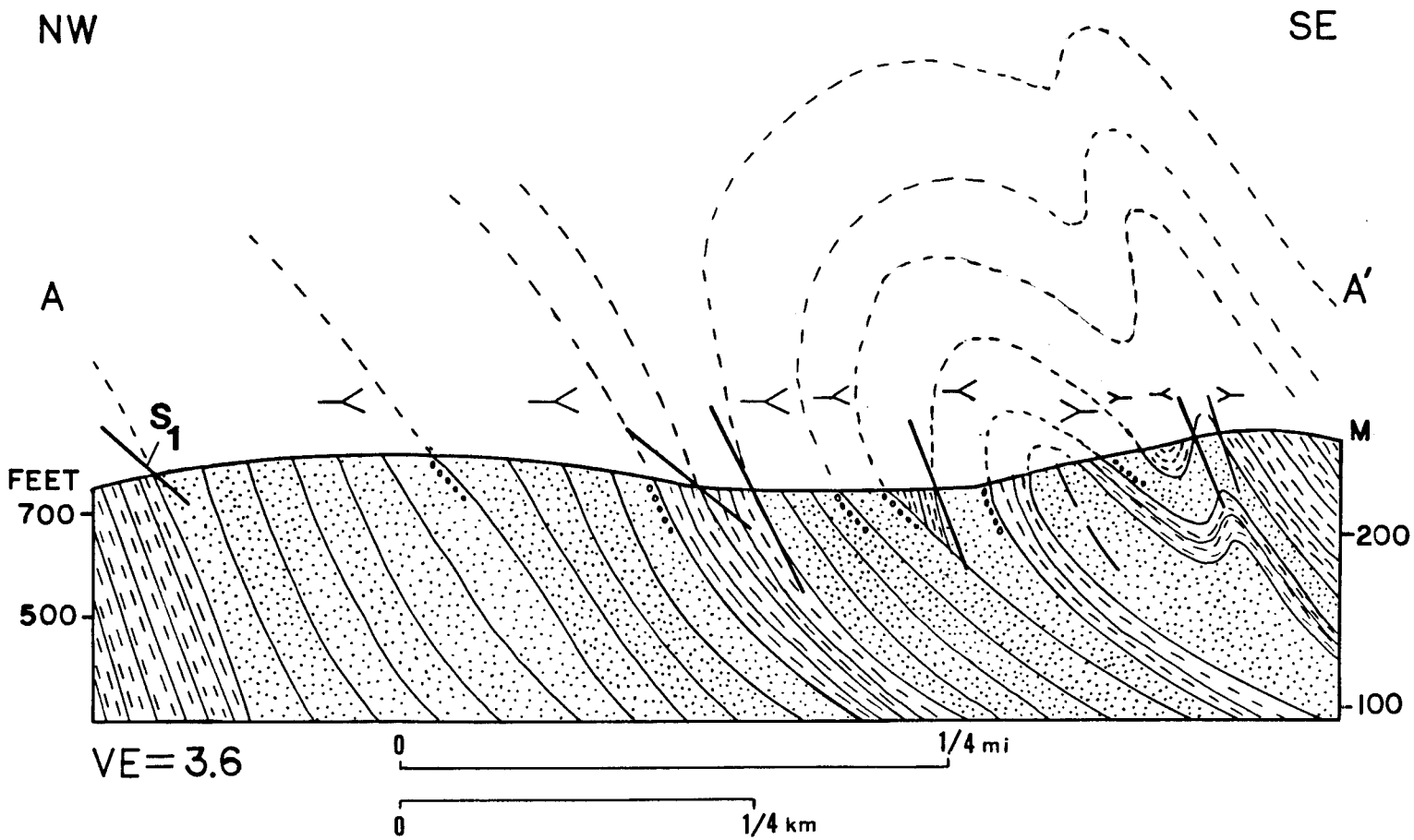

Figure 3-7: Structural profile A-A' from Galice vicinity reveals a Nevadan fold overturned to the northwest. Younging indicators determined from graded bedding.

Figure 3-8: Map of the Grave Creek vicinity showing bedding, cleavage, and the calculated Nevadan fold axes' (S_0 x S_1) measurements of Galice shales. Approximate trend of F_3 fold axis located for reference. Jvt=Rogue Formation, Js=Galice Formation, and hd=hornblende diorite porphyry dike.

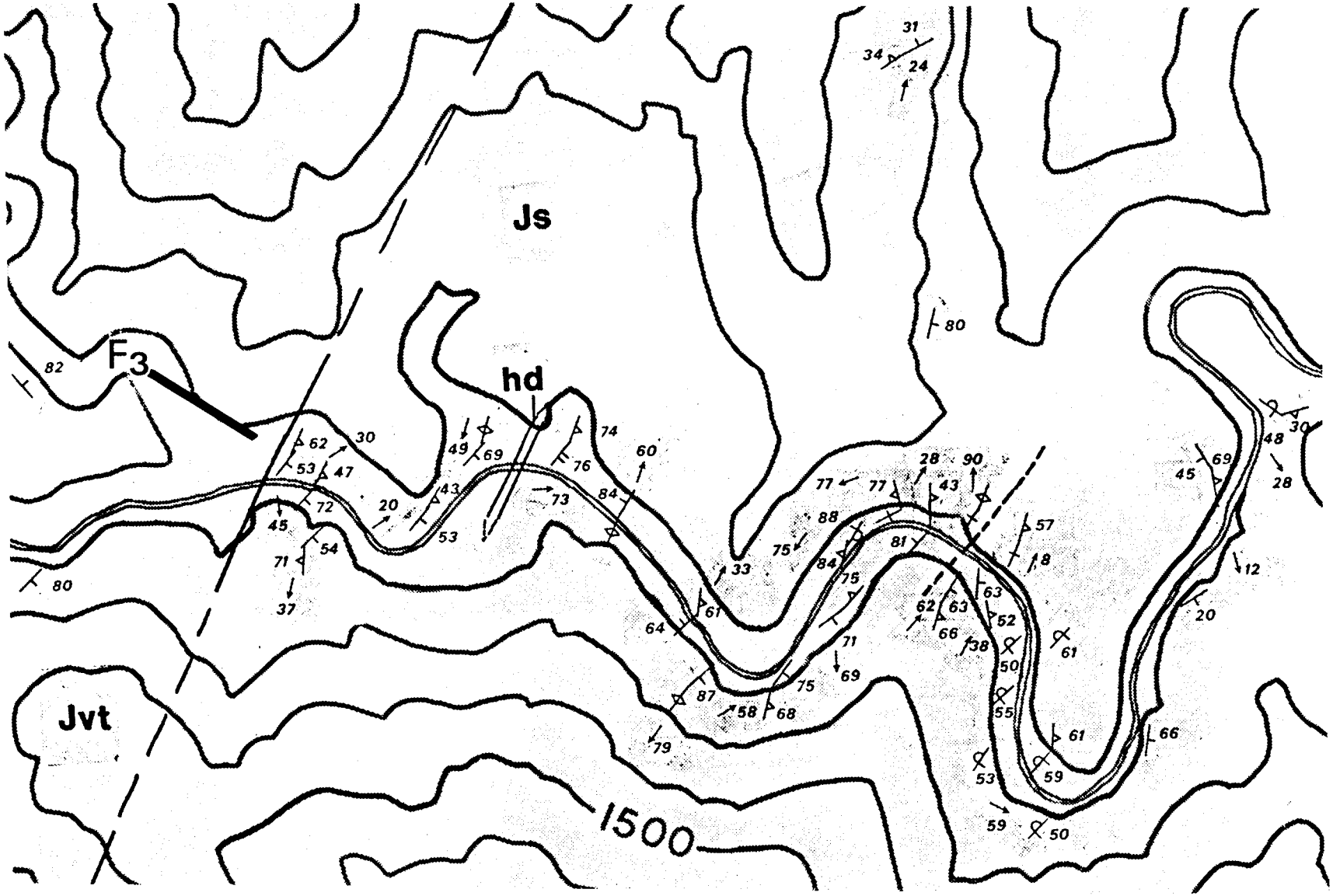
Js
Jvt
F3
hd
1500

Figure 3-9: Locality map and structural profile B-B' for the Grave Creek locality. The locality map shows the location of stations used in the construction of the vertical cross-section and the plot of F_1 fold axes (*see* Figure 3-20). Younging directions and the trace of apparent cleavage S_1 are shown on the profile. The Rogue-Galice contact is interpreted as a fault parallel to subparallel to bedding whose displacement and times of displacement are uncertain.

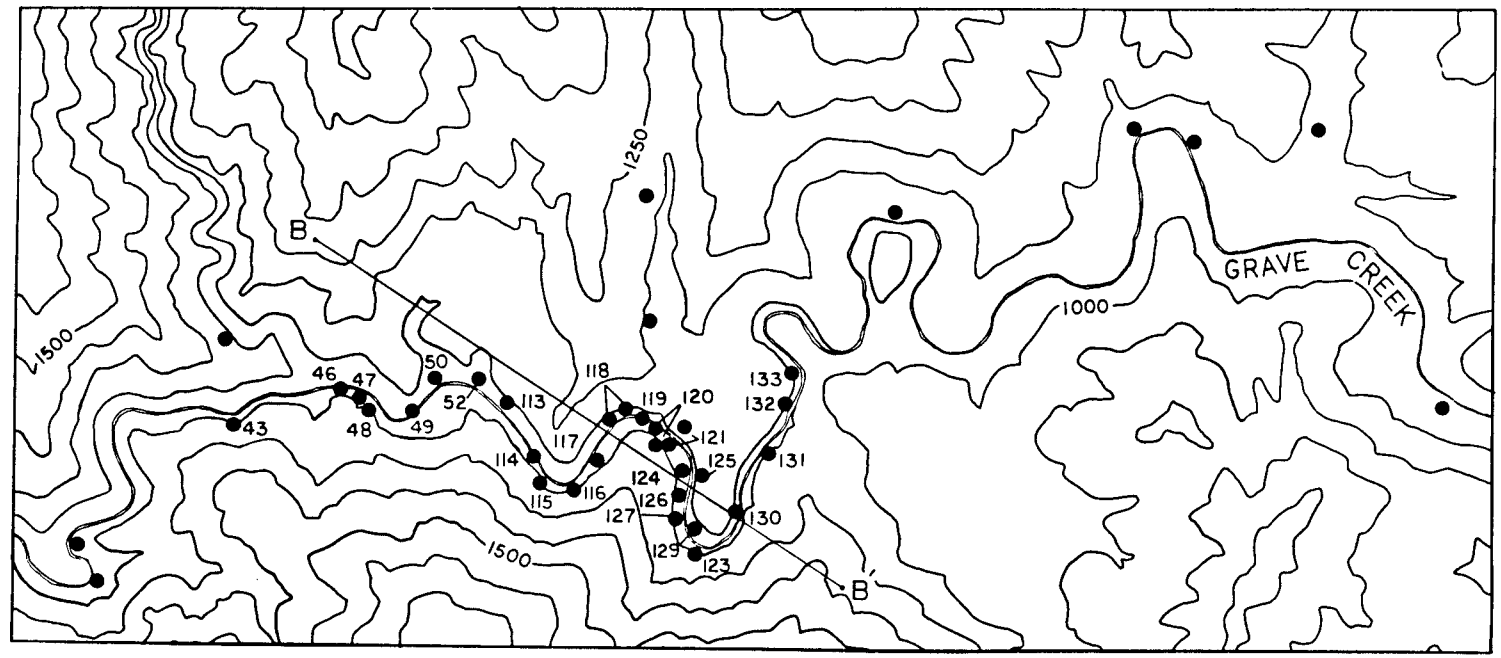
B
B′
1250
1500
1000
GRAVE CREEK
43
46
47
48
49
50
52
113
114
115
116
117
118
119
120
121
124
125
126
127
129
130
131
132
133
123
NW
GRAVE CREEK
SE
B
B′
FEET
1400
800
200
Rogue
Fault
Galice
dike
S1
S1
Fault
METERS
400
100
0
1/4 MI
0
1/4 KM
VE=2.1

of maximum finite shortening. Figure 3-2 shows a fold at locality 118 cut by pervasive, axial planar cleavage, presumably produced syn- or pene-contemporaneously with Nevadan underthrusting of the western Jurassic belt, and subsequent fold development. Most shale beds observed in the type Galice, however, show cleavage at an acute angle to bedding.

Cleavage is a commonly observed feature in pelitic rocks. Its origin has been studied since 1857, when H. C. Sorby noted that pre-existing sediment and tectonic preferred orientation are important factors governing cleavage development. The origin of axial planar cleavage has been studied experimentally (Tullis, 1976), yet the relative importance of mechanisms such as crystal growth, rotation, flattening, diffusion, and the relationship of strain to fold geometry are not well understood (Hobbs *et al.*, 1976, p. 231-232). Nevertheless, pencil cleavage and crenulation cleavage have been studied in the past decade as a way to decipher progressive stages of deformation, and both of these types of cleavage development are found in the study area.

Pencil cleavage is a term used in slate districts for long, narrow strips of shale with rhombic cross-sections. They form during the initial stage of metamorphism of shale into slate, and are strain-induced (Engelder and Geiser, 1979). The pencils are produced by the intersection of cleavage and bedding, such that stress relaxation by the removal of overburden induces fracturing, and subsequent weathering enhances pencil cleavage development (Reks and Gray, 1982).

Pencil cleavage is found in the study area along Grave Creek in some outcrops, such as at locality 152 (Figure 3-10), and it commonly weathers out as "pencils" which are found in the stream bed. Wells et al. (1949) first noted that pencil structure is present in the Galice Formation, yet they believed that pencil structure is found on fold crests and could be useful for determining the locations of fold hingelines, which isn't necessarily the case.

Figure 3-10: Pencil cleavage outcrop along Grave Creek at locality 152.

Reks and Gray (1982) deduced that pencil development is most likely found in areas of warped strata with moderate dips and in zones that have experienced approximately 9-25% shortening. They studied middle Ordovician mudstone and siltstone from the Appalachian Valley and Ridge Province. They correlated pencil development with corresponding incremental strain measurements derived from measurements of syntectonic fibers growing in the pressure fringes around pyrite framboid concretions. According to Reks and Gray (1982), bedding is prevalent in areas that have undergone less than 9% shortening, pencil development is found in areas that have undergone 9-25% shortening, while cleavage forms in zones that have experienced more than 26% shortening. In a follow-up paper, Reks and Gray (1983) conclude that cleavage-dominated rocks occur in fold hinge and fault regions, while rocks dominated by pencil structure are found along limbs of regional folds.

Crenulation cleavage is a type of cleavage found in low to medium-grade metamorphic rocks (Gray, 1979) in which the microlithons have a pre-existing grain alignment that has been systematically deformed into microfolds. Crenulation cleavage is thought to form by microfolding and solution transfer, as the cleavages represent residual accumulations of insoluble material, such as clay, mica, chlorite, and opaque minerals. The cleavage may be enhanced by grain growth or prograde metamorphism (Gray, 1979).

Kinks or crenulated cleavage are found in the study area at stations 22, 87, 88, and 89. The zone that includes sites 87, 88, and 89 is a 1 km stretch along a logging road, located 2 km north of major NW-trending faults that bound the serpentinized ultramafic bodies. At station 89, two sets of cleavage are observed, with the second cleavage clearly refolding the earlier cleavage (see Figure 3-11). Other outcrops from stations 87-89 show sets of kink folds in shales that have a strong phyllitic schistosity. Station 22 is located along the Rogue River about 1/2 km east of the Rogue-Galice contact. The significance of these kinks to large-scale structures is not great (Hobbs *et al.*, 1976, p.

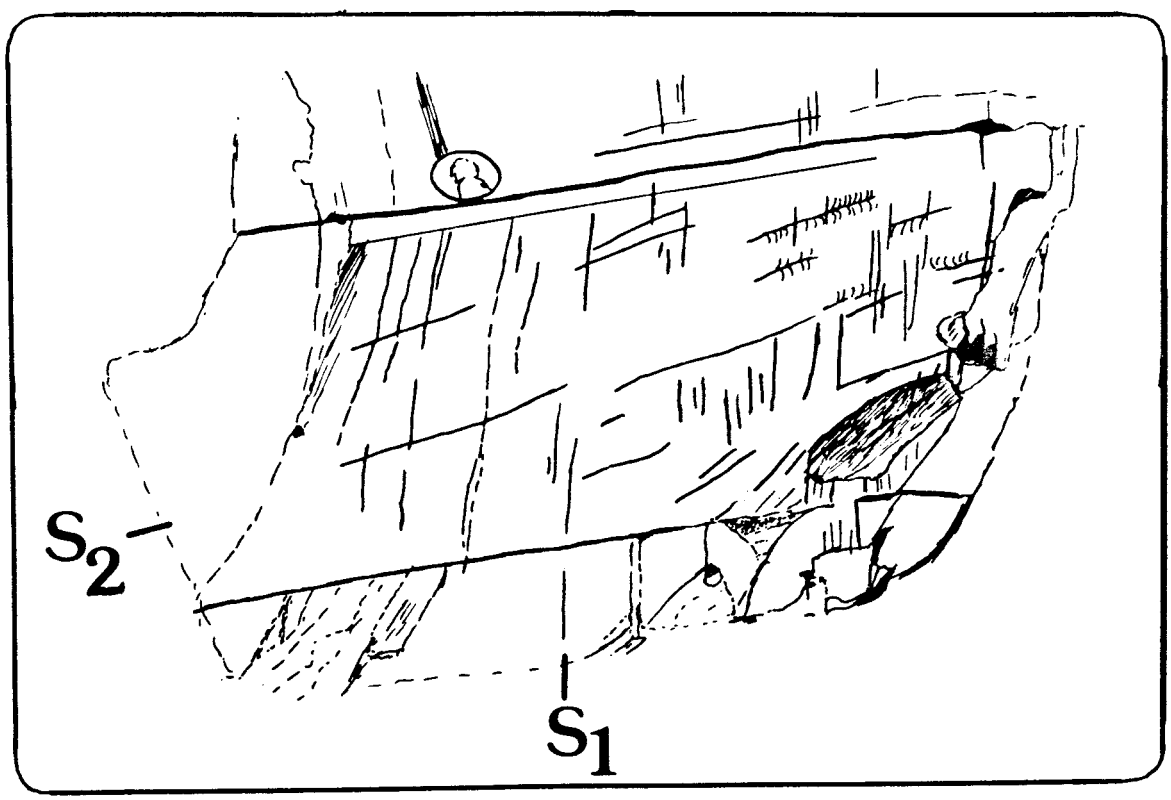

Figure 3-11: Photo and sketch of two sets of cleavage such that S_2 refolds S_1, from locality 89. Nickel for scale. Photo taken looking southwest (253°).

404), except that they usually occur in areas near large faults, or they may be related to a second folding episode. In this instance, the occurrence of kinks and crenulation cleavage in Galice shales and phyllitic rocks is probably related to large, nearby faults.

3.2.3 Faults

Numerous faults were observed throughout the study area in serpentinized ultramafic rocks, shale, and volcanic tuff. A previous section, Section 2.6.2, discussed in detail the nature of the Rogue-Galice contact, not repeated in this section. Instead, smaller-scale faults in the study area are discussed and illustrated.

Shiny, dark green serpentinized ultramafic rocks are found east of Indian Mary Campground. These masses occur as north-northeast trending, fault-bounded bodies. Wells and Walker (1953) discuss the high-angle reverse faults (*i.e.*, West Hellgate and East Hellgate) that separate the ultramafic rocks from surrounding volcanic tuffs and tuff breccias of the Rogue Formation. Within these serpentinites, shear zones are commonly found, such as at location 27 (Figure 2-11). At station 165, rodingite rinds with an orientation of $330^{o}/25^{o}$E are found between serpentinites with whitish-weathering volcanic tuffs. The south side of the road across from station 165 has a fault plane (orientation $050^{o}/70^{o}$SE) that separates volcanic tuff from serpentinites. Excellent slickensides are found along the fault plane in the down-dip direction.

Approximately 270 meters (880') east of the Rogue-Galice contact, a high-angle fault separating Galice beds of different attitudes is found at station 23 (Figure 3-12). The beds on the northwest side (left side of photo) dip steeply to the east and are overturned. At station 120, a nearly vertical fault dissects two apparent limbs of a tight fold along Grave Creek. Fault gouge occupies a sinuous zone that is 5-10 cm wide, and the beds on either side of the fault are not significantly disturbed (Figure 3-13). A moderately-dipping fault at station 102 divides greywackes and overlying shales from shales of a different orientation.

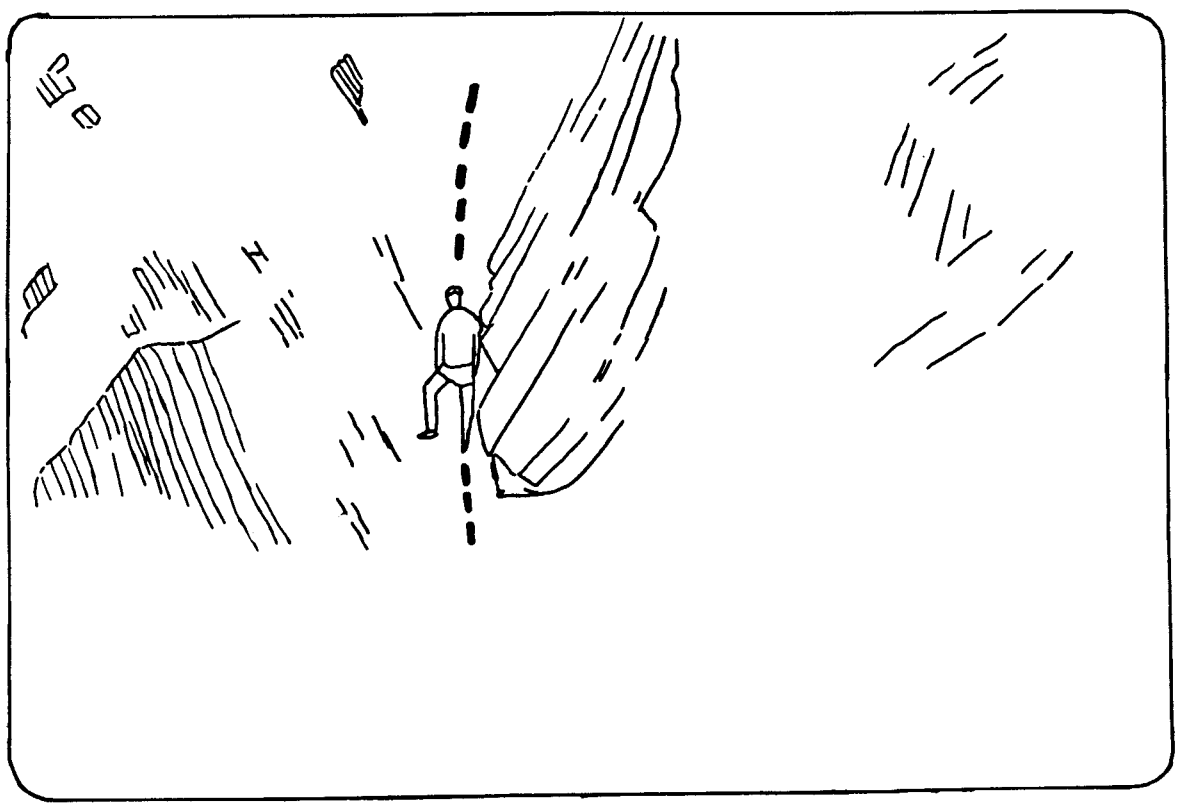

Figure 3-12: High-angle fault separating shale beds of different attitudes at locality 23, approximately 270 meters (880') east of the Almeda mine. Small lenses of sandstone are present in the shale beds. Beds on the northwest side (left side of photo) are overturned and strike 011° and dip 86°E (cleavage 009°/84°E). Beds on the southeast side have an attitude of 010°/65°NW (cleavage 004°/78°NW). Photo taken looking NE (027°).

Figure 3-13: Photos of a vertical fault and sinuous fault gouge zone 5-10 cm wide from locality 120 along Grave Creek. Fault gouge is white, powdery unconsolidated material. Veining is also present in fault zone. This fault separates shale beds with an attitude of $036^{o}/90^{o}$ (left side) from shale and greywacke beds with an attitude of $213^{o}/63^{o}$SE. Photo taken looking northeast.

Numerous faults are found in the volcanic tuff and tuff breccia of the Rogue Formation along the logging roads in the vicinity of Butte Creek. Station 72 has well-developed slickenlines along a large fault surface (orientation $216^{o}/74^{o}$NW) at an outcrop of bedded tuffs. The surface appears milky-white due to the presence of quartz or calcite on the fault surface, and the slickenlines have a pitch of 40^{o} south.

A low-angle fault exposed in the Rogue River canyon, 800 m west of Almeda mine dips gently to the north at about 25^{o}. This fault separates cherty tuffs from underlying amygdaloidal lava, and has a reported reverse displacement of 183 meters (Wells and Walker, 1953). This low-angle fault is shown in Figure 3-14.

Numerous NW-trending faults are present in the study area. These faults offset the trend of the Rogue-Galice NE-trending contact, and the flysch-volcanic contact west of Stratton Creek. These NW-trending faults are small and not continuous features. Other examples of NW-trending faults are found in the multiply-faulted serpentinized ultramafic bodies near Hell's Gate Canyon.

3.3 Analysis of Structural Elements

3.3.1 Bedding and Cleavage

Structural analysis of the Galice Formation has been done using data collected during the summer of 1985. Measurements of bedding for the Galice shales and greywackes are shown in the lower hemisphere, equal-area projections of Figure 3-15. These data, expressed as poles to bedding, show that bedding generally strikes northeast. Note that steeply southeast-dipping beds predominate. Eighteen out of 118 beds were found to be clearly overturned. The data points are scattered in a diffuse girdle pattern indicative of "near-cylindrical" macroscopic folding (Davis, 1984, p. 366). The term

Figure 3-14: Low-angle fault dipping 25^{o} north exposed in the Rogue River canyon 800 meters west of Almeda mine. According to Wells and Walker (1953), this fault separates cherty tuffs from underlying amygdaloidal lava and has a reverse displacement of 183 meters.

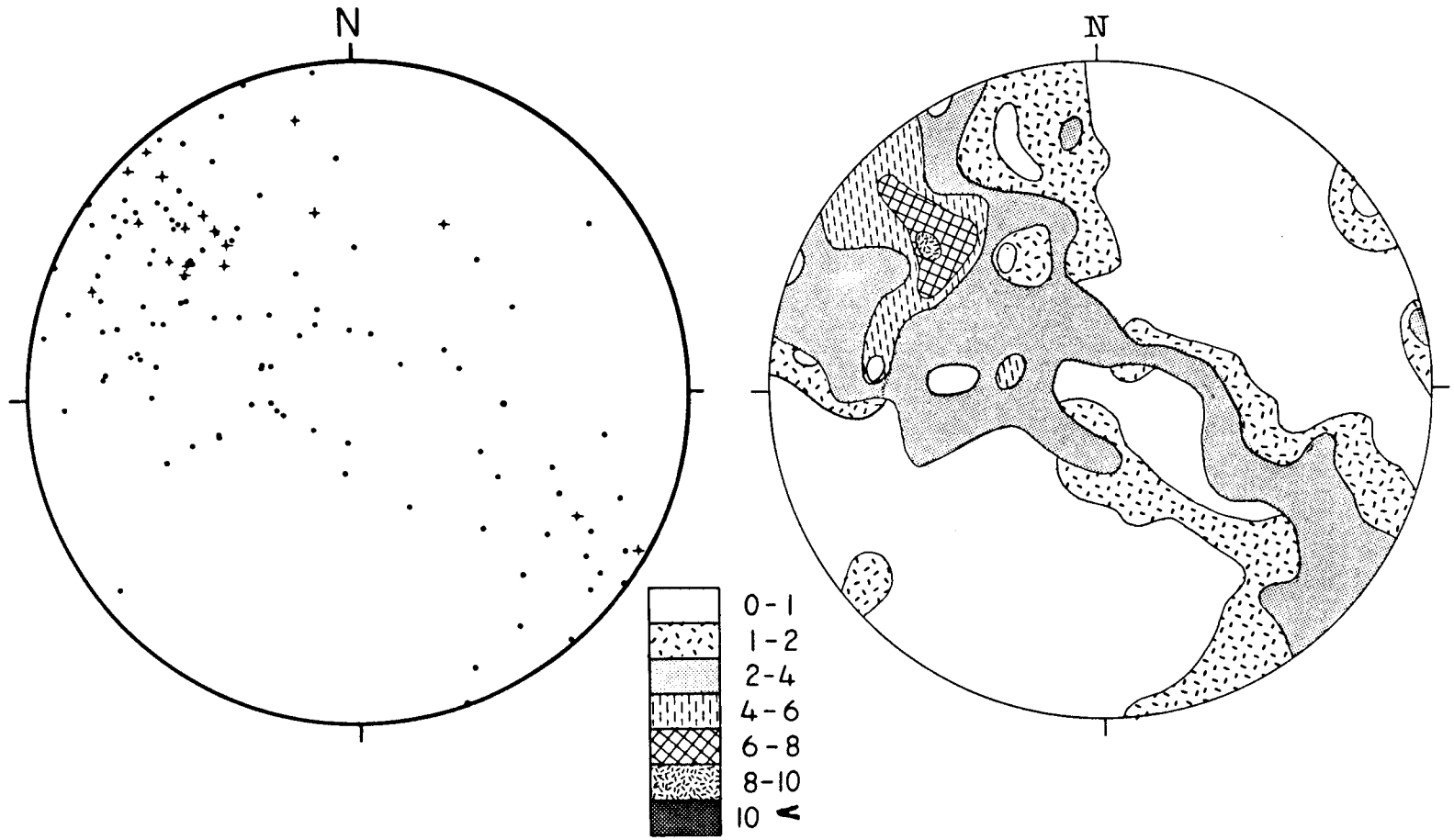

Figure 3-15: Equal-area, lower hemisphere projections of poles to bedding for Galice shales and greywackes (n=118). Overturned beds are represented by crosses.

"near-cylindrical" is preferred over the term "non-cylindrical" because of the following reasons:

-- Non-cylindrical folds do not possess linear fold axes since the hingelines are very irregular in orientation. Equal area projections are so complex that the field area must be broken into smaller fold domains (*e.g.*, Weiss and McIntyre, 1957). An attempt to break this study area's data into uniform fold domains did not produce identifiable clusters of fold axes within small sections of the study area.

-- The contoured plot of poles to bedding for "areas" on the net showing greater than 2% of the total data points per 1% area shows that a majority of points falls along a great circle with a strike of 126^{o}. These poles to bedding fall within 20^{o} of a best-fit circle and meet the criteria of a near-cylindrical fold (Davis, 1984, p. 371).

-- Considerable scatter of poles to bedding can be attributed to later folding, as the trend and plunge of the fold axes vary widely over short distances.

The density distribution of these data points is shown in the pole-density diagram of Figure 3-15, constructed by use of a Kalsbeek counting net, contouring of the data points, and recalculation of the values of the data points in terms of the percentage of total data points per 1% area of net (Davis, 1984; Ragan, 1973). This contoured diagram shows the point maximum to lie in the northwest quadrant, which translates to a point maximum orientation of Galice beds of $039^{o}/057^{o}$SE. This pattern is interpreted as representing asymmetrical folding with an inclined axial plane, i.e., folds are overturned to the northwest. These folds would be classified as "plunging inclined" folds according to the fold classification scheme of Hobbs et al. (1976, p. 180).

A plot of poles to bedding for the limited number of measurements made on the Rogue volcanics shows a similar diffuse girdle pattern and point maximum lying in the northwest quadrant (Figure 3-16). The contoured diagram is shown for qualitative purposes only, as not enough data points were measured to make it statistically valid. But the similarity of bedding (and thus, folding) patterns shown by the Galice and Rogue Formations indicates that they were folded into the same overall geometry during D_1, the Nevadan orogeny.

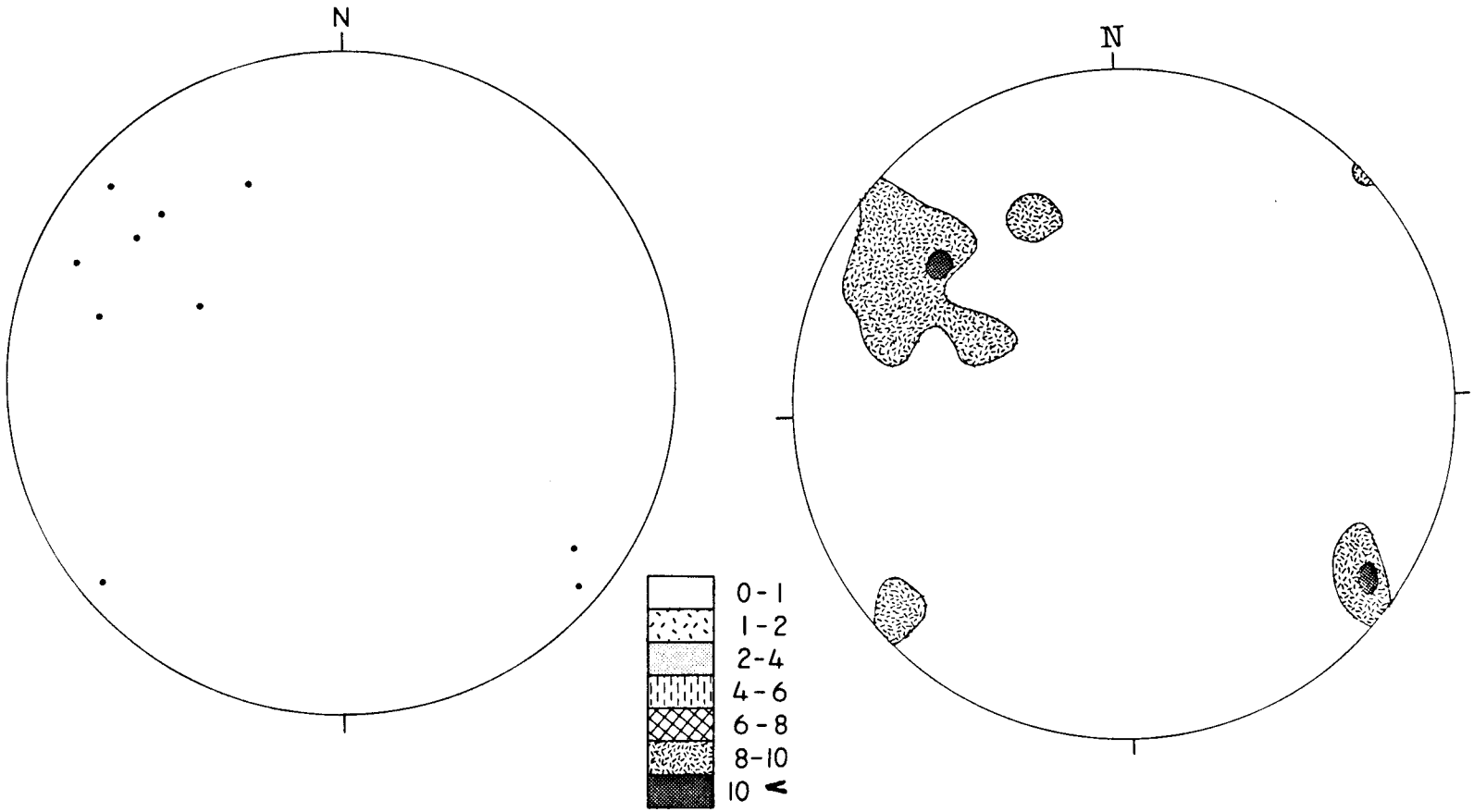

Figure 3-16: Equal-area, lower hemisphere projections of poles to bedding for Rogue volcanics, shown for comparison purposes only (n=10). Note the pattern similarity to Figure 3-15.

A plot of poles to cleavage and the corresponding contoured diagram of these points is shown in Figure 3-17. Note that the cleavage generally trends north-northeast and dips steeply to the southeast. The dense cluster of points in the west-northwest section of the stereonet corresponds to a cleavage orientation of $021^{o}/60^{o}$SE. The fact that cleavage data do not cluster in a single maxima, but are scattered into a girdle indicates that the foliation has been dispersed by later folding during a post-Nevadan deformation phase. A strong maximum in the northwest quadrant is present, however, which supports the supposition that the later deformation was a less-pronounced deformation phase than the Nevadan deformation.

A combination of the point maxima from the contoured diagrams for the Galice and Rogue Formations shows that the poles to bedding lie along a full girdle, from which a best-fitting great circle (π-circle of Ramsay, 1967) can be constructed (Figure 3-18a). This great circle contains the point maxima of both units. From this plane, a good estimate of the average F_1 fold axis orientation (Hobbs *et al.*, 1976, p. 366) can be deduced. A good estimate of the axial plane AP_1 is found normal to the best-fitting great circle that describes the plot of poles to cleavage (Figure 3-18b). The axial plane trends 022^{o} with a dip of 60^{o}SE. The F_2 fold axis trends 197^{o} and plunges 10^{o}SW and has a similar orientation to F_1, which may represent late-stage Nevadan folding. Together, the axial plane, fold axes F_1 and F_2, and plot of poles to bedding and cleavage are interpreted as representing the orientation of asymmetrical, overturned (to the NW) and gently-plunging Nevadan folds near Galice, Oregon.

3.3.2 F_1, F_2 and F_3 Fold Axes

Nevadan (F_1) fold axes or bedding-cleavage intersection lineations (S_0 x S_1) for the Galice area are shown in Figure 3-19. They define a weak northeast-southwest girdle which is especially evident by the contoured diagram of Figure 3-19(b). The contoured

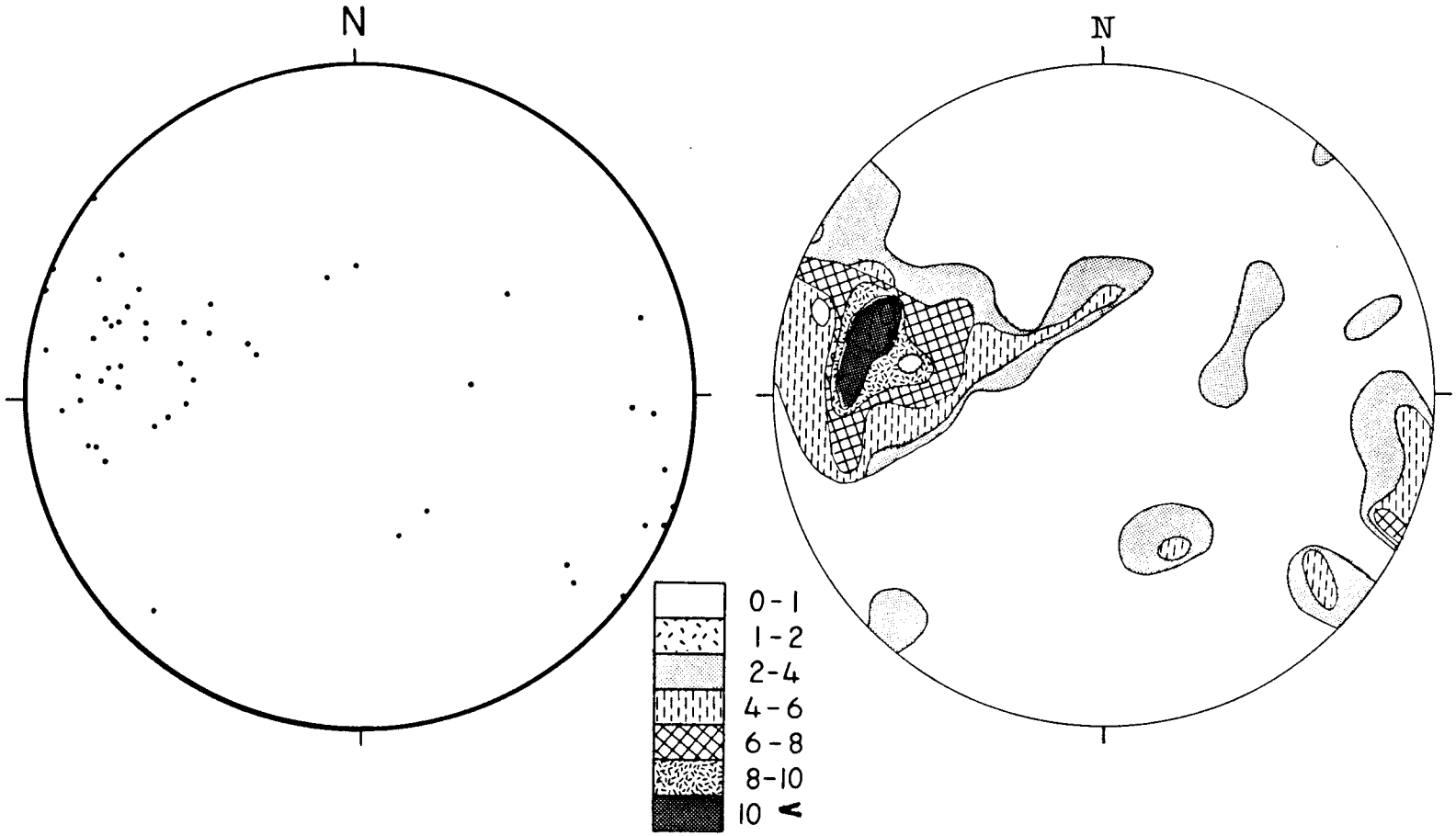

Figure 3-17: Equal-area, lower hemisphere projections of poles to cleavage for Galice shales (n=48).

Figure 3-18: (a) Contoured point maxima for poles to bedding of Galice flysch and Rogue volcanics. Dashed contour line=Galice maxima, dotted contour line=Rogue maxima, x=intersection of point maxima. The π-circle contains the point maxima of both formations. The F_1 fold axis is normal to the point maxima of both units (x). (b) Contoured point maxima for poles to cleavage for Galice shales from which is shown the estimated axial plane AP_1 and F_2 fold axis. The F_2 fold axis has a similar orientation as the F_1 fold axis.

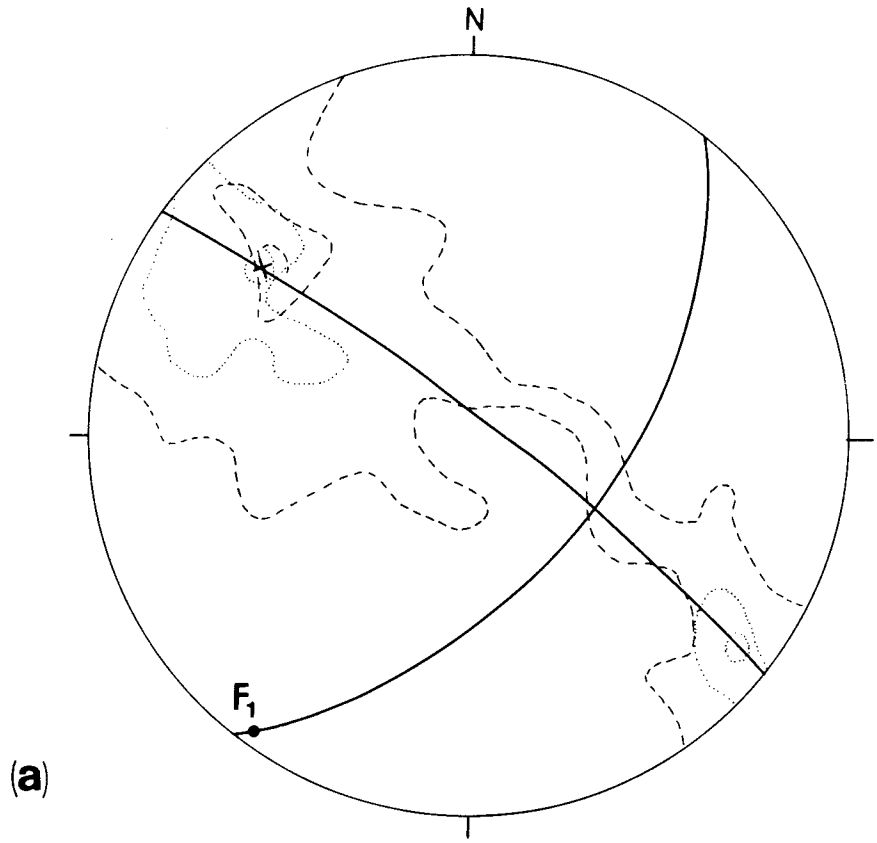

(a)

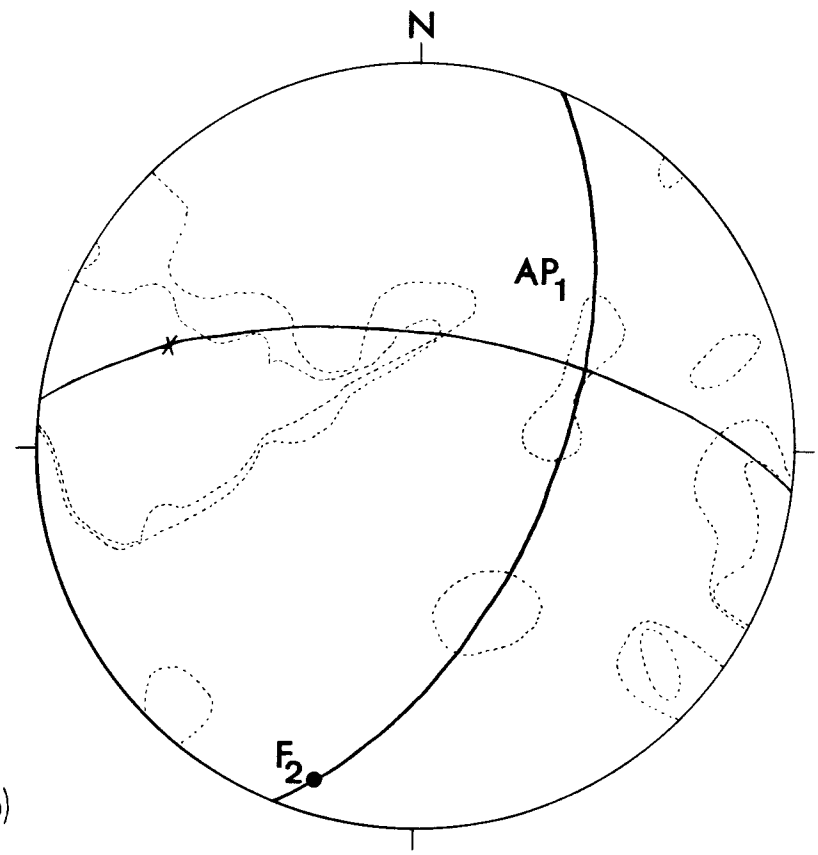

(b)

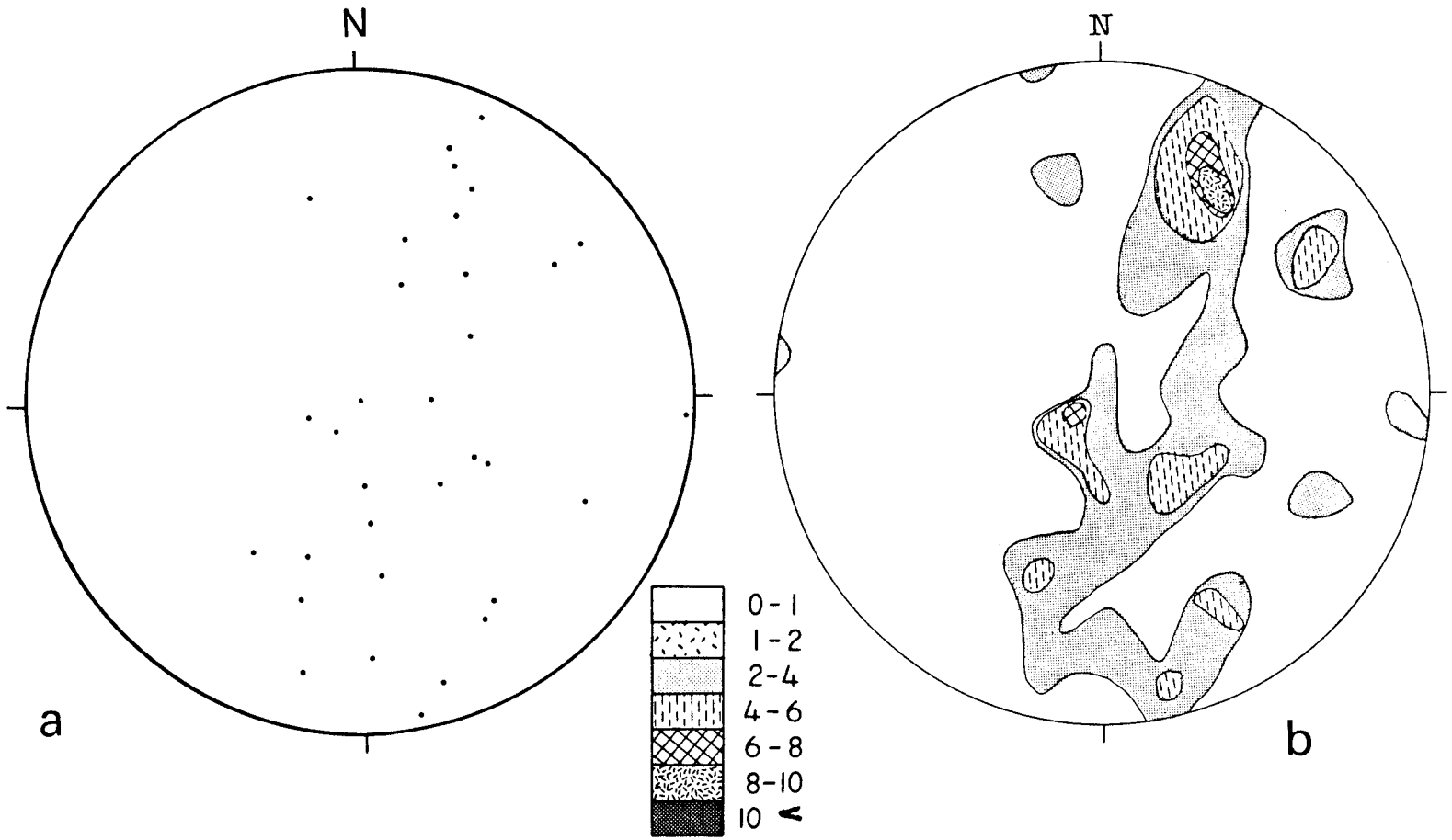

Figure 3-19: Plot of Nevadan F_1 fold axes (bedding-cleavage intersections) for the Galice Formation.

diagram is very similar to the contoured fold axes shown by M. A. Kays for roughly the same area, which he refers to as Zone II (his Figure 3, p. 27, 1968).

An indepth examination of fold axes and their systematic variation was carried out for the well-exposed section along Grave Creek. Figure 3-9 shows the location of the stations utilized in constructing a vertical profile B to B', from which was taken the calculated fold axes plotted in Figure 3-20. These Nevadan fold axes delineate three interesting points. First, the fold axes appear to fall along two similarly-oriented NE-SW great circles or small circles of large angle. The Nevadan fold axes are plotted as solid circles or triangles depending on which great circle (or small circle of large angle) they lie nearest. Second, the fold axes systematically change vergence from northeast to southwest as one walks towards the east along Grave Creek. Third, the calculated post-Nevadan fold axes (F_3) lie in the northwestern and west-northwestern quadrants (diagrammed by an open circle or triangle), approximately 90^0 apart from the mean F_1 and F_2 fold axes.

Another method by which the post-Nevadan (F_3) fold axis orientation can be determined is by use of bedding-plane intersections. Intersection of two fold limbs for each fold drawn on the profile B to B' (Figure 3-9) gives the approximate hingeline or fold axis, and these calculated fold axes (Figure 3-21) lie near or along a best-fit great circle (or small circle of large angle). Post-Nevadan folding is assumed to have been nearly cylindrical, judging from the distribution of fold axes given in Figure 3-21. The approximate F_3 fold axis in this diagram trends 301^0 and plunges 10^0 to the northwest. The mean of the three F_3 fold axes from Figures 3-20 and 3-21 trends 303^0 and plunges 14^0NW. From the map of Grave Creek (Figure 3-8) it appears that the wavelength of the F_3 folds is on the order of 0.3-0.4 km.

Field data from station 18 supports a post-Nevadan fold axis of about $303^0/014^0$NW. The bedding-cleavage intersection lineation for this station trends 116^0

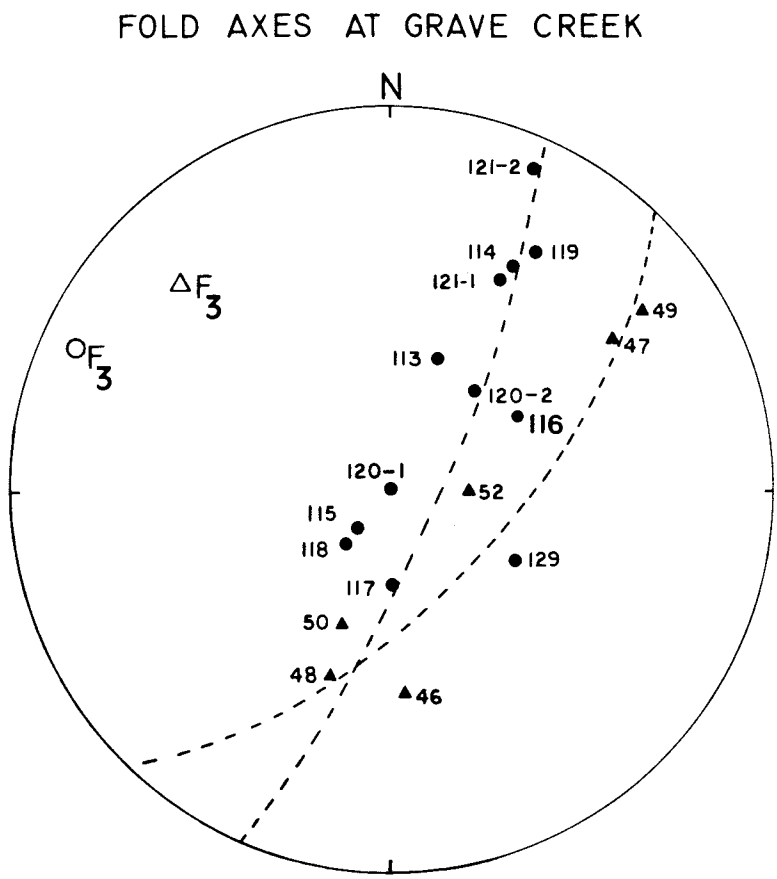

Figure 3-20: Plot of bedding-cleavage intersection lineations (solid circles and triangles) for Grave Creek stations as numbered, from which the F_3 fold axes (open circle and triangle) were derived. Note that the lineations or Nevadan fold axes lie along two great circles or small circles of large angle, and are steeply plunging and consistently changing plunge direction from NE to SW about an F_3 fold axis. See Figure 3-9 for Grave Creek locations.

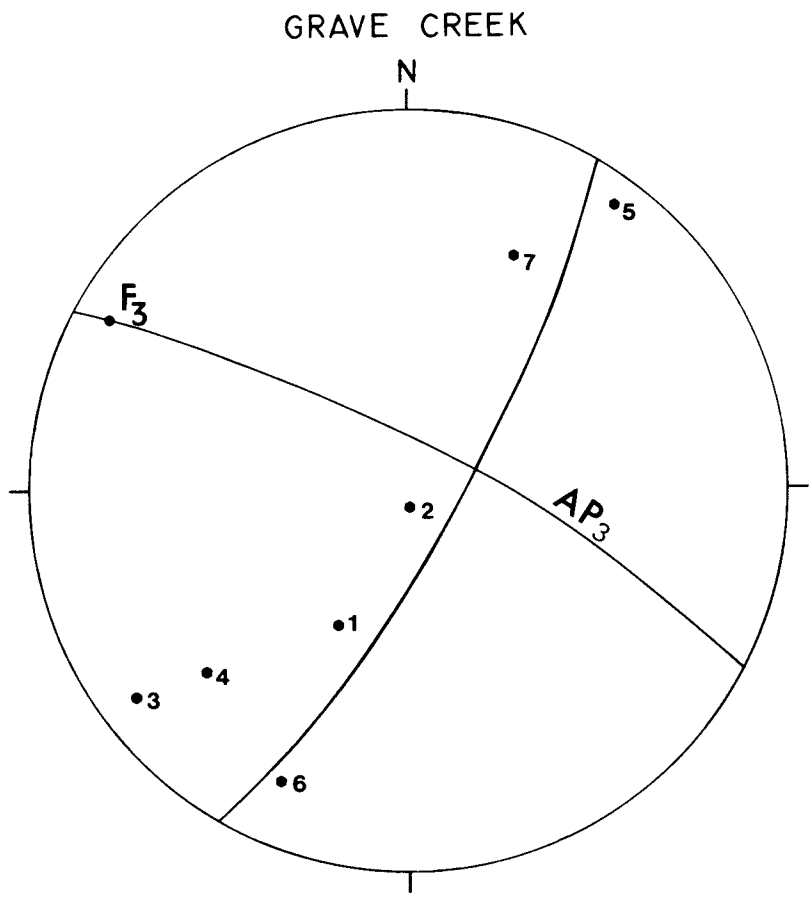

Bedding–plane intersections

1 = 117 ∧ 118	5 = 120-1 ∧ 120-2
2 = 118 ∧ 115	6 = 120-2 ∧ 121-2
3 = 115 ∧ 114	7 = 121-2 ∧ 121-1
4 = 119 ∧ 117	

Figure 3-21: Estimate of F_3 fold axis determined by use of bedding-plane intersections (labelled 1-7) for contiguous fold limbs. Fold limb pairs listed at lower right. Stations used are the same as those used in Figure 3-21 (Grave Creek).

and plunges 27^{o}E, approximately 2^{o} off of the calculated orientation of $AxPl_3$, as shown in Figure 3-22.

In conclusion, the type Galice shales and greywackes display evidence of three phases of folding. The Nevadan folds are asymmetrical and overturned to the NW, with an axial plane AP_1 orientation of $022^{o}/060^{o}$SE. The F_1 and F_2 fold axes lie in the southwestern quadrant and have orientations of $215^{o}/004^{o}$SW and $197^{o}/010^{o}$SW, respectively. From the plots of poles to cleavage and bedding-cleavage intersections, it is apparent that these girdles have been broadened or dispersed by F_1 and F_2 folding in a NW-SE sense. The post-Nevadan deformation is characterized by folds that warp the hingelines of Nevadan folds, as is seen in the Grave Creek map (Figure 3-8) and analysis of the bedding-cleavage intersections and bedding-plane intersections from Grave Creek stations. The orientation of the post-Nevadan axial plane AP_3 is $119^{o}/080^{o}$SE and the F_3 fold axis is inferred to trend 303^{o} with a 14^{o} northwestern plunge. A summary of the structural data for the Galice Formation and a stereographic block diagram are provided in Table 3-1 and in Figure 3-23.

3.3.3 Fold Interference

Ramsay (1967) defined two angles α and β in his classification scheme of fold interference patterns. These angles are diagrammed in Figure 3-24. Alpha is defined as the angle between the fold axis for the second-formed folds (b_2) and f_1. Alpha is approximately 87^{o} for this area. Beta is defined as the angle between the pole of the first axial plane and a_2, the normal to b_2 that lies in the axial plane of the second-formed folds. In this case, β for the Galice data is 69^{o}. From these two angles, α and β, Ramsay (1967) classified fold interference patterns (Figure 10-13 of Ramsay, 1967). The Galice area has evidence of superposed folds that are transitional between type I and type II fold interference patterns.

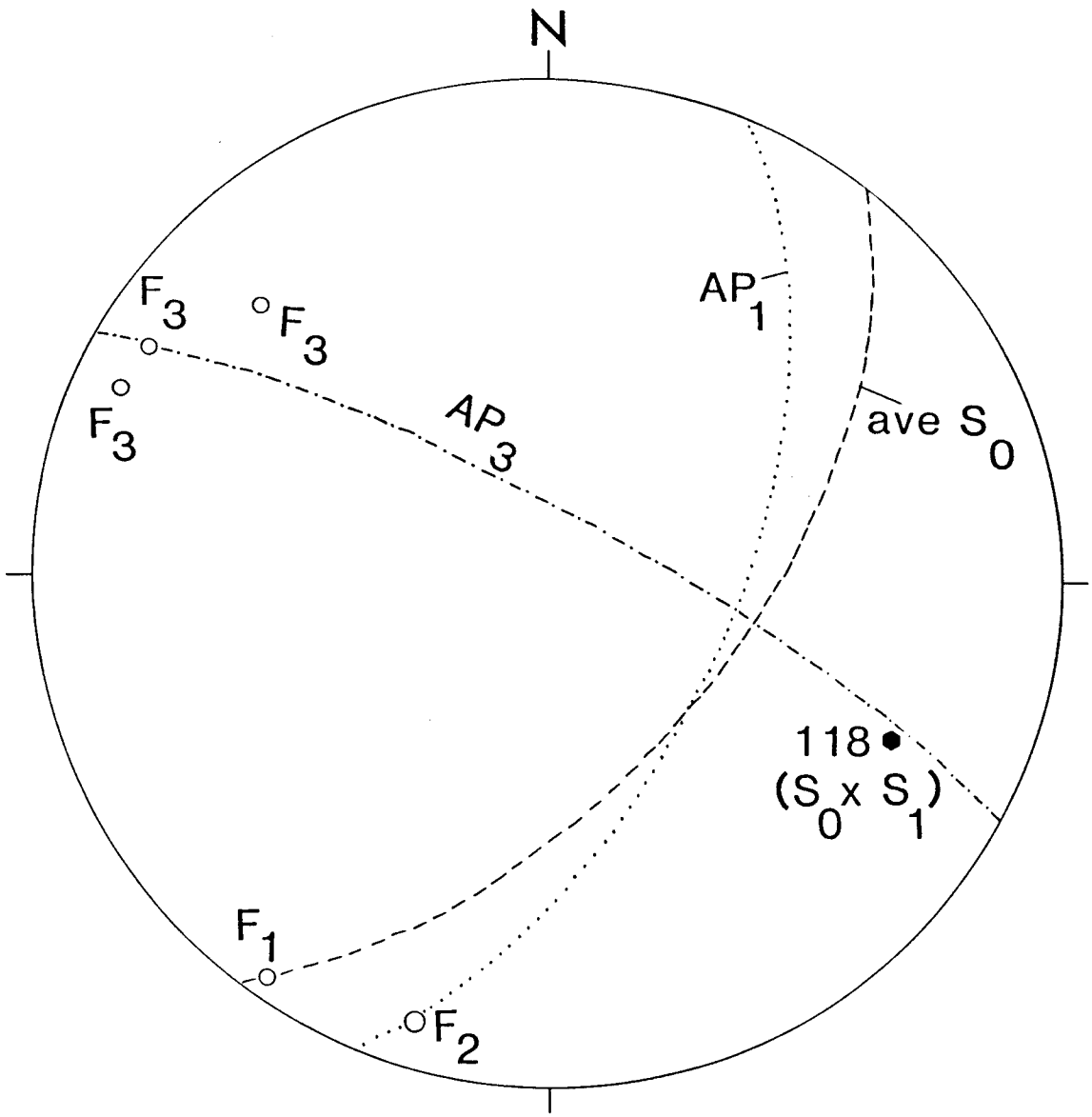

Figure 3-22: The bedding-cleavage intersection lineation from locality 118 is plotted along with the calculated locations of F_1, F_2, and F_3 fold axes. The bedding-cleavage intersection lies approximately 35^{o} off of the trend of the mean F_3 fold axis orientation and is 2^{o} off of the F_3 axial plane. Photo of this locality in Figure 3-5.

NEVADAN AND POST-NEVADAN DATA

Description	Strike	Dip	Trend	Plunge
Nevadan Data				
Mean S_0 orientation	038°	059°SE		
Mean S_1 cleavage or AP_1	022°	060°SE		
Mean trend of bedding-cleavage intersections (n=43)			019°	
F_1 fold axis			215°	004°SW
F_2 fold axis			197°	010°SW
Post-Nevadan Data				
F_3 fold axis			314°	024°NW
F_3 fold axis			295°	010°NW
F_3 fold axis (bedding-plane intersection)			301°	010°NW
Mean F_3 fold axis			303°	014°NW

Table 3-1: Compilation of all Nevadan and post-Nevadan data.

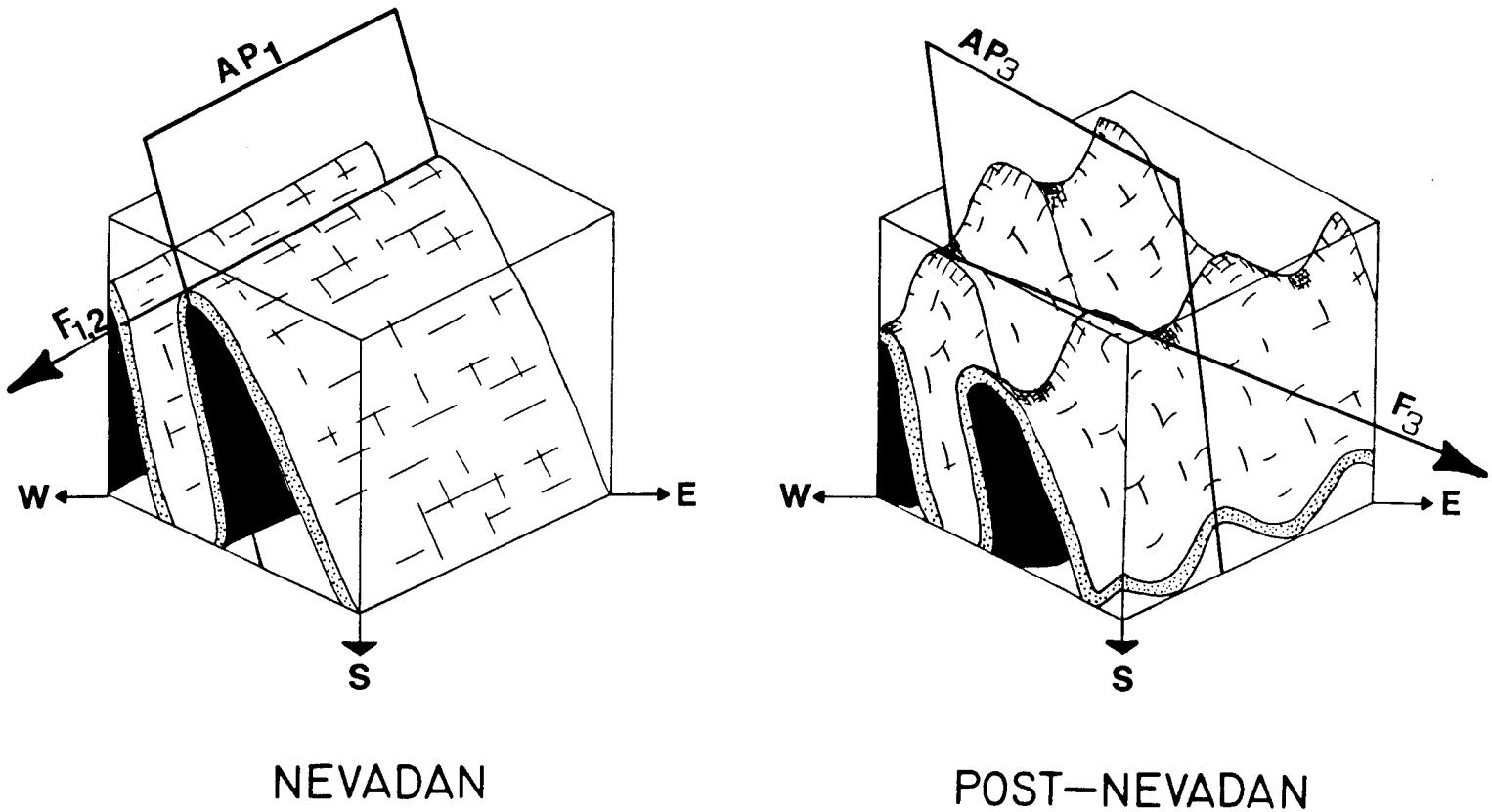

Figure 3-23: Stereographic block diagrams illustrating the mean orientation of Nevadan folds and the effects of post-Nevadan (F_3) folding superposed onto F_1 and F_2 folds.

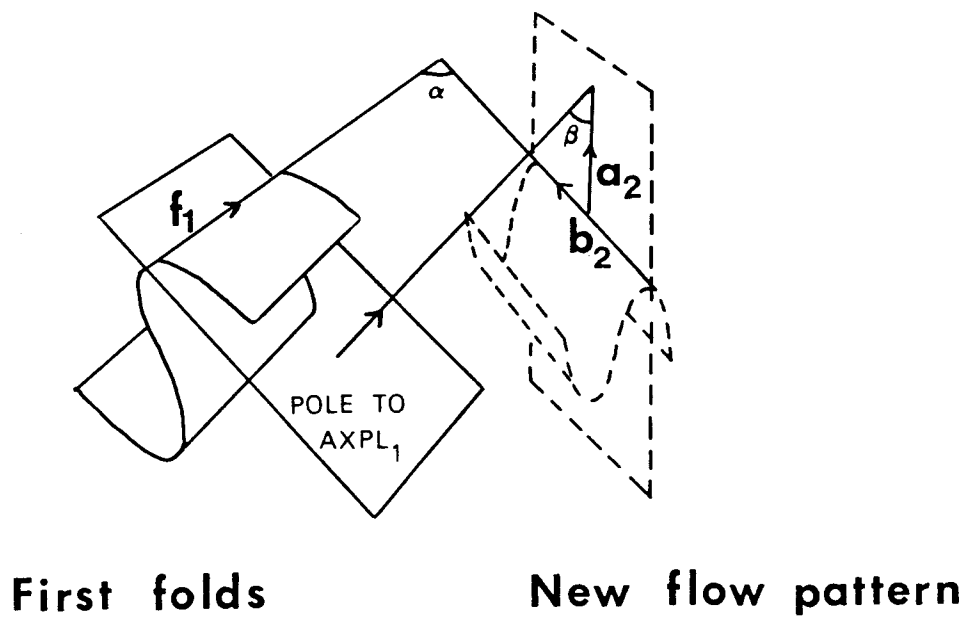

Figure 3-24: Drawing illustrating the angular relationships α and β, from Ramsay (1967).

Thiessen and Means (1980) modified this classification system by introducing additional angular parameters γ and δ. Gamma is defined as the angle between the pole to the second axial plane, c_2, and f_1. Gamma was found to be 07^{o} for the data under consideration. The angular relationships between α, β, and γ define sixteen fold interference patterns and four major types of folds (Thiessen and Means, 1980). Even with this expanded classification scheme, the calculated values of α, β, and γ indicate that the interference pattern can be best be described as transitional between types I and II. Thiessen and Means (1980) point out that for this particular fold interference pattern, triangular closed outcrop patterns are likely.

3.4 Gravity Data

Gravity data for the Galice area published by Kays and Bruemmer (1964) reflect the areal distribution of dense and less dense lithologies (see Figure 3-25). Gravity minima correspond to the metasedimentary rocks of the Galice Formation (2.64-2.69 g/cc) while gravity maxima correspond to the ultramafic, gabbroic, and metavolcanic rocks present (2.85-2.97 g/cc).

The gravity map manifests the overall pattern of northeast-trending Nevadan folds and faults and seems not to be greatly disturbed by later deformation(s). A hatchured, closed gravity low in the vicinity of station 147 is tentatively suggested to result from Galice metasediments that are bordered on the east and west by denser rocks, such as interbedded tuffs, shales, and lava flows found at stations 1-7 and 26. The Rogue-Galice contact is approximately located at the bottom of the gradients that surround the gravity high just west of the town of Galice, which is consistent with the observed steeply-dipping contact. A less-pronounced gravity high is evident in the vicinity of the serpentinized ultramafic slivers in the southeastern corner of the study area.

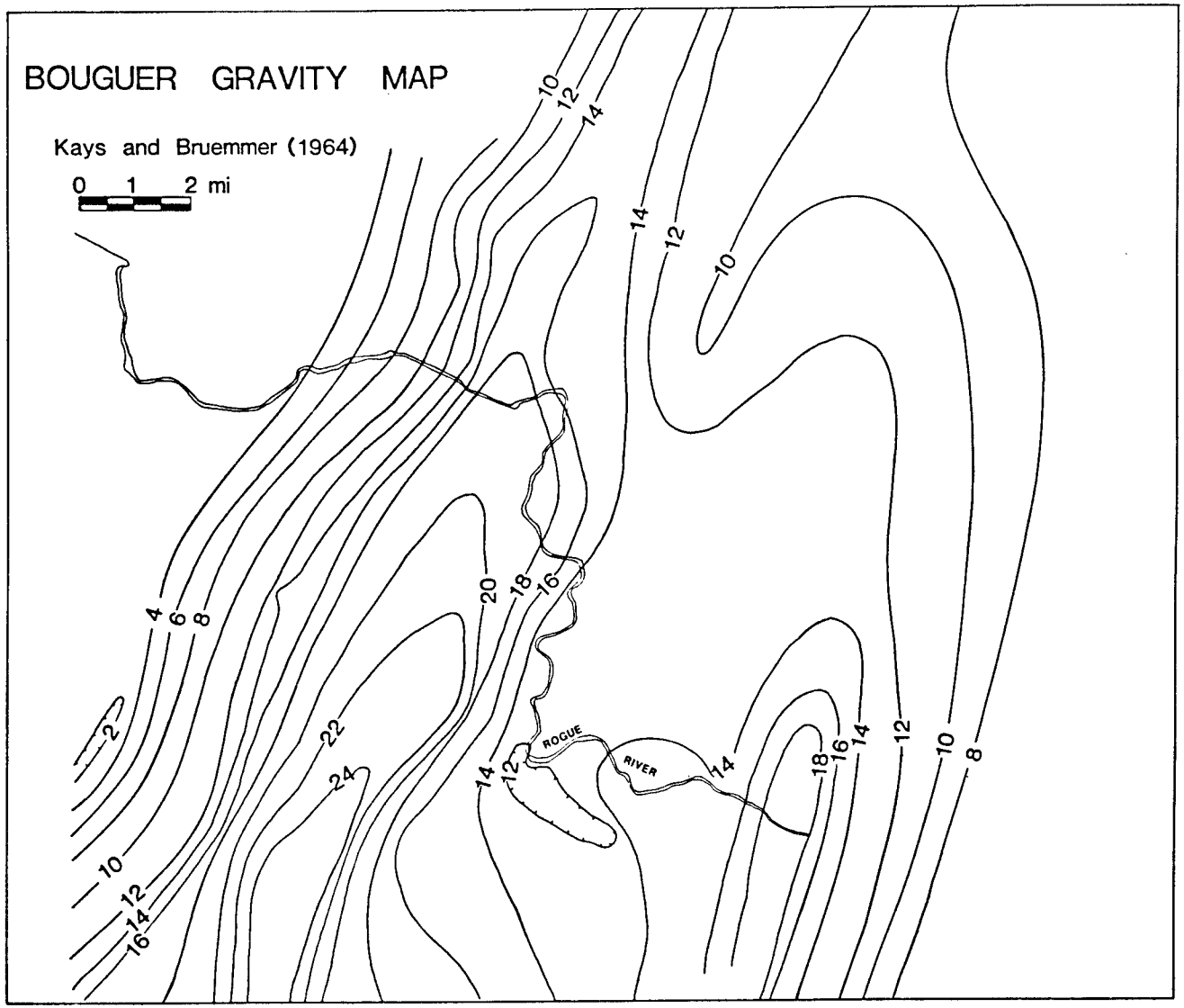

Figure 3-25: Bouguer gravity map of the study area from Kays and Bruemmer (1964).

CHAPTER 4: SEDIMENTOLOGY

4.1 Submarine Fan Sedimentation

Submarine fan studies proliferated during the 1970's as geologists examined transport mechanisms by which sediments are distributed in channel and basin environments. Deep marine clastic deposition can be characterized by a continuum of depositional processes that range from sliding, slumping, debris flow, high-density turbidity currents, turbidity currents, grain flow, fluidized flow, hemipelagic transport, and nepheloid layer deposition (Bouma, 1987). It is a general axiom that major fan accumulation occurs during periods of relatively low sea level (Bouma and others, 1985).

Fan development requires a sediment source, a submarine canyon, and a decrease in slope at the end of the fan (Nelson and Nilsen, 1974). A submarine fan is in reality a channel-levee-overbank system such that the overbank system consists primarily of muds and thin-bedded turbidites (Bouma *et al.*, 1985). Grain size and the rate of sediment supply are more important parameters than basin shape and relief (Normark, 1978). Additionally, the sandstone/shale ratio or the thickness of bedding do not indicate the relative proximity of a deposit to the original sediment supply source (Nilsen, 1980). Thus, inferences about the depositional environment and the original configuration of ancient submarine fan deposits are made based on the observed sedimentary structures, measurements of exposed stratigraphic sequences, and measurements of paleoflow indicators, with subsequent calculation and restoration of beds. This is the approach that has been taken for the Galice turbiditic sandstones and shales.

4.2 Sedimentary Structures

The type Galice Formation consists of thin-bedded (2-25 cm) dark grey to black shales interbedded with sandstone laminae, and massive thick greywackes typically on the order of 1-3 meters that are exposed in sequences of beds up to 44 meters across. The greywacke units are composed of volcanic lithic grains, detrital chert, monocrystalline quartz, plagioclase, and metamorphic lithic fragments (Harper, 1980b; Saleeby *et al.* 1982; Miller and Saleeby, 1987). Sedimentary structures observed in the study area include: (1) shale rip-up clasts (up to 12 cm diameter) in matrix-supported coarse sandstone and pebble conglomerate units, (2) graded beds in Galice siltstone and greywacke, and Rogue cherty tuff, (3) small-scale ripple cross-lamination in thin sandstone lenses, and finally, (4) scour marks and bottom structures in massive greywacke units. These structures and their respective stations in the study area are listed in Appendix I.

The presence of ripped-up shale clasts imply erosion of the substrate by turbidity current scour, which most likely occurred in a channel margin environment rather than in a basin-plain environment (*e.g.*, May *et al.*, 1983; Walker, 1978). The subrounded to rounded, elliptical shale clasts (Figure 2-4) have no preferred orientation. Additionally, they are often associated with poorly-sorted, coarse sandstone or pebble conglomerate beds that are typically 1-2 meters thick. The lack of grading and sorting together with the random orientation of the shale clasts indicates that flow conditions were dominated by debris flow (Leeder, 1982, p. 81). In most cases, the shale rip-up clasts are located at the base of a coarse sandstone bed (stations 102, 133), or less commonly, at the top of a coarse-grained sandstone bed (station 115). In summary, shale rip-up clasts are found in coarse sandstone beds along the banks of the Rogue River across from the town of Galice, as well as along McKnobe Creek, and along Grave Creek. These structures are interpreted as indicators of paleochannels in an upper or mid-fan environment, that were filled by debris flow deposits.

Graded bedding in Galice siltstone, greywacke, and in the Rogue cherty tuffs is common at many localities in the study area. Graded beds together with scour marks, load casts, and current ripple cross-lamination were used as younging indicators. Graded beds were most often found at stations along the Rogue River from Galice to Almeda mine. Graded bedding is produced as a result of waning flow strength, as the mean grain size is proportional to the flow strength. Figure 4-1 shows an overturned graded bed from locality 133.

Small-scale ripple cross-lamination is evident in thin sandstone lenses interbedded with shale. The amplitudes of the ripples are on the order of 1-2 cm. Climbing ripple cross-lamination is found in silty-sandy lenses within shale beds at stations 23, 24, 50, 118, and 133. Figure 4-2 shows some climbing ripple cross-lamination from station 23. At station 24, small sandstone balls were noted (Figure 4-3). These sandstone balls are simply downbulges of sandy-silty material that are detached from the overlying laminated siltstone beds, due to diapiric injection of liquified mud from below. Figure 4-3 shows this feature at the level of the pocket knife. The internal laminations appear to have not been strongly deformed. According to Leeder (1982, p. 114), the shape of these structures and their wavelengths are controlled by density, viscosity, and the thickness of the layers. Sandstone balls are commonly associated with liquified flows.

Scour marks and bottom structures are well-developed in massive, generally overturned, greywacke beds. Scour or sole marks are cut by turbulent fluids that may have been aided by suspended and bedload grains and detritus carried by the flow. These bedforms are preserved by later infill of coarse-grained sands, and they record the sudden appearance of a turbidity current in an area formerly characterized by quiet water and mud and fine silt deposition. Sole marks include flute casts, longitudinal ridges (in the sense of Dzulynski and Walton, 1965) minor grooves and prod marks. The flute and related longitudinal ridges tend to show clustered assemblages. The flute casts are well-defined, narrow and parabolic, while the longitudinal ridges are elongate

Figure 4-1: Overturned graded bedding in a coarse pebbly conglomerate and greywacke from locality 133.

Figure 4-2: Climbing ripple cross-lamination in silty lenses of Galice shale from station 23. Dime for scale.

Figure 4-3: Small sandstone balls at the level of the pocket knife, most probably produced by detachment and diapiric injection of mud from below. From station 24.

Figure 4-4: Flute casts and longitudinal ridges on the underside of an overturned greywacke bed ($038^{O}/54^{O}E$) from locality 11.

troughs clustered together, all with the same general orientation (see Figure 4-4). Load casts are bottom structures found in association with liquified flows, produced in a similar manner to sand pillows, that is, by diapiric injection of liquified muds. A two-dimensional example of load casts was found at locality 50. Parting lineation is produced under upper flow regime conditions of turbulent flows, commonly found in Bouma B beds. Parting lineation indicates the paleoflow axis (Walker, 1978) and was identified at stations 124, 126, and 128.

4.3 Stratigraphic Section

A carefully measured stratigraphic section of Galice sandstones and shales extends over 200 meters at the type locality. This section is shown in Figure 4-5 and illustrates many of the characteristics of turbidite deposits, including scour marks, graded beds, coarse-grained sandstone beds with shale rip-up clasts, and a repeated thinning and fining-upwards sequence. Examination of the megasequences of greywacke beds reveals four thick packages of greywacke, each section greater than or equal to 20 meters thick.

4.4 Paleoflow Data

Paleocurrent flow directions were determined by use of bidirectional indicators such as longitudinal ridges, minor grooves, parting lineation, and by flute casts, which are unidirectional flow indicators. Measurements were taken along Grave Creek and at the type locality across from Galice. At both localities, most of the beds are overturned and they expose the scour marks in three dimensions, since the underlying shale has weathered out.

Paleoflow data are presented in the rose diagram of Figure 4-6 and these data demonstrate that flow was dominantly to the west and north, as determined from longitudinal ridges, grooves and flutes from Grave Creek and Galice. Each measurement represents the best determined reading from a single bed; thus measurements taken from

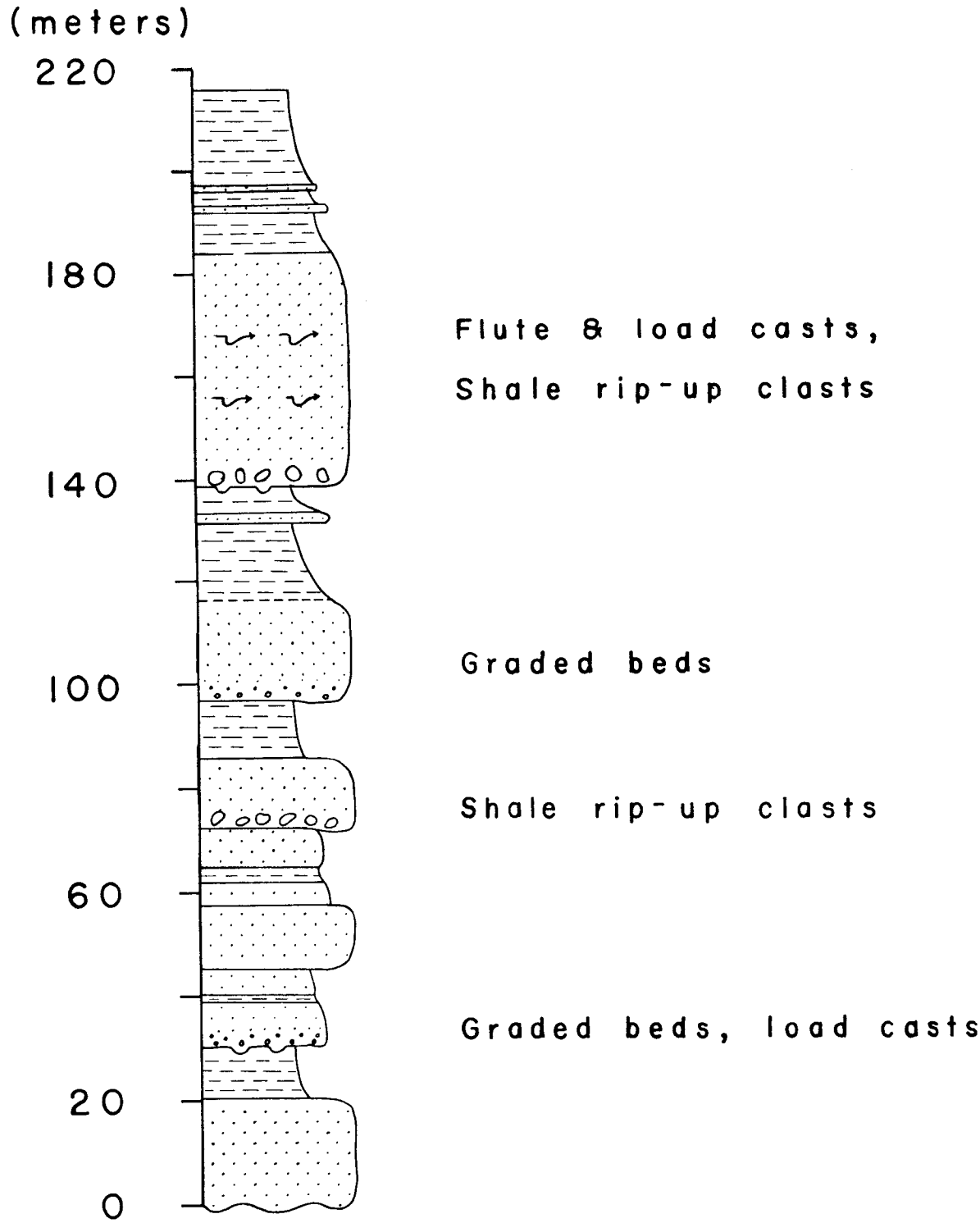

Figure 4-5: Stratigraphic section of one continuous outcrop located along the eastern bank of the Rogue River across from the hamlet of Galice, within the type section of this unit.

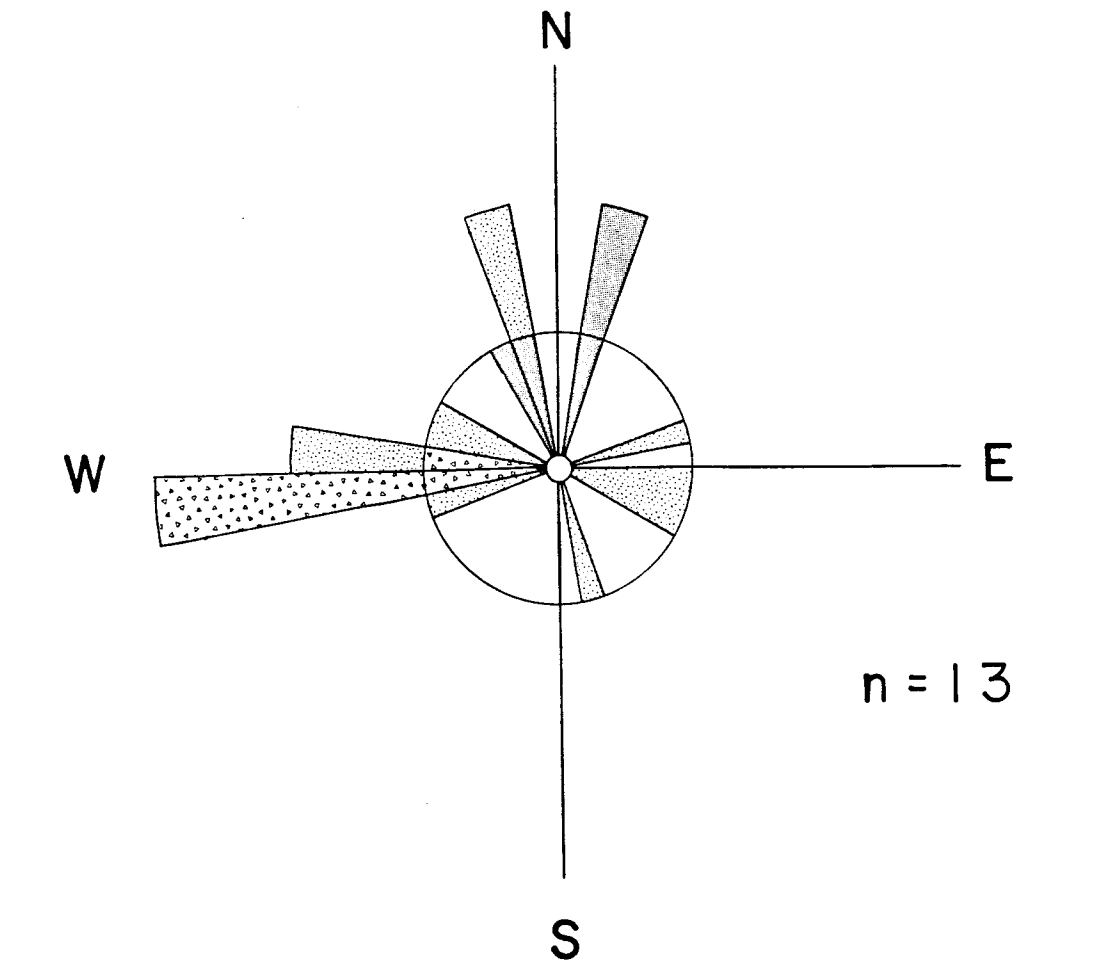

Figure 4-6: Rose diagram summarizing corrected paleoflow data from the Grave Creek and Galice localities.

the bases of thirteen different beds with good scour marks are presented in Figure 4-6. The original measurements for each of these scour marks were corrected for local folding effects and overturned bedding. The scour marks were restored to their original orientation. The corrected data are presented in Appendix II. It should be noted that *if* the type Galice has rotated *90° clockwise* due to oroclinal bending as suggested by Bogen's study (*see* Chapter 1.6), then all of the paleocurrent directions presented in this section should probably be rotated approximatedly 90° in an *anti-clockwise* direction (Harper, personal communication, 1988). According to G. Harper (personal communication, 1988) later effects due to possible Cretaceous tilting/folding do not substantially alter Bogen's paleomagnetic data or results.

The best hypothesis that accounts for the 90° difference in observed paleoflow directions is that the primary flow was directed northward or westward, with flow towards the west or north by longitudinal turbidity currents that paralleled the margin. This 90° difference in paleoflow direction is a common occurrence on many modern day submarine fans (Nelson and Nilsen, 1974). Turbidity currents are believed to start by the slumping of sediments along the flanks of a trough, and later after the channel and fan are built, turbidity currents turn and flow along the axis of the depression.

In this scenario, the Galice appears to represent detrital material shed from an uplifted, eroding continental margin to the east, which was periodically delivered to a deep ocean basin, as indicated by the abyssal trace fossils (Chapter 2). Presumably, this detritus was derived from and deposited near an active arc, as the Galice greywacke is volcanic-rich. Snoke (1977), Harper (1980a, 1983), Saleeby et al. (1982) and Harper and Wright (1984) have suggested that the likely sources of detritus in Galice sandstones are older terranes of the Klamath Mountains. Triassic and Jurassic chert and argillite are common rock types of the western Paleozoic and Triassic belt, and the Western Hayfork terrane is the proposed remnant arc, located in the southern part of the Klamath Mountains (*see* discussion in Chapter 3.1).

Other possible hypotheses that could account for the calculated differences in paleoflow direction include the following: (1) stratigraphic variation, from a probable lower section (type Galice) to a probable higher stratigraphic section (Grave Creek localities) with a concomitant change in source area of sediment supply (indicated from the paleoflow directions), or (2) abandonment and change in channel orientation, such that the suprafan lobes that splay outwards from the major channel(s) change orientation over time.

CHAPTER 5: SEDIMENTARY GEOCHEMISTRY

5.1 Introduction

Shales make up at least 75% of most sedimentary basins (Johnston, 1987) and as much as 75% of the geologic record (Blatt, 1982), yet they remain poorly understood. Provenance studies of ancient terranes in the last few decades have emphasized transport mechanisms, petrology, and geochemistry of sandstones, rather than the analysis of fine-grained siltstones and mudstones. Mudstones in the past were usually described as interlaminated beds with little attention given to their internal characteristics (Gorsline, 1985). The rationale often given is that fine-grained sediments were difficult to study largely because of grain size (Stow, 1985).

Recently, however, interest in mudstones and siltstones has surged due to the realization that mudrocks have lower permeabilities and hence, a greater potential for preserving accessory minerals and feldspars (Blatt, 1985). Shales represent fine-grained sediments of three possible facies groups, namely, turbidites, contourites, and pelagites/hemipelagites, the products of (respectively): gravity-driven turbidity currents, thermohaline and wind-driven bottom currents, and vertical settling through the water column (Stow, 1985). These latter two processes transport and deposit muds in a continuous manner over long periods of time, as opposed to the singular, episodic bursts of deposition by turbidity flows. Thus with the assumption that shales and fine-grained sediments represent a more continuous record of deposition than turbiditic sandstones, one could argue that shales have the potential of providing more information than sandstones. This information could reveal subtle changes over time in provenance, relief, weathering, sorting and diagenesis, which are the main factors that influence the final composition of a sedimentary rock (Bhatia, 1983).

The recent focus on shales is the result of the growing recognition that authigenetic and diagenetic processes dissolve sandstone detrital mineral assemblages, particularly by

intrastratal dissolution. These processes involve the formation of authigenic clay rims and coatings around detrital grains, authigenic pore-filling cements, and diagenetic calcite pore-filling cements (Galloway, 1974). Other burial diagenetic reactions form silicate overgrowths and replace rock fragments and plagioclase with chlorite and calcite (Galloway, 1974). Feldspars in sandstones are now viewed as unreliable indicators of ancient paleogeology (Blatt, 1985). Accessory minerals have been recognized as commonly unrepresentative of the detrital input to sandstones, and the more chemically unstable heavy minerals are absent from ancient sandstones (Blatt, 1985). As a consequence, heavy mineral studies on ancient sandstones have been nearly abandoned except for the most stable heavy minerals such as zircon (Blatt, 1985). Conventional methods of point-counting framework grains are now done only for those sandstones that are inferred to have been largely unaffected by dissolution (Shanmugam, 1985). Furthermore, it has been concluded by Morad (1984) (*see also* Galloway, 1974; Whetten and Hawkins, 1970) that greywacke matrices are largely of diagenetic origin, based on examination of recent North Atlantic depositional environments which suggests that sands are rarely found with abundant silt and clay matrices.

The upshot of these inferences and discoveries has been an increase in the number of studies examining shale deposits. Attempts at classifying fine-grained sediments by use of different parameters have been made by Dean and others (1985) and Bhatia (1985a). Dean and others (1985) classified mudrocks on the basis of the calcareous, siliceous, and biogenic components present. Bhatia (1985a) utilized the relative proportion of phyllosilicates to the total (phyllosilicates + quartz + feldspar) against the ratio of K_2O to Na_2O. Since about 1980, some workers (*e.g.*, Bhatia, 1983, 1985a, 1985b, 1985c; Roser and Korsch, 1985, 1986; and Bhatia and Crook, 1986) have attempted to employ geochemical analysis of sediments in order to disclose the original source of the grains and the general tectonic setting in which they were emplaced.

The overall intent of this chapter is to present geochemical data from the Galice shales and greywackes in the belief that it will help to delineate and add to the current on-going controversy linking geochemical parameters to a corresponding tectonic regime and source area. Major and trace element data of the Galice shales and greywackes obtained by XRF analysis will be set forth and discussed in Section 5.3, followed by presentation of rare earth element (REE) instrumental neutron activation analyses (INAA) of selected Galice shale and greywacke samples in Section 5.4.

5.2 Analytical Methods

Samples of type Galice shales were collected during field work (1985). Type Galice shale samples collected for geochemical analysis were chosen from nine stations located throughout the two NE-SW trending "belts" of type Galice that cross the study area (Figure 5-1). "Galice" shales overlie the Josephine ophiolite in a structurally higher thrust sheet to the south of the study area. Ten "Galice" shale samples were collected during the summer of 1986 by Ross Jones from outcrops near Cave Junction, Oregon and in areas south of the California-Oregon border (*see* Table 5-1). Type Galice and "Galice" shales chosen for analysis were black, very fine-grained shales that appeared unaffected by weathering and alteration. Hand-sized samples of these shales with approximate masses of 130 to 220 grams were ground up in a tungsten-carbide shatterbox at SUNY-Albany, from which 6-8 grams of each sample were sent to McGill University for XRF analysis. Approximately 6 grams of each sample were taken to Cornell University, where 0.30-0.53 grams were loaded into sealed high-purity silicon glass tubes, which were subsequently irradiated.

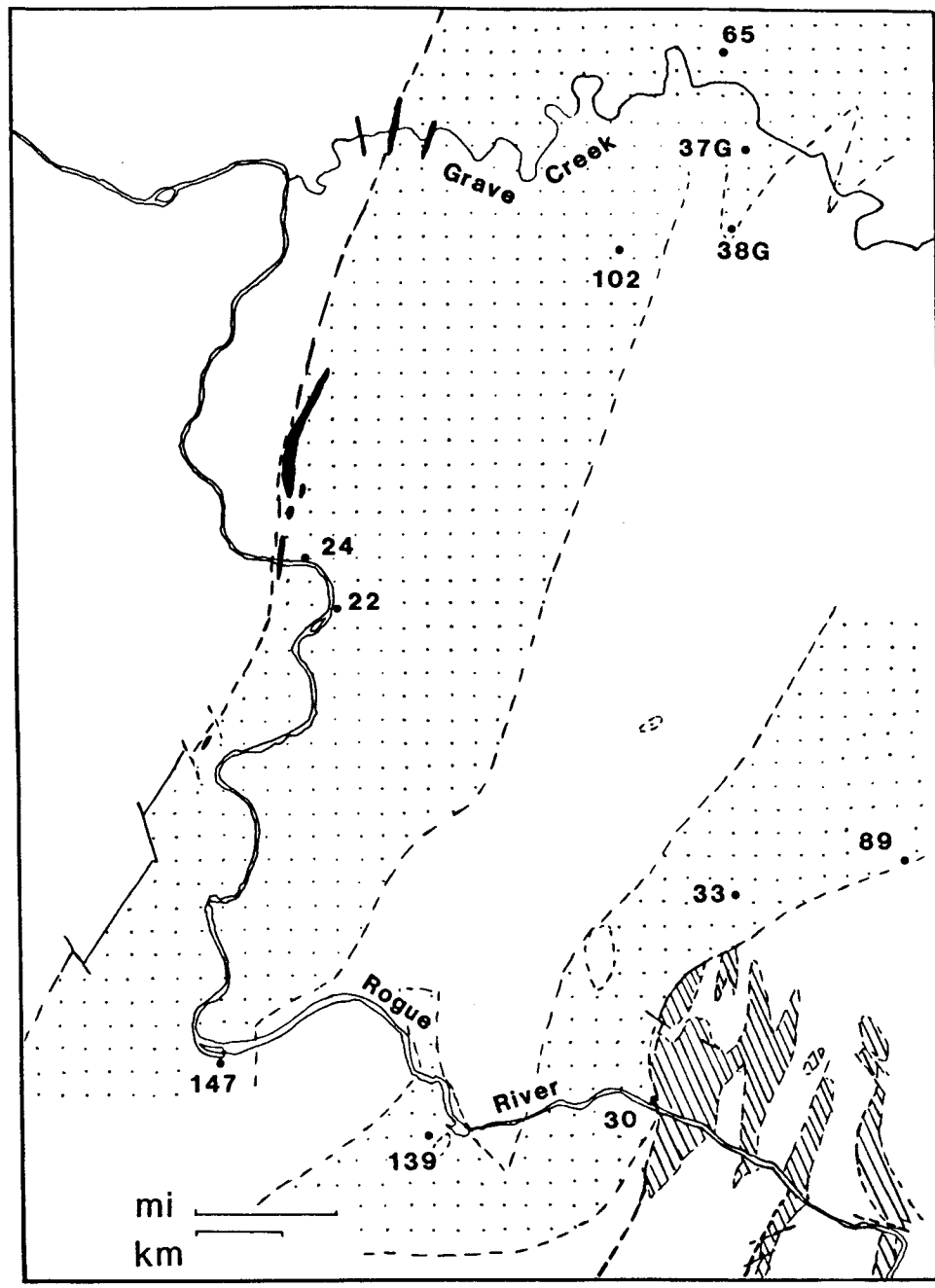

Figure 5-1: Localities of the type Galice shales and greywackes (37G, 38G) analyzed by x-ray fluorescence for major and trace element abundances. The type Galice is shown by the stippled pattern.

Table 5-1: Sample localities of "Galice" Formation Near Cave Junction, Oregon
G1= 0.5 km east of Kerby, Oregon on Holton Creek Road
G2= Along the West Fork of the Illinois River, 2.25 km south of Pomeroy Dam
G3= Northeast of Kerby, Oregon, 2.5 km east of U.S. Route 199, 2.5 km due south of Reeves Creek Road
G4= Along Cheney Creek Road, 3.2 km south of Wilderville, Oregon
G5= Along Sanger Peak Road, 3.2 km north of the California-Oregon border
G6= 0.5 km north of Pomeroy Dam, east bank of the West Fork of the Illinois River
G7= South of Kerby, Oregon 0.75 km and approximately 0.5 km east of U.S. Route 199
G8= Along Knopki Creek Road 7.2 km south of the California-Oregon border
G9= 0.25 km west of Pomeroy Dam on West Road
G10= Along Oregon Mountain Road, 1.6 km south of the Oregon-California border

Table 5-1: Sample localities of the "Galice" Formation to the south of the study area, from which samples were analyzed by x-ray fluorescence for major and trace element abundances.

5.3 Major and trace element data

The objectives of geochemical analysis of the Galice shales are twofold: (1) to characterize the components and sources of the type Galice shales; and (2) to compare these results with those obtained on the "Galice" shales that overlie the Josephine ophiolite to the south of the study area. It is important to discover if in fact these two units share the same geochemical signatures so as to warrant the inclusion of the "Galice" with the type Galice. Both Galice units contain *Buchia concentrica* (Sowerby) and show similar greywacke petrography. This was considered to be compelling evidence for correlation of the two Galice units by Cater and Wells (1953), and more recently by Harper and Wright (1984). However, Pessagno and Blome (in press) disagree. They are of the opinion that the sedimentary succession (*i.e.*, volcanopelagic succession and Galice *sensu lato*) above the Josephine ophiolite at Harper Locality 1 is not lithostratigraphically equivalent to that of the type Galice. They found thin-bedded layers or lenses of pelagic limestone in the volcanopelagic succession and Galice *sensu lato* which are not found anywhere in the type Galice. Pessagno and Blome (in press) reasoned that although the type Galice and "Galice" show a genetic relationship on a broad scale, they are not equivalent units.

X-ray fluorescence analysis of nine type Galice shales, two type Galice greywackes, one standard (SCo-1), and ten "Galice" shales from around Cave Junction, Oregon was performed by Dr. S.T. Ahmedali of McGill University. Standard x-ray fluorescence analysis procedures were followed on fused beads such that all iron was oxidized into the +3 state. The localities of the type Galice samples are shown in Figure 5-1, where the type Galice Formation is stippled and the serpentinite bodies are hatchured. The localities of the "Galice" shales near Cave Junction, Oregon are enumerated in Table 5-1.

Tables 5-2 and 5-3 list the original data of the Galice and "Galice" samples with major element abundances given in terms of weight percent, and trace element

	Major and Trace Element Data(XRF) Type Galice Shales and Greywackes												
	22	24	30	33	65	89	102	139	147	SCo-1	SCo-1*	37G	38G
SiO2	60.57	62.41	63.95	60.23	63.72	62.95	61.95	66.21	63.49	63.03	62.81f	65.77	73.57
TiO2	0.80	0.72	0.71	0.80	0.72	0.79	0.82	0.60	0.70	0.58	0.61 f	0.71	0.76
Al2O3	17.49	17.12	15.86	18.29	16.29	17.15	16.93	13.35	15.52	14.09	13.81f	16.75	11.26
Fe2O3	8.24	7.27	6.60	7.91	7.53	6.99	7.33	7.37	7.49	5.31	5.24 f	5.8	6.32
MnO	0.16	0.06	0.07	0.07	0.03	0.08	0.02	0.09	0.04	0.05	0.060f	0.02	0.02
MgO	2.49	2.70	3.03	2.60	2.41	2.82	2.87	2.71	3.29	2.76	2.33f	1.92	2.13
CaO	0.76	0.70	0.64	0.14	0.29	0.33	0.33	1.66	0.54	2.61	2.56 f	0.02	0.02
Na2O	2.18	2.00	2.21	0.84	1.59	1.78	2.24	1.26	1.99	0.96	0.78 f	1.08	0.37
K2O	2.23	2.32	2.80	2.49	2.01	2.56	2.47	1.84	1.85	2.79	2.65f	2.06	1.29
P2O5	0.30	0.30	0.12	0.14	0.20	0.19	0.21	0.61	0.36	0.18	0.198f	0.08	0.12
V	190	180	197	196	200	180	200	174	213	119	138f	142	156
Cr	112	101	110	104	100	125	148	85	120	65	75 ± 5m	198	281
Ni	54	60	47	85	50	23	75	48	39	19	29 f	50	81
Ba	638	584	856	756	439	726	674	494	597	519	571 ± 115m	635	385
Zr	159	152	145	178	143	173	176	131	144	173	164 ± 24 m	144	174
Y	31	27	24	34	27	36	28	30	25	25	22m	29	12
Sr	147	135	172	86	117	171	105	116	114	169	193 f	60	42
Rb	70	71	86	83	61	84	71	54	53	104	122 f	52	39
Pb	12	15	20	16	13	19	17	12	13	33	31 ± 5 m	12	14
LOI	5.32	5.07	4.26	6.75	5.47	4.72	5.26	4.13	5.05	8.02	---	6.13	4.47
TOTAL	100.65	100.77	100.40	100.38	100.32	100.48	100.56	99.92	100.43	100.47	91.05	100.46	100.43

* Cody Shale analysis from: fFabbi and Espos (1976);mMcLennan and Taylor (1980)

Table 5-2: X-ray fluorescence analyses of type Galice shale and greywacke powders that were prepared as pressed pellets. Detection limit for major elements is 0.01 wt. %. Total iron is reported as Fe_2O_3. Trace element abundances are reported in parts per million, with a detection limit of 5 ppm. Analyses were performed by Dr. S.T. Ahmedali of McGill University Geochemical Laboratories.

Major and Trace Element Data (XRF)
"Galice" shales near Cave Junction, OR

	G1	G2	G3	G4	G5	G6	G7	G8	G9	G10
SiO2	62.21	61.30	63.24	62.22	66.01	62.12	61.58	68.76	67.42	61.06
TiO2	0.77	0.77	0.84	0.94	0.76	0.77	0.87	0.62	0.59	0.87
Al2O3	17.17	15.90	18.52	19.23	15.29	16.06	17.49	14.05	14.16	18.55
Fe2O3	5.02	8.01	5.11	5.86	7.99	7.99	6.49	6.17	6.95	5.75
MnO	0.02	0.04	0.01	0.04	0.06	0.04	0.03	0.03	0.05	0.02
MgO	1.91	2.70	2.07	2.86	2.81	2.79	2.68	2.38	2.21	2.00
CaO	0.33	0.61	0.30	0.01	0.16	1.03	0.36	0.20	0.42	0.06
Na2O	1.30	1.61	0.72	<0.01	0.64	1.05	0.03	1.65	1.84	0.27
K2O	3.68	2.86	4.00	3.83	2.49	2.78	3.47	2.11	1.84	3.74
P2O5	0.18	0.21	0.02	0.09	0.21	0.22	0.18	0.16	0.20	0.18
V	177	159	210	252	157	170	206	154	106	220
Cr2O3	145	161	189	252	181	164	179	162	161	222
Ni	67	60	57	60	81	77	63	40	66	53
BaO	1060	872	1376	1660	990	846	1031	835	660	1370
Zr	157	169	180	181	173	170	166	141	143	178
Y	26	26	29	18	26	28	22	14	18	40
Sr	89	95	90	72	83	122	82	92	121	51
Rb	125	88	139	124	77	92	112	68	57	123
Pb	<5	11	31	27	34	35	25	34	32	34
LOI	7.16	5.75	5.43	5.42	4.26	5.70	6.08	3.86	4.46	7.76
TOTAL	99.88	99.89	100.29	100.69	100.81	100.68	100.40	100.12	100.23	100.45

Table 5-3: X-ray fluorescence analyses of "Galice" shale rock powders. Detection limit for major elements is 0.01 wt. % and 5 ppm for trace elements. Total iron is reported as Fe_2O_3.

concentrations listed in parts per million. Rock powder of the U.S.G.S. standard SCo-1 was included along with the Galice samples as a standard. The Cody Shale is an Upper Cretaceous, medium dark grey marine shale with thin, lighter-colored silty laminations (Schultz *et al.*, 1976). Other U.S.G.S. shale standards were considered unsuitable since the Green River shale (SGR-1) has a high volatile content (>40% weight loss when ignited) (McLennan and Taylor, 1980), and the Holocene Gulf of Maine marine mud (MAG-1) contains a significant quantity of NaCl (Manheim *et al.*, 1976). Table 5-2 compares the SCo-1 XRF analysis by Ahmedali with published analyses from Fabbi and Espos (1976) and McLennan and Taylor (1980). Analyses of two type Galice greywackes (37G, 38G) are included in this table in order to characterize the elemental composition of the sandstone on a first-order basis.

Tables 5-4 and 5-5 list recalculated major and trace element abundances for the two shale groups, after removal of volatiles (i.e., LOI) and CaO. These data are used in comparisons of immobile elements that are presented later in this section. Table 5-6 presents the mean values ($\pm$ 1σ) of the major and trace element abundances. In general, the two sets of analyses appear somewhat similar, with slight differences observed in the ranges for most elements.

Noticeable differences are seen in Mn, Mg, Na, K, Ba, Sr, and Rb concentrations in the mean shale values. However, all elemental abundances overlap at the 2σ level. Of these elements, the alkalies Mg, Na, and K, as well as the elements Sr and Rb are potentially mobile elements. These elements are highly soluble, as seen in Figure 5-2. Figure 5-2 plots log τ (residence time) against log K_y^{sw} of seawater (average upper continental crust water-rock partition coefficient), modified after Turner *et al.* (1980). The mobile elements listed above plot in the upper right hand corner, as high residence times indicate highly soluble elements. Conversely, elements with low solubilities in sea water have low residence times and are usually immobile during diagenesis.

Volatile- and CaO-free XRF Data											
Type Galice shales										Type Galice greywackes	
	22	24	30	33	65	89	102	139	147	37G	38G
SiO2	64.33	65.97	67.15	64.60	67.43	66.18	65.46	70.86	67.28	69.89	76.86
TiO2	0.85	0.76	0.74	0.86	0.76	0.83	0.87	0.64	0.74	0.75	0.79
Al2O3	18.57	18.10	16.65	19.62	17.24	18.03	17.89	14.29	16.45	17.80	11.76
Fe2O3	8.75	7.68	6.93	8.48	7.97	7.35	7.75	7.89	7.94	6.16	6.60
MnO	0.16	0.06	0.07	0.07	0.03	0.08	0.02	0.09	0.04	0.02	0.02
MgO	2.64	2.85	3.18	2.79	2.55	2.96	3.03	2.90	3.49	2.04	2.22
Na2O	2.32	2.11	2.32	0.90	1.68	1.87	2.37	1.35	2.11	1.15	0.39
K2O	2.37	2.45	2.94	2.67	2.13	2.69	2.61	1.97	1.96	2.19	1.35
V	202.3	190.3	206.9	210.2	211.6	189.2	211.3	186.2	225.7	150.9	163.0
Cr	119.2	106.8	115.5	163.0	105.8	131.4	156.4	91.0	127.2	210.4	293.6
Ni	57.5	63.4	49.4	91.2	52.9	24.2	79.2	51.4	41.3	53.1	84.6
Ba	679.3	617.3	898.8	905.2	464.6	763.3	713.2	528.7	632.6	674.8	402.2
Zr	169.3	160.7	152.3	190.9	151.3	181.9	186.0	140.2	152.6	153.0	181.8
Y	33.0	28.5	25.2	36.5	28.6	37.8	29.6	32.1	26.5	30.8	12.5
Sr	156.5	142.7	180.6	92.2	123.8	179.8	110.9	124.1	120.8	63.8	43.9
Rb	74.5	75.0	90.3	89.0	64.5	88.3	75.0	57.8	56.2	55.3	40.7
Pb	12.8	15.9	21.0	17.2	13.8	20.0	18.0	12.8	13.8	12.8	14.6

Table 5-4: Volatile- and CaO-free type Galice shale and greywacke XRF data.

Volatile- and CaO-free XRF Data
"Galice" shales

	G1	G2	G3	G4	G5	G6	G7	G8	G9	G10
SiO2	67.56	65.78	67.08	65.79	69.06	66.59	65.82	71.67	70.87	66.23
TiO2	0.84	0.83	0.89	0.99	0.79	0.82	0.93	0.65	0.62	0.94
Al2O3	18.65	17.06	19.64	20.33	15.99	17.21	18.69	14.64	14.88	20.12
Fe2O3	5.45	8.60	5.42	6.19	8.36	8.56	6.94	6.43	7.30	6.24
MnO	0.02	0.04	0.01	0.04	0.06	0.04	0.03	0.03	0.05	0.02
MgO	2.07	2.90	2.19	3.02	2.94	2.99	2.86	2.48	2.32	2.17
Na2O	1.41	1.73	0.76	<0.01	0.67	1.12	0.03	1.72	1.93	0.29
K2O	4.00	3.07	4.24	4.05	2.60	2.98	3.71	2.19	1.93	4.06
V	192.2	170.6	222.6	267.1	164.2	182.2	220.0	160.2	111.3	237.6
Cr	107.5	118.0	136.7	182.3	129.7	120.1	119.6	115.4	115.5	164.2
Ni	72.7	64.4	60.4	63.6	84.7	82.5	67.3	41.6	69.3	57.2
Ba	1030.6	838.1	1305.9	1576.2	927.8	812.6	986.8	777.9	620.6	1325.2
Zr	170.5	181.4	190.8	191.9	181.0	182.2	177.3	146.6	150.2	192.2
Y	28.2	27.9	30.7	19.1	27.2	30.0	23.5	14.6	18.9	43.2
Sr	96.7	101.9	95.4	76.3	86.8	130.8	87.6	95.7	127.1	55.1
Rb	135.7	94.4	147.3	131.4	80.5	98.6	119.6	70.7	59.9	132.8
Pb	<5	11.8	32.9	28.6	35.6	37.5	26.7	35.4	33.6	36.7

Table 5-5: Volatile- and CaO-free "Galice" shale XRF analyses.

Mean values of Type Galice and "Galice" samples
Volatile- and CaO-free data

	Galice mean	Galice 1σ	"Galice" mean	"Galice" 1σ	Greywacke 37G	Greywacke 38G
SiO2	66.58	1.84	67.65	2.06	69.89	76.86
TiO2	0.78	0.07	0.83	0.11	0.75	0.79
Al2O3	17.43	1.44	17.72	1.98	17.80	11.76
Fe2O3	7.86	0.51	6.95	1.15	6.16	6.60
MnO	0.07	0.04	0.03	0.02	0.02	0.02
MgO	2.93	0.27	2.59	0.36	2.04	2.22
Na2O	1.89	0.47	0.97	0.69	1.15	0.39
K2O	2.42	0.32	3.28	0.80	2.19	1.35
V	203.7	12.3	192.8	42.8	150.9	163.0
Cr	124.0	22.2	130.9	22.9	210.4	293.6
Ni	56.7	18.6	66.4	11.8	53.1	84.6
Ba	689.2	141.9	1020.2	280.8	674.8	402.2
Zr	165.0	16.8	176.4	15.4	153.0	181.8
Y	30.9	4.1	26.3	7.6	30.8	12.5
Sr	136.8	28.8	95.3	21.0	63.8	43.9
Rb	74.5	12.3	107.1	28.9	55.3	40.7
Pb	16.1	2.9	27.9	11.8	12.8	14.6

Table 5-6: Mean values and 1 σ uncertainty for type Galice and "Galice" data.

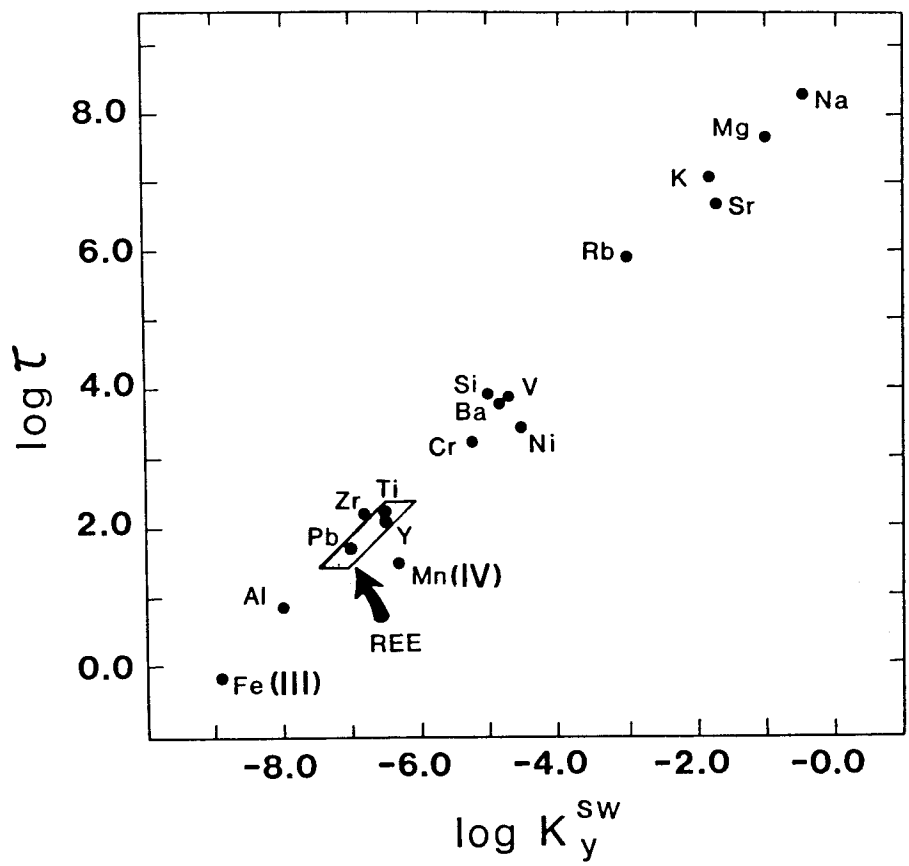

Figure 5-2: Plot of residence time, log τ versus water-rock partition coefficient, K_y^{SW}. Modified after Turner *et al.* (1980).

The elements Mn and Ba show differences in abundance between the mean values of type Galice and "Galice" shales. Possible explanations for the observed variation in Ba and Mn concentrations are many. The rate of accumulation of Ba is a function of latitude, as the maximum rate of accumulation occurs in the biologic high productivity zone due to scavenging of barium by organisms (Goldberg, 1958; Goldberg and Arrhenius, 1958). Manganese, on the other hand, is an element that is redox sensitive, changing valence state from +2 to +4 during oxidation, and in the +2 state it is highly soluble in pore water solutions of sediments. Determining factors of Mn abundance are the sedimentation rate, the diffusion of O_2, and the organic concentration of the sediment (Heggie *et al.*, 1987; deLange, 1986; Colley *et al.*, 1984). In short, absolute differences in abundances of individual elements can be attributed to multiple factors. It can be concluded that a comparison between the type Galice and "Galice" shale samples is more logically carried out by examination of the ratios of immobile elements, to better determine the geochemical behavior of these two groups of Galice sediments.

In order to carry out the aforementioned objectives, it will be necessary to first examine plots of immobile elements against other immobile elements, to see if diagenesis or other processes have affected their distribution. Second, immobile elements will be contrasted against other relatively immobile elements (*i.e.*, potassium) that are mobile only under certain conditions. Finally, two different pairs of elements will be examined that illustrate the sharp differences in geochemical behavior shown by the type Galice and "Galice" shales, which will shed some light as to the source rock(s) and components that have contributed to both shale units.

Figure 5-3 shows the plot of Al_2O_3 versus TiO_2 for both shale units. Both aluminum and titanium are immobile elements (Figure 5-2), and in this plot, show a strong positive correlation. These elements have low solubilities in pore fluids and hence are not usually fractionated by diagenetic processes. The distribution of immobile

Figure 5-3: Plot of Al_2O_3 versus TiO_2 for the type Galice shales and "Galice" shales. Volatile- and CaO-free data.

Figure 5-4: Plot of Zr versus Al_2O_3 for the type Galice shales and "Galice" shales. Volatile- and CaO-free data.

Figure 5-5: Plot of K_2O versus TiO_2 for the type Galice and "Galice" shales. Volatile- and CaO-free data.

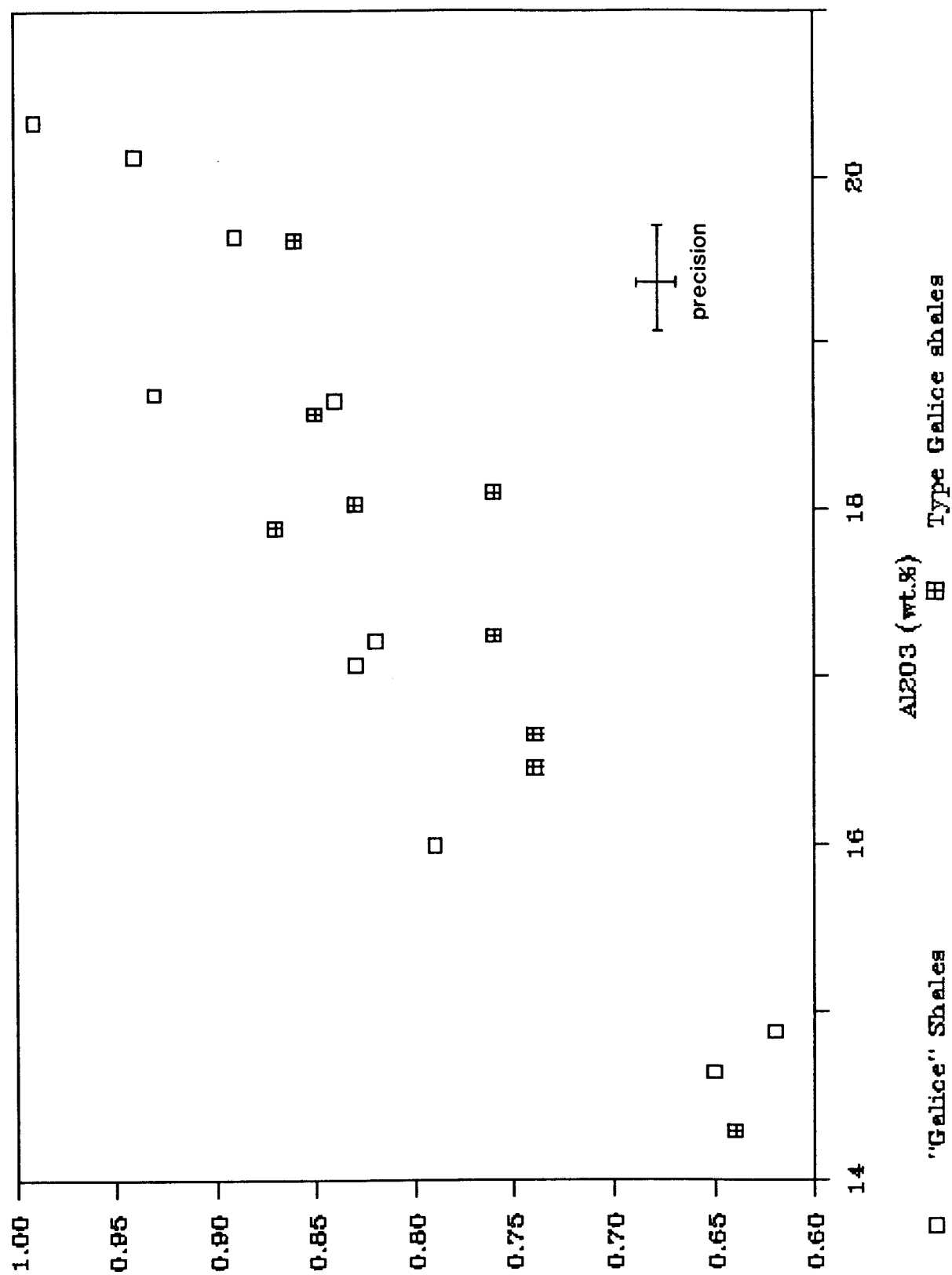
TiO2 (wt. %)
1.00
0.95
0.90
0.85
0.80
0.75
0.70
0.65
0.60
14
16
18
20
Al2O3 (wt.%)
precision
"Gelice" Shales
Type Gelice shales

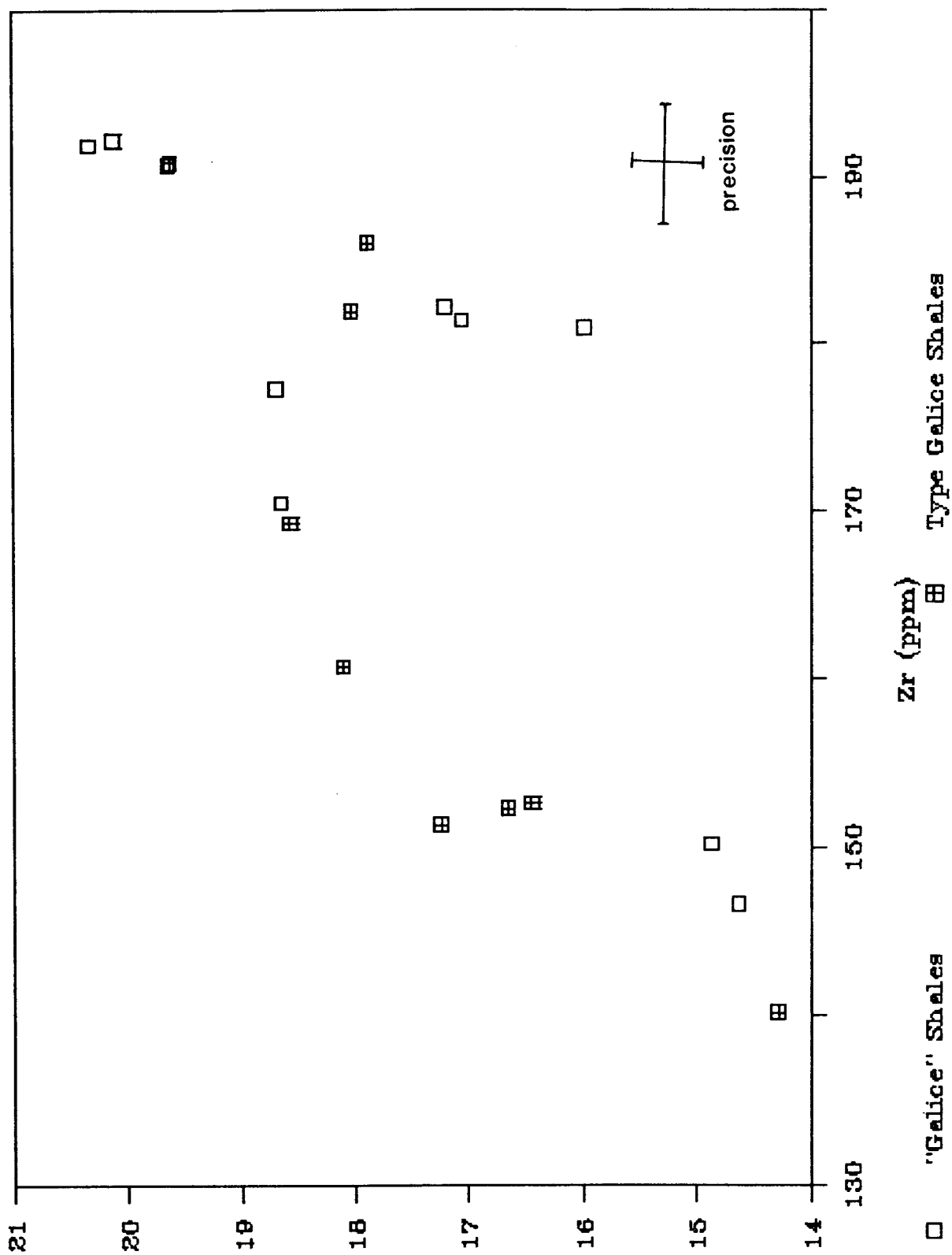
Al2O3 (wt. %)
21
20
19
18
17
16
15
14
130
150
170
190
Zr (ppm)
precision
"Galice" Shales
Type Galice Shales

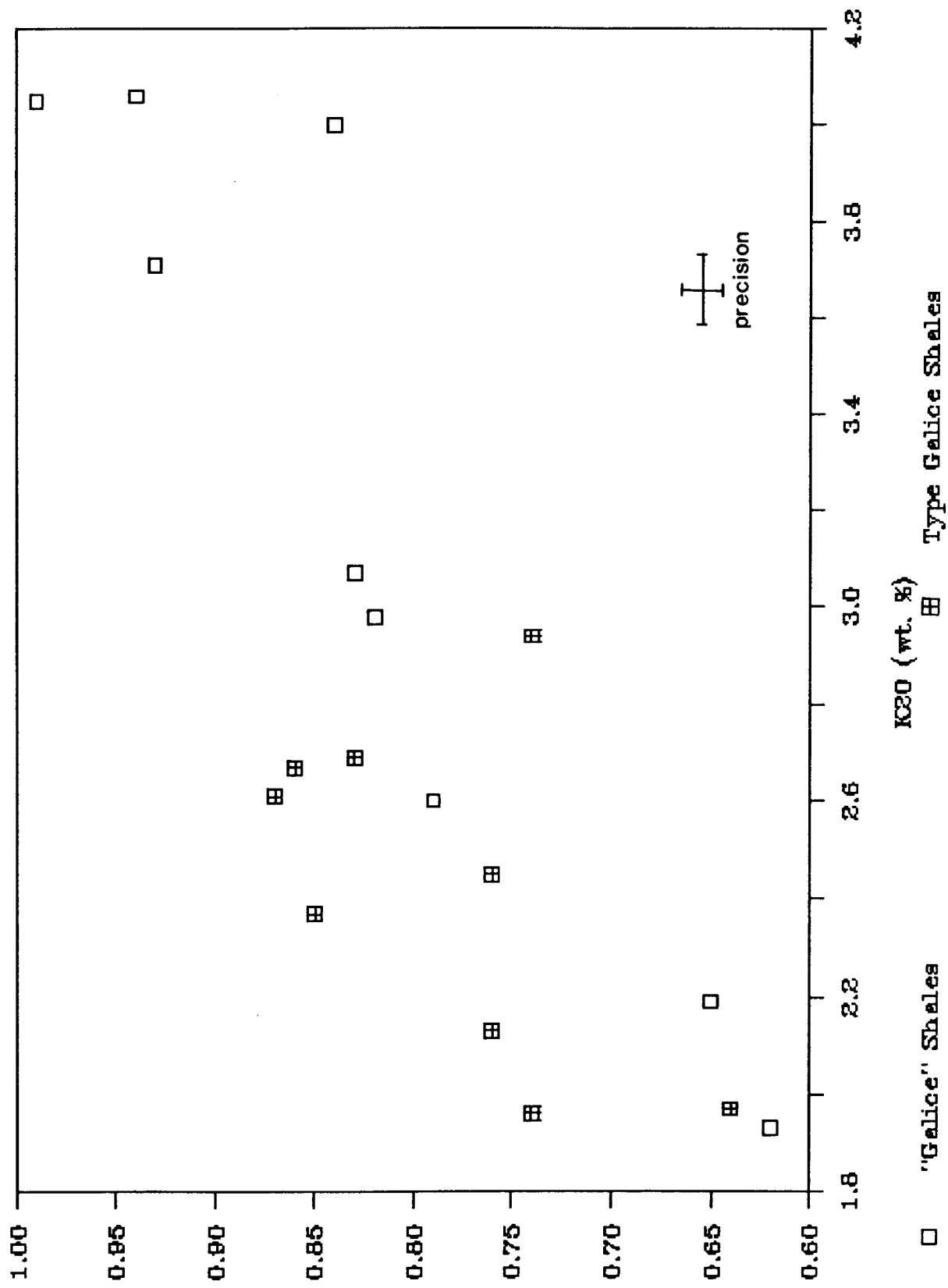
TiO2 (wt. %)
1.00
0.95
0.90
0.85
0.80
0.75
0.70
0.65
0.60
1.8
2.2
2.6
3.0
3.4
3.8
4.2
K2O (wt. %)
precision
"Galice" Shales
Type Galice Shales

elements can be affected in most cases only by physical parameters such as (a) sorting by wind or water and (b) changes in provenance.

Zirconium is another immobile element, and it has been compared to aluminum oxide (Figure 5-4). The type Galice shales show a fairly well-defined positive correlation of Zr versus Al_2O_3, while the "Galice" shales show a poorer correlation.

A comparison of K_2O versus TiO_2 in Figure 5-5 reveals a positive correlation that is fairly well-defined for the "Galice" shales, and poorly defined for the type Galice shales. In this case, it is important to consider the relative mobilities of K and Ti during chemical weathering and diagenesis. Potassium can be mobile (log τ is 7.1), but it is immobile if it is adsorbed onto the clay structure. Volcanic glasses tend to gain potassium from solution (*i.e.*, seawater) during devitrification that can lead to elevated K concentrations for marine shales having a significant volcanic component (*e.g.*, Ailin-Pyzik and Sommer, 1981; Böhlke *et al.*, 1980; Staudigel and Hart, 1983). Titanium is an immobile element (except in highly acidic solutions) that is unaffected by weathering or diagenesis. Thus, these two elements are assumed to be immobile in clays and one would predict a strong correlation in both plots. The fact that the type Galice shale plot does not show a good correlation indicates that at least three differentiable sedimentary components have produced this scatter on a two-dimensional plot. Multivariate analysis would probably delineate the other factor(s) producing the observed dispersal of data.

The positive correlation between potassium and titanium on the "Galice" shale plot establishes another important point. Potassium is an element primarily found in the mica group minerals, especially in illite, the chief constituent of many shales. Titanium is generally found in the clastic fraction, most notably in the detrital accessory minerals of rutile, sphene, and ilmenite. If variation in grain size of these shale samples was significant, one would expect a negative correlation between potassium and titanium, as the potassium concentration would be highest in the clay-size fraction, with titanium held mainly in the sand-size fraction. The exact opposite correlation is observed for the

"Galice" shales, from which it can be assumed that grain size (i.e., sorting) is not interfering in these analyses, and also not contributing to the observed trends.

In summary, the positive correlation in Figure 5-5 shown by the "Galice" shales must be produced by a factor other than grain size. It is inferred that either (1) the solubility or mobility of potassium has been affected, or (2) potassium concentrations have been elevated by the presence of volcanic glasses.

Figure 5-6 illustrates the plots of K_2O versus Al_2O_3 for the type Galice and "Galice" shales. Again, potassium is assumed to be immobile since it is adsorbed onto the clay structure, and aluminum is an immobile element. Both potassium and aluminum are common constituents of clay minerals, and a strong correlation is predicted for the black type Galice and "Galice" shales. The "Galice" shales near Cave Junction, Oregon verify this prediction, while the type Galice shales show a weaker correlation between K_2O and Al_2O_3.

A comparison of the immobile elements yttrium and aluminum reveals an unexpected outcome (Figure 5-7). Yttrium is commonly a component of clay minerals and accessory minerals. The type Galice shales show a positive correlation between these two immobile elements, except for one sample (#139) which is low in both Al and Y abundances. By contrast, the "Galice" shales near Cave Junction do not show any type of correlation between Y and Al and show a wide scatter. The evidence conveyed in these two plots is significant, as it implies that the two shales show different geochemical behaviors, most likely due to differing source regimes and constituents. It appears likely that in the north (type Galice), yttrium and aluminum concentrations are linked together (*i.e.*, both may be contained in clay structures), whereas to the south, yttrium and aluminum concentrations appear not to be correlated at all, suggesting a complex relationship between multiple variables does exist.

Figure 5-6: Plot of K_2O versus Al_2O_3 for the type Galice and "Galice" shales. Data are volatile- and CaO-free.

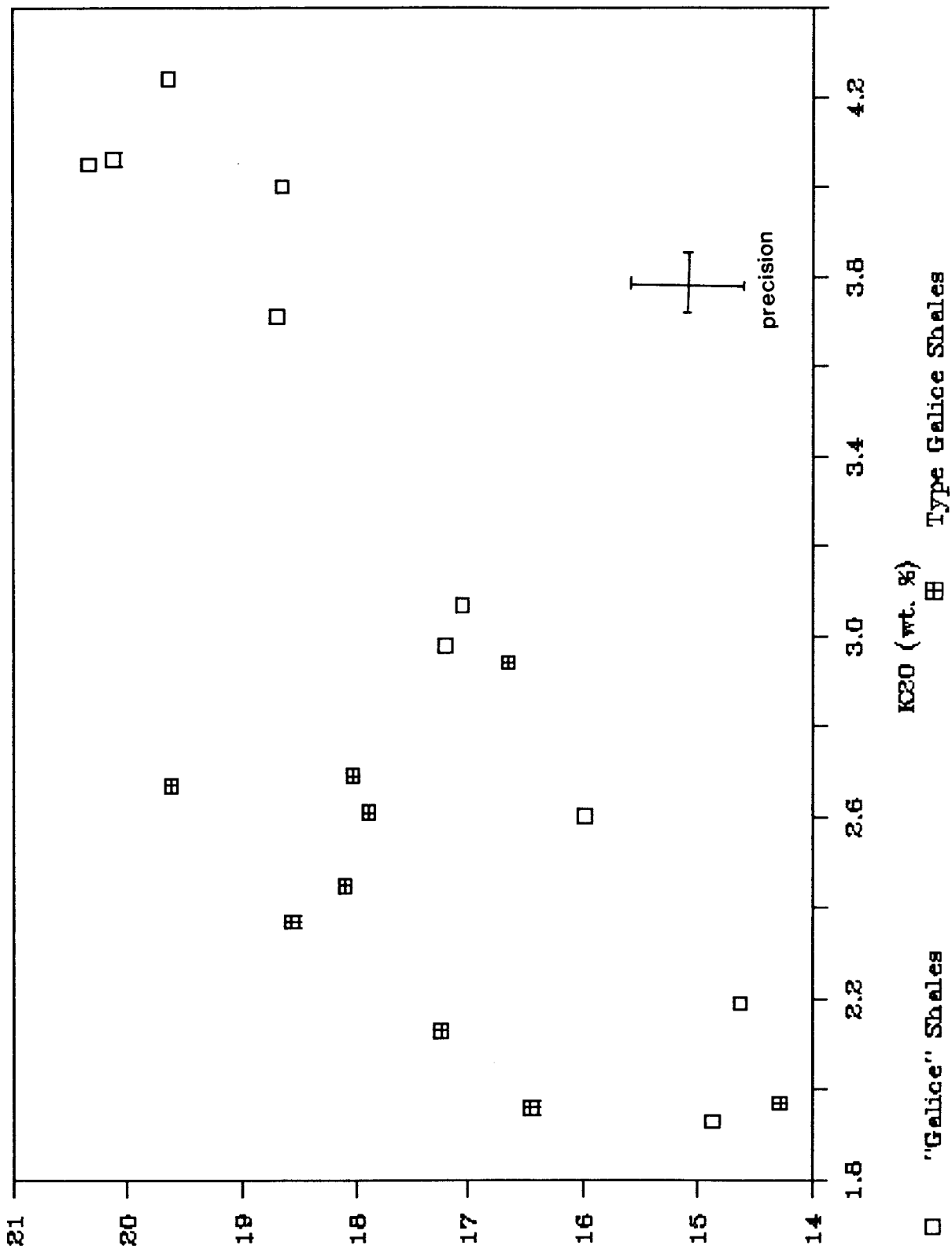
Al2O3 (wt. %)
21
20
19
18
17
16
15
14
1.8
2.2
2.6
3.0
3.4
3.8
4.2
K2O (wt. %)
precision
"Gelice" Shales
Type Gelice Shales

Figure 5-7: Plot of Y versus Al_2O_3 for the type Galice and "Galice" shales. Data are volatile- and CaO-free.

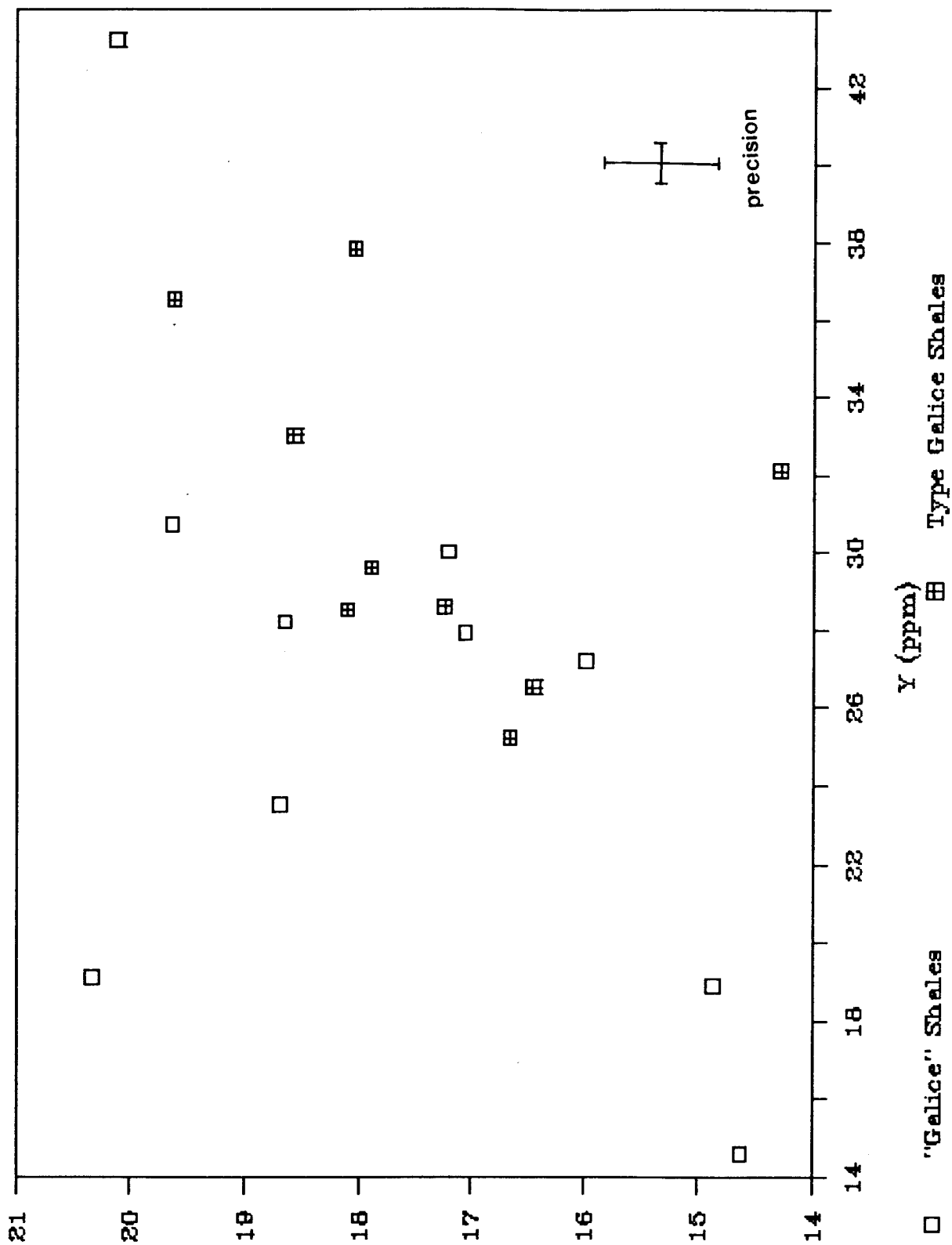
Al2O3 (wt. %)
21
20
19
18
17
16
15
14
14
18
22
26
30
34
38
42
Y (ppm)
precision
"Gelice" Shales
Type Gelice Shales

The plot of K_2O versus V is seen in Figure 5-8 for both sets of shale data. The source of vanadium in marine shales is thought to be from (1) V-rich marine organisms (such as ascidians), (2) preferential adsorption/reduction by organic constituents, or (3) volcanic ash (Premovic *et al.*, 1986; Goldberg and Arrhenius, 1958). A recent study of estuary data, however, suggests that the adsorption and complexation of vanadium by organic matter is a relatively unimportant process (Shiller and Boyle, 1987). Shiller and Boyle (1987) concur that vanadium behaves as a bioactive element linked to the distribution of phosphate, an indicator of a zone of high productivity.

Figure 5-8 conveys the fact that the elements K and V have different geochemical behaviors in the two Galice shale sets. The type Galice shales show a wide scatter of data points, with no clear positive or negative trend. On the other hand, the "Galice" shales near Cave Junction, Oregon show a well-defined, positive correlation between K and V. The inference is that *if* volcanic ash was a significant component at the time of deposition of the black shales, it would be indicated by elevated potassium concentrations and potassium would be positively correlated with vanadium derived from volcanic ash (Premovic *et al.*, 1986). This is indeed what is observed in Figure 5-8 for the "Galice" shales, although the problem with this deduction is the fact that vanadium can be attributed to multiple factors which can not be ruled out as contributing sources. The only sound conclusion drawn from these plots is that the type Galice shales show no correlation between the two elements K and V, indicating complex geochemical behavior. The "Galice" shales verify a fairly well-defined positive correlation between K and V.

Figure 5-8: Plot of K_2O versus V for the type Galice shales and "Galice" shales. Volatile- and CaO-free data.

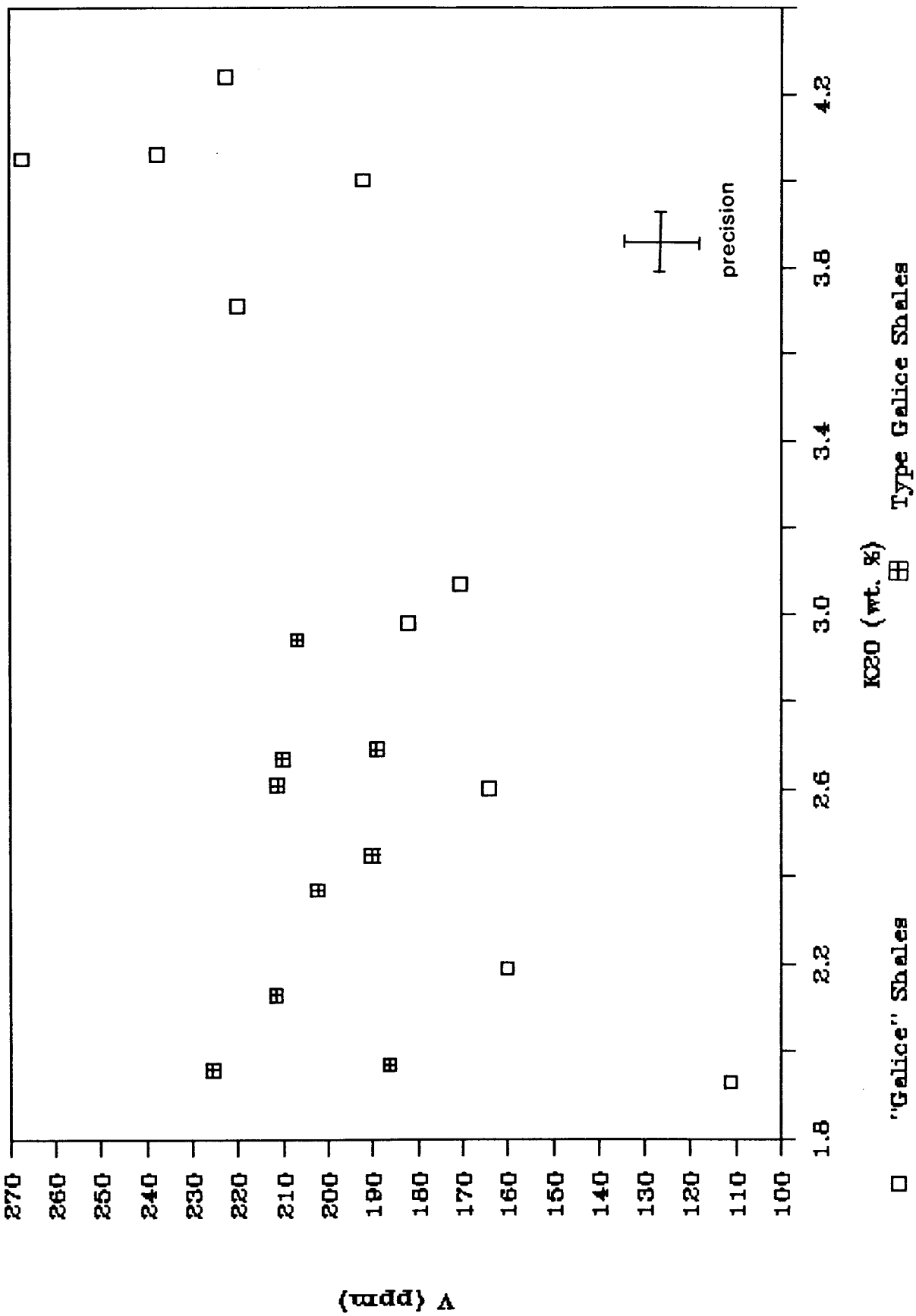
V (ppm)
270
260
250
240
230
220
210
200
190
180
170
160
150
140
130
120
110
100
1.8
2.2
2.6
3.0
3.4
3.8
4.2
K2O (wt. %)
precision
"Galice" Shales
Type Galice Shales

5.4 REE Studies

The rare earth elements (REE) are believed to fractionate by igneous rock-forming processes (Haskin, 1984), and in most common minerals, they are considered to be refractory, incompatible, immobile elements (Taylor and McLennan, 1985; Haskin, 1984; Boynton, 1984; McLennan and Taylor, 1980; Muecke *et al.*, 1979). The REE behave as a geochemically coherent group due to their (a) linear contraction of ionic radii with increasing atomic number and (b) common 3+ valence state. Thus, the relative abundances of REE in crustal rocks record the net-effects of primary differentiation by igneous processes of their constituent grains (Haskin, 1984). Shales, for example, are thought in most cases to represent the end-product of wide-scale sampling of the exposed crust, and to preserve a record of the upper crustal average REE pattern (McLennan and Taylor, 1980).

Sedimentary rocks with clay minerals have much higher concentrations of REE than carbonate or quartz-rich sandstones (Roaldset and Rosenqvist, 1971; Haskin *et al.*, 1966). The bulk of REE are contained in clay minerals, while minor amounts are contained in accessory minerals, such as monazite and apatite. Clays develop and acquire REE by surface adsorption during weathering (Roaldset, 1975), a reaction favored under neutral or basic conditions in the weathering profile (Cullers *et al.*, 1979). The clays in this manner inherit the average REE distributions of their sources (Clark, 1984).

Although the rare earth elements generally appear unaffected by diagenesis (Chaudhuri and Cullers, 1979) and metamorphism (Frey *et al.*, 1968; Muecke *et al.*, 1979), some mobility may occur (Elderfield and Sholkovitz, 1987). During sedimentary processes such as erosion and transport, the REE tend to be fixed. Mobilization is most likely to occur during weathering (Fleet, 1984). Some studies have suggested that during intense chemical weathering under strongly acidic conditions, REE are mobile

(Chaudhuri and Cullers, 1979; Balashov *et al.*, 1964), and are easily removed from clays (Elderfield and Sholkovitz, 1987; Brown *et al.*, 1955).

REE are relatively immobile elements with short residence times (Figure 5-2), typically on the order of 100-200 years (Taylor and McLennan, 1985). Minor amounts of REE go into solution, so that only a few percent of all the REE that enter the oceans are ever in the dissolved state (Martin *et al.*, 1976). Elderfield and Greaves (1982) have shown that REE are scavenged and regenerated about five times before they are buried. They suggest that a longer residence time of approximately 2,500 years may be more accurate. Thus, a small percentage of the REE go into solution and are biogenically recycled. Surface waters tend to be enriched in dissolved REE relative to the water column, most likely due to the presence of calcareous plankton tests that preferentially remove the light rare earth elements (LREE) from seawater (Fleet, 1984), or else due to aeolian contributions (Elderfield and Greaves, 1982). Elderfield and Greaves (1982) found evidence of deep-water enrichment in REE near the ocean floor. They attributed this phenomenom as the result of transport of REE to the deep ocean.

Comparison of crustal rocks that have experienced igneous differentiation with rocks that have not undergone igneous differentiation is the best method of determining relative fractionation and for the identification of source materials. Type 1 carbonaceous chondrites (C1) are the best available records of primordial abundances of the solar system. Comparison of the elemental abundances in these meteorites against the composition of selected sedimentary rocks reveals the relative amount of differentiation that the source rock(s) has(have) undergone, as well as the extent to which oxidizing or reducing conditions prevailed (Haskin, 1984). Normalized plots provide a good method of finger-printing the source rocks by detecting whether or not a sample has a typical REE content (*i.e.*, average REE of the upper crust), or if there is a relative enrichment or deficiency in certain elements (Fleet, 1984). The relative abundances of REE in most shales is very similar, while the absolute concentrations of

REE may vary. Typically, shale samples show small Eu depletions and REE patterns that are enriched in the LREE's with respect to the HREE's when normalized to C1 chondrites.

In this study, five samples of type Galice and "Galice" shales, one type Galice greywacke, and one standard (SCo-1) were analyzed by instrumental neutron activation analysis (INAA) at Cornell University. The type Galice shales are samples taken from localities 22, 24, and 147. The "Galice" shale samples chosen for analysis are G1 and G2. The INAA data are presented in Table 5-7 on a CaO- and volatile-free basis. This removal of volatiles and CaO was calculated for each of the samples and accordingly, this factor was multiplied by the original Fe_2O_3 values. The "dry" Fe_2O_3 values are presented in Table 5-7 which were used to calculate the REE and trace element concentrations by the INAA reduction program.

Analysis and irradiation of the samples were performed at Cornell's TRIGA reactor with reduction of the data completed at Snee Hall during the fall of 1986. The run including sample #147 was re-reduced during March, 1988, due to a minor entry error. Good results from neutron activation analysis are contingent on accurately weighed samples sealed in high-purity silicon tubing that are then exposed to a high flux of neutrons in a reactor core. This flux of neutrons produces transmutation of the naturally-occurring stable isotopes into synthetic radioactive isotopes in the rock powder. The abundances of these synthetic isotopes are quantitatively determined by a detector that records the distinct energies given off by the induced gamma rays.

The data presented in Table 5-7 are listed along with the error or uncertainty values calculated by the reduction program for each element. In general, the uncertainty of the REE and trace element abundances is very low, which indicates the high reliability of these data.

The INAA rare earth data for each of the samples were normalized relative to Type I carbonaceous chondrite abundances of Evensen *et al.* (1978) in Table 5-8. Both the

	INAA Data (CaO-free, volatile-free) Type Galice Shale		"Galice" Shale			Galice Greywacke	Cody Shale
	22	24	147	G1	G2	38G	SCo-1
La	31.02 ± 0.44	29.08 ± 0.47	25.48 ± 0.34	37.51 ± 0.70	30.76 ± 0.48	25.19 ± 0.39	38.15 ± 0.66
Ce	62.64 ± 1.42	60.26 ± 1.31	50.86 ± 1.92	70.23 ± 1.55	63.52 ± 1.33	45.36 ± 1.17	73.21 ± 1.42
Nd	33.60 ± 4.54	31.85 ± 4.93	24.67 ± 2.72	34.72 ± 5.46	31.49 ± 4.96	18.66 ± 3.65	32.62 ± 4.57
Sm	7.71 ± 0.09	7.02 ± 0.10	6.28 ± 0.07	7.41 ± 0.12	7.01 ± 0.09	4.16 ± 0.06	7.26 ± 0.11
Eu	1.53 ± 0.03	1.42 ± 0.03	1.68 ± 0.05	1.41 ± 0.03	1.42 ± 0.03	0.89 ± 0.02	1.33 ± 0.03
Tb	1.15 ± 0.07	1.09 ± 0.10	0.93 ± 0.14	0.99 ± 0.12	1.05 ± 0.11	0.47 ± 0.07	0.91 ± 0.05
Yb	4.32 ± 0.42	3.76 ± 0.40	3.39 ± 0.33	4.19 ± 0.45	3.66 ± 0.40	2.15 ± 0.27	3.26 ± 0.36
Lu	0.54 ± 0.03	0.47 ± 0.03	0.47 ± 0.02	0.55 ± 0.03	0.49 ± 0.03	0.28 ± 0.02	0.43 ± 0.03
Hf	4.69 ± 0.20	4.41 ± 0.19	4.68 ± 0.30	5.06 ± 0.21	5.78 ± 0.19	5.43 ± 0.17	5.72 ± 0.18
Sc	23.89 ± 0.19	23.56 ± 0.19	27.20 ± 0.36	26.19 ± 0.25	21.44 ± 0.17	20.28 ± 0.17	14.98 ± 0.14
Ta	0.90 ± 0.08	0.95 ± 0.09	0.61 ± 0.09	1.16 ± 0.10	0.87 ± 0.09	0.67 ± 0.07	1.18 ± 0.10
Cr	153.19 ± 3.46	134.82 ± 3.13	150.31 ± 4.85	128.08 ± 3.45	152.54 ± 3.22	393.58 ± 5.03	98.98 ± 2.83
Th	9.83 ± 0.41	9.46 ± 0.39	6.91 ± 0.25	13.29 ± 0.54	10.41 ± 0.43	6.59 ± 0.29	12.70 ± 0.51
U	3.68 ± 0.62	3.40 ± 0.59	2.67 ± 0.23	4.18 ± 0.72	3.90 ± 0.67	2.94 ± 0.51	4.97 ± 0.83
Co	20.94 ± 0.36	21.21 ± 0.35	10.21 ± 0.33	8.67 ± 0.24	27.29 ± 0.41	15.56 ± 0.33	14.57 ± 0.28
Ni	75.57 ± 14.55	89.66 ± 14.11	65.53 ± 20.17	49.01 ± 13.81	93.99 ± 14.27	109.58 ± 14.11	33.80 ± 11.05
Cs	4.38 ± 0.28	5.07 ± 0.29	2.34 ± 0.31	12.24 ± 0.58	8.42 ± 0.42	1.32 ± 0.17	9.97 ± 0.48
Fe2O3	8.75	7.68	7.94	5.45	8.60	6.60	5.93

Table 5-7: Volatile- and CaO-free INAA data for the type Galice shales and greywacke, "Galice" shales (G1 and G2), and the USGS standard, SCo-1. Analyses performed at Cornell University's TRIGA reactor. All analyses are corrected for flux and counting geometry relative to GSP1 KAY. Rare earth element abundances are based on each sample's total iron content, expressed as Fe_2O_3.

	SAMPLE/CHONDRITE						
		Galice		"Galice"		Galice	Cody
	22	24	147	G1	G2	38G	SCo-1
La	83.4	78.2	68.5	100.9	82.7	67.8	102.6
Ce	64.6	62.1	52.4	72.4	65.5	46.8	75.5
Nd	46.6	44.2	34.3	48.2	43.7	25.9	45.3
Sm	32.9	30.0	26.8	31.7	29.9	17.8	31.0
Eu	17.4	16.1	19.1	16.0	16.1	10.1	15.1
Tb	20.2	19.1	16.3	17.4	18.4	8.2	16.0
Yb	17.2	15.0	13.5	16.7	14.6	8.6	13.0
Lu	14.0	12.2	12.2	14.2	12.7	7.3	11.1

Table 5-8: Chondrite-normalized data for analyzed lanthanide elements. Chondrite-normalizing factors utilized are from Type 1 carbonaceous chondrite abundances of Evensen *et al.* (1978) that have been multiplied by 1.52 for removal of volatiles. SCo-1 REE data were also obtained by INAA at Cornell. All data are "dry."

original data and chondrite abundances are reported "dry", i.e., CaO- and volatile-free. Figure 5-9 plots these normalized data on a logorhythmic plot with the lanthanide elements plotted along the x-axis, with increasing atomic number to the right. The normalized plot of the type Galice shales and "Galice" shales appear indistinguishable from one another, except for sample #147. Sample #147 has an atypical shale plot, with no apparent Eu anomaly, i.e., Eu was not reduced to the +2 state in significant amounts. The rationale behind this relationship for shale sample #147 is unclear, except that the record retained in this sample of its source rock(s) appear to have been different from other Galice and "Galice" shale samples. Possibly, this sample is enriched in plagioclase, which would affect the Eu anomaly (Delano, personal communication, 1988).

Table 5-9 presents analyses of the rare earth and trace element concentrations of the seven samples (INAA data) that are normalized by PAAS, the Post-Archean average Australian shale of Nance and Taylor (1976) and Taylor and McLennan (1985). The V and Ba values were derived by XRF analysis, as indicated. This table reveals that the five Galice and "Galice" shales do not show significantly different trends when normalized to PAAS. In Figure 5-10, the data from Table 5-9 are plotted to show the differences in the normalized abundances of the Galice and "Galice" shales and Cody Shale (SCo-1).

5.5 Discussion of Results

A comparison of the type Galice and "Galice" shales against the standard SCo-1 shows the two Galice shales have higher V, Cr, and Ni abundances (Tables 5-2 and 5-9). The elevated V, Cr, and Ni concentrations are thought to be the result of an arc volcaniclastic component or an ophiolitic component.

Differences were noted in the mean values of the type Galice and "Galice" shales in the abundance of Mn, Mg, Na, K, Sr, and Rb, but these differences are not significant at the 2σ level.

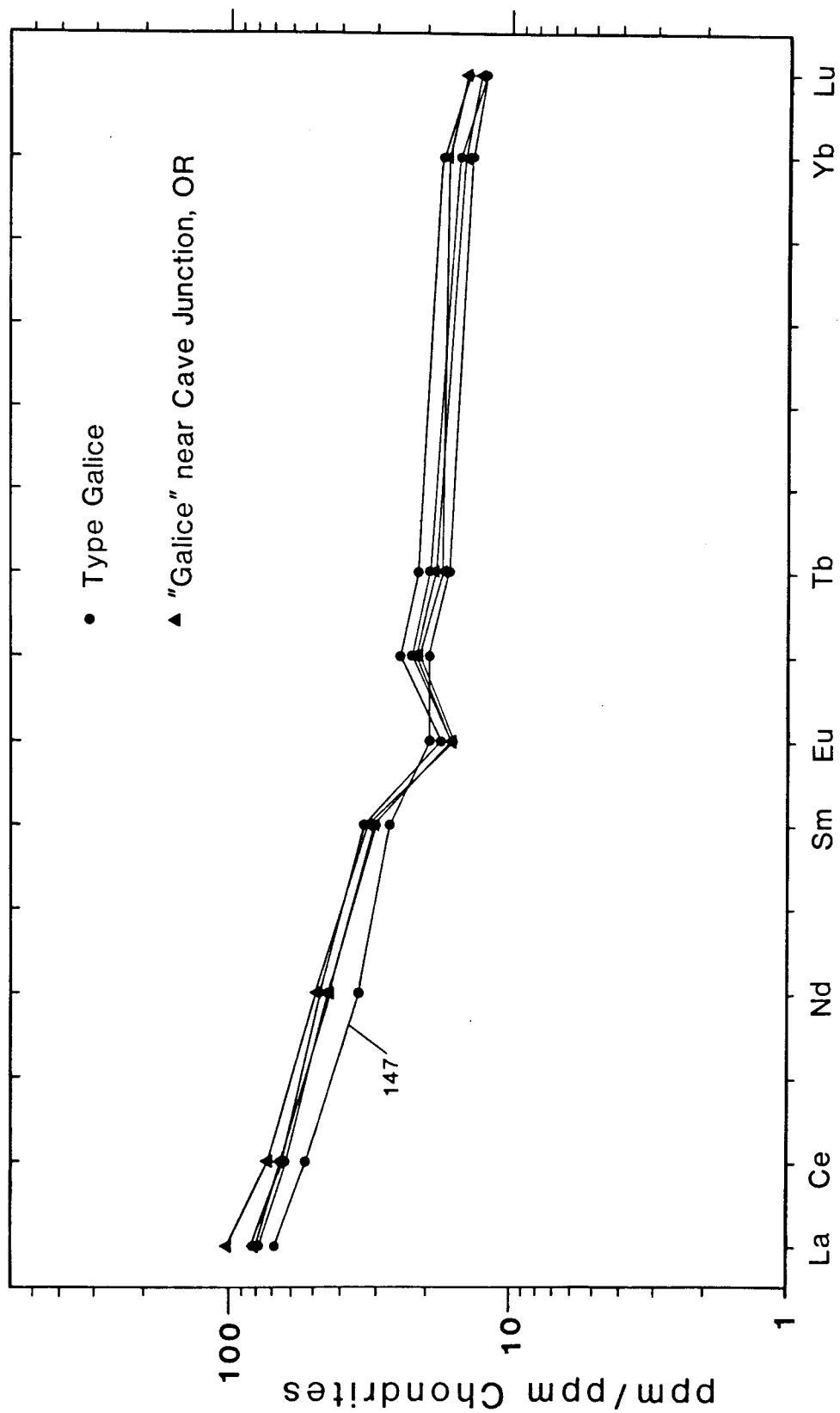

Figure 5-9: Chondrite-normalized diagram of the type Galice and "Galice" shales. Type Galice greywacke 38G is not plotted on this diagram.

	SAMPLE/PAAS INAA data						
	22	24	147	G1	G2	38G	SCo-1
La	0.82	0.77	0.67	0.99	0.81	0.66	1.00
Ce	0.78	0.75	0.64	0.88	0.79	0.57	0.92
Nd	1.05	1.00	0.77	1.09	0.98	0.58	1.02
Sm	1.38	1.25	1.12	1.32	1.25	0.74	1.30
Eu	1.39	1.29	1.53	1.28	1.29	0.81	1.21
Tb	1.49	1.42	1.21	1.29	1.36	0.61	1.18
Yb	1.54	1.34	1.21	1.50	1.31	0.77	1.16
Lu	1.26	1.09	1.09	1.28	1.14	0.65	1.00
Hf	0.94	0.88	0.94	1.01	1.16	1.09	1.14
Sc	1.49	1.47	1.70	1.64	1.34	1.27	0.94
Cr	1.39	1.23	1.37	1.16	1.39	3.58	0.90
Th	0.67	0.65	0.47	0.91	0.71	0.45	0.87
U	1.19	1.10	0.86	1.35	1.26	0.95	1.60
Ni	1.37	1.63	1.19	0.89	1.71	1.99	0.61
Cs	0.29	0.34	0.16	0.82	0.56	0.09	0.66
V*	1.35	1.27	1.50	1.28	1.13	1.09	0.89
Ba*	0.98	0.90	0.92	1.46	1.20	0.59	0.80

Post-Archean average Australian shale of Nance and Taylor (1976) and Taylor and McLennan (1985)
*V and Ba from XRF data of S.T. Ahmedali

Table 5-9: Table of INAA data normalized to PAAS for the type Galice and "Galice" shales, one type Galice greywacke, and SCo-1. All data are INAA data except for V and Ba, for which XRF data are utilized. The normalizing factor is PAAS, the Post-Archean average Australian shale, from Nance and Taylor (1976) and Taylor and McLennan (1985).

Figure 5-10: INAA and XRF data (Table 5-9) normalized to PAAS for the type Galice and "Galice" shales and SCo-1. PAAS from Nance and Taylor (1976) and Taylor and McLennan (1985).

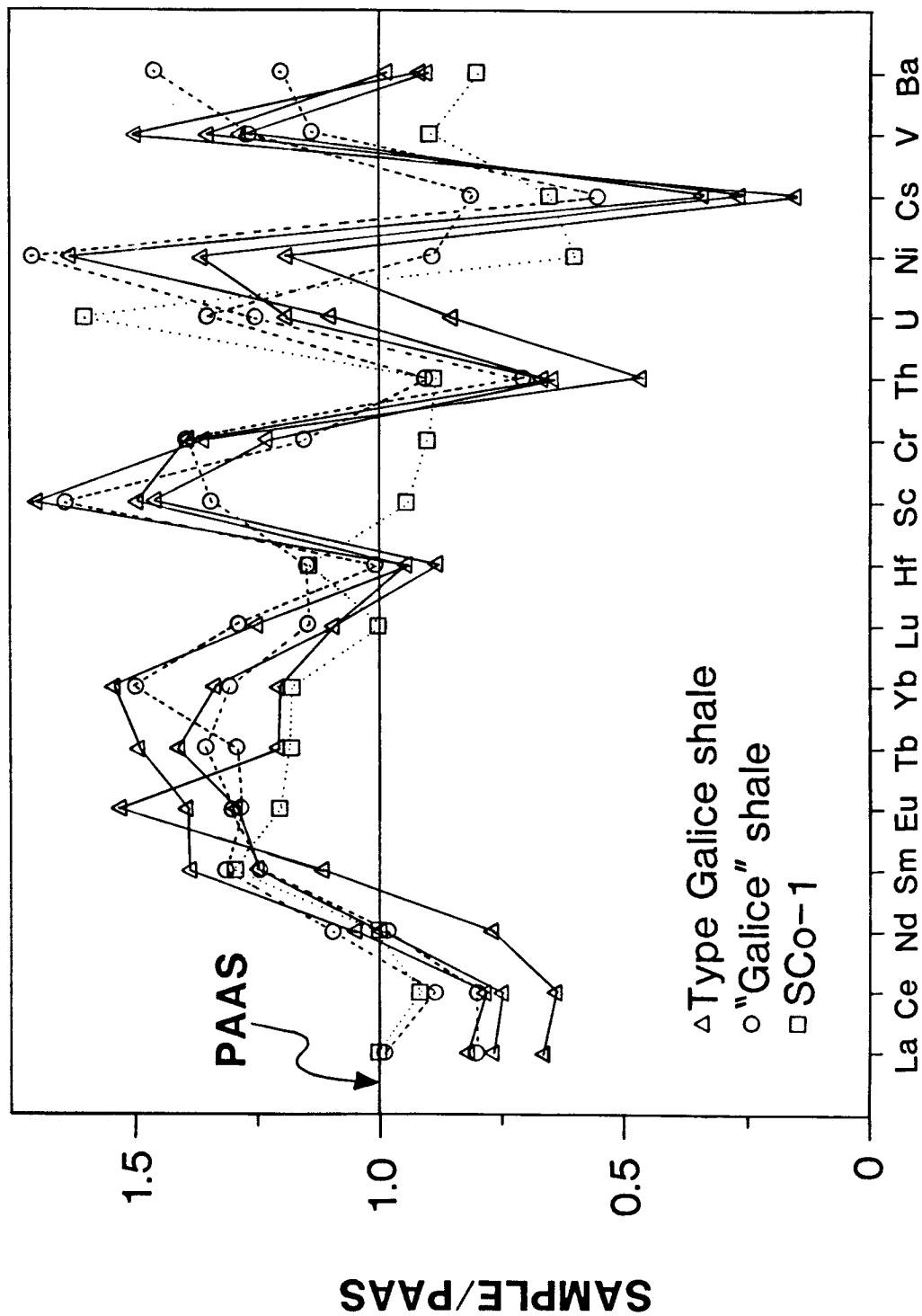
SAMPLE/PAAS
1.5
1.0
0.5
0
PAAS
△Type Galice shale
○"Galice" shale
□SCo-1
La Ce Nd Sm Eu Tb Yb Lu Hf Sc Cr Th U Ni Cs V Ba

Comparisons of immobile element abundances between the two Galice units revealed some interesting points. First, both Galice shales showed a strong positive correlation in the diagram of Al_2O_3 versus TiO_2. Second, differences were observed in the behavior of the two Galice shales in the other plots. The type Galice shales show well-defined positive correlations for Zr versus Al_2O_3 and for Y versus Al_2O_3. The "Galice" shales show a poor correlation or no correlation for these same plots. The "Galice" shales do show a well-defined positive correlation between K_2O versus TiO_2, K_2O versus Al_2O_3, and K_2O versus V, while the type Galice shales show very poor correlations or total scatter in these plots.

Attempts were made at discriminating the type Galice from the "Galice" shales on ternary diagrams, in order to better understand the complex, multi-component behavior exhibited by these shales. Elements chosen for comparison included Si, Ti, and Al, and Zr, Cr, and Ti. The attempts at discriminating the two shales on ternary diagrams were not successful in defining separate domains or any observable trends.

In conclusion, it appears evident that there are identifiable differences and complex relationships between immobile elements for these units which differentiate the type Galice from the "Galice" shale.

CHAPTER 6: SUMMARY AND CONCLUSIONS

The study area consists of metasedimentary rocks of the Galice Formation and metavolcanic rocks of the Rogue Formation. The Galice structurally overlies the Rogue, which has previously been interpreted as an island arc assemblage (Garcia, 1979).

The Rogue consists of greenish-grey lava flows, lithic tuffs, and breccia of andesitic to dacitic composition. The Pb/U zircon ages for the type Rogue are 157 ± 2 Ma (Saleeby, 1984). Work done by Riley (1987) suggests that multiple magma chambers were probably present in the Rogue, and that the extrusives represent a relatively young island arc with a tholeiitic parent magma. The Rogue volcanics in the study area exhibit tight to isoclinal folds that are overturned to the northwest. Dismembered pillow lavas are found near the confluence of Grave Creek and the Rogue River east of the Grave Creek bridge. Dark grey to greyish-green cherts are found along with Rogue lithic tuffs between Taylor and Galice Creek. An island arc association of the cherts is inferred.

The Galice Formation consists of thin-bedded, dark grey to black slaty shales with a prominent cleavage. Coarse-grained pebbly sandstone beds with large shale rip-up clasts are present locally and are interpreted as representing water-cut channels. Chert-pebble conglomerate is found along Galice Creek. It is poorly sorted, lithologically diverse, and dominantly made up of grey chert. This conglomerate appears to have an aligned fabric produced by imbrication. It is interpreted as a quickly deposited conglomerate produced by the exposure and erosion of a basement pelagic sequence, with minor contribution of quartzite and sandstone clasts apparently coming from older Klamath terranes to the east.

The Galice is dated as late middle Oxfordian to middle Kimmeridgian on the basis of a bivalve, *Buchia concentrica* (Sowerby), the characteristic fossil of the Galice (Imlay, 1980). The basal Galice is assigned to mid-middle Oxfordian (154-157 Ma) on the basis of the radiolarian assemblages present (Pessagno and Blome, in press).

Plant fragments consisting of carbonaceous broken stems and possible leafy material are preserved in Galice shales, indicative of organic-rich turbiditic material. Apparent trace fossils found parallel to sub-parallel to bedding are interpreted as feeding and grazing traces produced at the sediment-water interface by deep-water organisms. Other deep water trace fossils have been previously identified in the Galice slate that overlies the Josephine ophiolite in northern California (Harper, 1980a, 1982a, 1983).

Ultramafic rocks crop out in the southeastern portion of the study area in narrow, highly dissected, offset and sheared belts. Many NE-trending high-angle reverse faults are found along the contacts between the serpentine and volcanic lithic tuffs and flows. Later NW-trending faults have offset the serpentinized ultramafic rocks. Amygdaloidal basalt is found east of Stratton Creek. Hornblende diorite porphyry dikes and sill-like intrusions trend northeast and are found near or along the Rogue-Galice boundary.

The Galice Formation has minor interbedded volcaniclastics which appear indistinguishable from the Rogue Formation volcanics. A stratigraphic section of interbedded shales and volcanic tuffs was measured at station 26 across from the Indian Mary boat ramp. Flattened shale clasts were observed in the banded tuff.

Both the Rogue and Galice Formations generally strike N to NE and dip steeply to the southeast at the type locality. This contact is possibly depositional, however it has since been faulted parallel or nearly parallel to bedding. The interpretation of this boundary is that it represents a high-angle fault whose displacement and times of displacement are uncertain.

Figure 6-1 shows a simplified geologic map of the study area, modified after Hotz (1971) and Riley (1987). Hotz (1971) mapped the Rogue-Galice contact and sampled along it from the Almeda mine to Sailor Jack Creek (southeast of the study area). Riley (1987) mapped the Rogue Formation from the Rogue-Galice contact west to Rainie Falls. His subdivisions of the Rogue are shown in Figure 6-1. A schematic cross-section A to A' is shown in Figure 6-2.

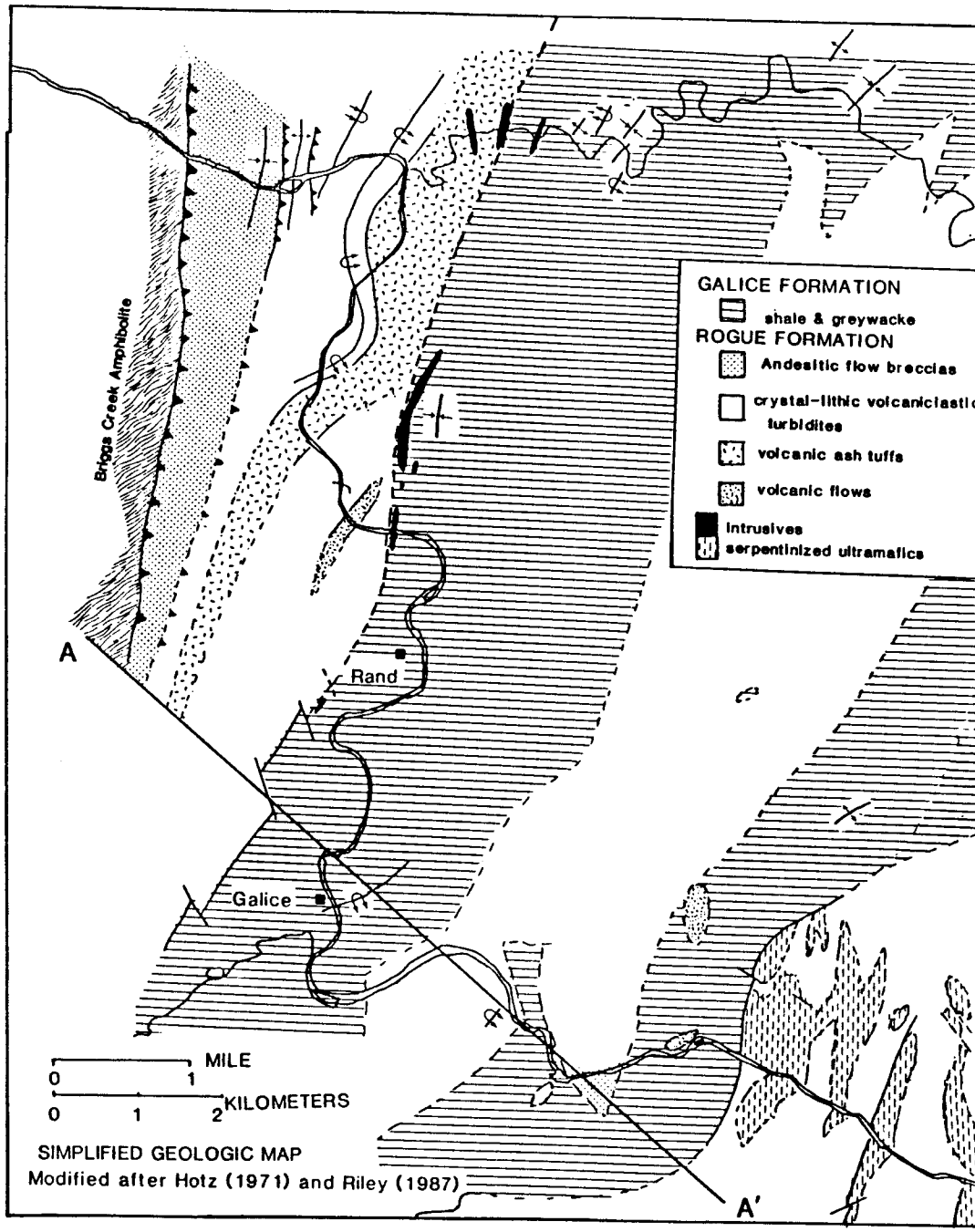

Figure 6-1: Simplified geologic map of the study area.

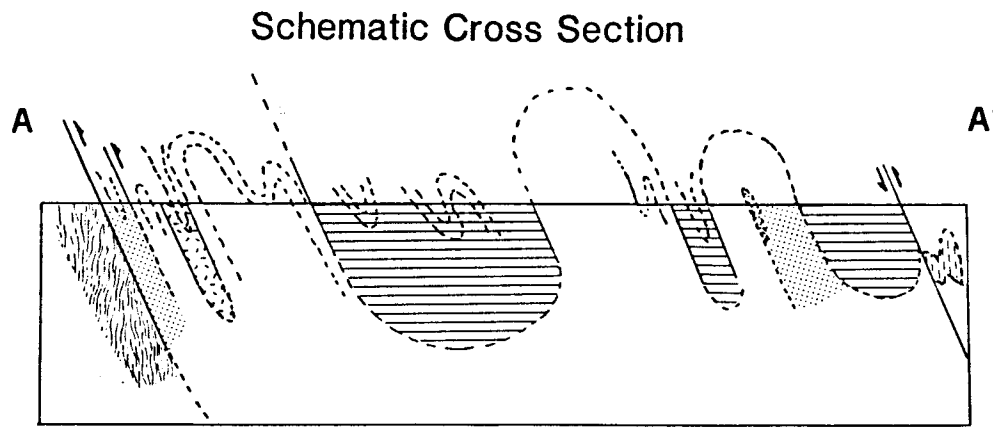

Figure 6-2: Schematic cross-section A-A' showing the Rogue-Galic contact as a thrust fault that is parallel or subparallel to bedding. Symbols same as in Figure 6-1, with the Galice Formation shown in a horizontal lined pattern.

Nevadan folds possessing an axial-planar cleavage are found throughout the study area. Post-Nevadan folds are defined as those folds that have refolded the axial-planar cleavage. Cleavage is most commonly found at an angle to bedding in the type Galice shales. Kinks and crenulation cleavage are found at a few localities in the study area, usually in areas near large faults. Numerous faults are found in the volcanic tuff and tuff breccia of the Rogue Formation in the vicinity of Butte Creek.

An asymmetric Nevadan fold overturned to the NW was identified across from the town of Galice. Along Grave Creek, the plunge of Nevadan fold axes alternates in a systematic way from NE to SW. Proposed F_3 (post-Nevadan) folds trend NW-SE and account for the dispersal of the Nevadan fold axes as observed in map view and on stereonet plots of Grave Creek data.

Type Galice shales and greywackes show evidence of at least two phases of folding. F_1 and F_2 fold axes have similar orientations as they both trend SSW and plunge gently to the SW at 4-10^{o}. They are interpreted as Nevadan fold axes with F_2 representing a possible late-stage Nevadan folding episode. The Nevadan axial plane AP_1 strikes 022^{o} and dips 060^{o}SE. The post-Nevadan deformation is characterized by F_3 folds that warp the hingelines of Nevadan folds. The orientation of the post-Nevadan axial plane (AP_3) is 119^{o}/080^{o}NE and the mean F_3 fold axis trends 303^{o} with a 14^{o}NW plunge. The fold interference pattern is transitional between types I and II of Ramsay (1967).

The thickness of the Galice Formation at the type section can not be accurately measured due to the presence of intense folding, faulting, and intrusions. A minimum thickness of 1510 meters (4960') is estimated from the map (back flap) in the vicinity north of Centennial Gulch, an estimate that takes into account structural repetition of bedding due to tight to isoclinal folding.

Sedimentary structures observed in the Galice include (1) shale rip-up clasts, (2) graded beds of Galice siltstone and greywacke and Rogue cherty tuff, (3) small-scale ripple cross-lamination, and (4) scour marks and bottom structures. Paleoflow data were calculated from measurements of flute casts, parting lineation, grooves, and longitudinal ridges found across from the town of Galice and along Grave Creek. Paleoflow was found to be dominantly towards the west (Grave Creek section) and north (Galice type section) after corrections for local folding and overturned bedding. A 90^{o} anti-clockwise rotation of the type Galice paleoflow data would be necessary if the type Galice section has rotated clockwise 90^{o}, as suggested by Bogen (1986).

XRF and INAA analyses show differences exist between the type Galice and "Galice" shales. First, a comparison of the type Galice and "Galice" shales against the standard SCo-1 reveals that the two Galice shales have higher V, Cr, and Ni abundances, thought to represent an arc volcaniclastic component or ophiolitic component. Second, differences were noted in the mean values of the type Galice and "Galice" in the abundance of Mn, Mg, Na, K, Sr, and Rb, but these differences are not significant at the 2σ level. Comparison of immobile elements elucidated distinct differences in the geochemical behavior between the two shales in the plots of Zr versus Al_2O_3, K_2O versus TiO_2, K_2O versus Al_2O_3, Y versus Al_2O_3, and K_2O versus V. These differences in geochemical behavior are presented as preliminary, general findings worthy of more detailed study to more accurately characterize the similarities and differences between the type Galice and "Galice" shales.

APPENDIX I: OBSERVED GALICE SEDIMENTARY STRUCTURES

	Stations
Shale rip-up clasts	11, 13, 14, 16, 102, 115, 118, 120, 123, 133
Graded beds	12, 13, 14, 16, 24, 118, 133, 143
Climbing ripple cross-lamination	23, 24, 50, 118, 133
Flute casts	10, 11, 14, 118, 123, 127, 128
Grooves, prod marks	10, 125, 127
Load structures	11, 13, 50, 52, 115, 118, 125, 128, 133, 152
Parting lineation	124, 126, 128
Bioturbation, trace fossils	17, 22, 23, 24, 58

APPENDIX II: CORRECTED PALEOFLOW DATA

Location	*Type of Sole Mark*	*Direction*
Galice	flute cast	011°
Galice	flute cast	339°
Galice	flute cast	342°
Galice	flute cast	016°
Grave Creek	flute cast	263°
Grave Creek	flute cast	261°
Grave Creek	flute cast	276°
Grave Creek	flute cast	262°
Grave Creek	grooves	162°/342°
Grave Creek	groove	113°/293°
Grave Creek	groove	077°/257°
Grave Creek	parting lineation	100°/280°
Grave Creek	parting lineation	098°/278°

REFERENCES CITED

AILIN-PYZIK, I.B., AND SOMMER, S.E., 1981, Microscale chemical effects of low temperature alteration of DSDP basaltic glasses, *Journal of Geophysical Research*, v. 86, p. 9503-9510.

ALTSCHULER, Z.S., 1980, The geochemistry of trace elements in marine phosphorites, 1. Characteristic abundances and enrichment, *Society of Economic Paleontologists and Mineralogists, Special Publication 29*, p. 19-30.

BALASHOV, YU.A., AND GIRIN, YU.P., 1969, On the reserve of mobile rare earth elements in sedimentary rocks, *Geochemistry International*, v. 7, p. 649-659.

BALASHOV, YU.A., RONOV, A.B., MIGDISOV, A.A., AND TURANSKAYA, N.V., 1964, The effect of climate and facies environment on the fractionation of the rare earths during sedimentation, *Geochemistry International*, v. 10, p. 995-1014.

BALDWIN, E.M., 1969, Thrust faulting along the lower Rogue River, Klamath Mountains, Oregon, *Geological Society of America Bulletin*, v. 80, p. 2047-2052.

BARNES, C.G., RICE, J.M., AND GRIBBLE, R.F., 1986, Tilted plutons in the Klamath Mountains of California and Oregon, *Journal of Geophysical Research*, v. 91, p. 6059-6071.

BATEMAN, P.C., AND CLARK, L.D., 1974, Stratigraphic and structural setting of the Sierra Nevada batholith, *Pacific Geology*, v. 8, p. 78-89.

BHATIA, M.R., 1983, Plate tectonics and geochemical composition of sandstones, *Journal of Geology*, v. 91, p. 611-627.

BHATIA, M.R., 1985a, Composition and classification of Paleozoic flysch mudrocks of eastern Australia: Implications in provenance and tectonic setting interpretation, *Sedimentary Geology*, v. 41, p. 249-268.

BHATIA, M.R., 1985b, Rare earth element geochemistry of Australian Paleozoic graywackes and mudrocks: Provenance and tectonic control, *Sedimentary Geology*, v. 45, p. 97-113.

BHATIA, M.R., 1985c, Plate tectonics and geochemical composition of sandstones: A reply, *Journal of Geology*, v. 93, p. 85-87.

BHATIA, M.R., and Crook, K.A.W., 1986, Trace element characteristics of graywackes and tectonic setting discrimination of sedimentary basins, *Contributions to Mineralogy and Petrology*, v. 92, p. 181-193.

BLACKWELDER, E., 1914, A summary of the orogenic epochs in the geologic history of North America, *Journal of Geology*, v. 22, p. 633-654.

BLATT, H., 1982, Sedimentary Petrology, Freeman, San Francisco, Calif., 564 p.

BLATT, H., 1985, Provenance studies and mudrocks, *Journal of Sedimentary Petrology*, v. 55, p. 69-75.

BOGEN, N.L., 1986, Paleomagnetism of the Upper Jurassic Galice Formation, southwestern Oregon: Evidence for differential rotation of the eastern and western Klamath Mountains, *Geology*, v. 14, p. 335-338.

BÖHLKE, J.K., AND HONNOREZ, J., AND HONNOREZ-GUERSTEIN, B.-M., 1980, Alteration of basalts from Site 396B, DSDP: Petrologic and mineralogic studies, *Contributions to Mineralogy and Petrology*, v. 73, p. 341-364.

BOUMA, A.H., 1987, Megaturbidite: An acceptable term?, *Geo-Marine Letters*, v. 7, p. 63-67.

BOUMA, A.H., NORMARK, W.R., AND BARNES, N.E., 1985, COMFAN: Needs and initial results, *in* Bouma, A.H., Barnes, N.E., and Normark, W.R., eds., Submarine Fans and Related Turbidite Sequences, Frontiers in Sedimentary Geology, Springer-Verlag, New York, p. 7-11.

BOYNTON, W.V., 1984, Cosmochemistry of the rare earth elements: Meteorite studies, *in* Henderson, P., ed., Rare Earth Element Geochemistry, Developments in Geochemistry 2, Elsevier, New York, p. 63-114.

BRENNER, R.L., 1983, Late Jurassic tectonic setting and paleogeography of western interior, North America, *in* Reynolds, M.W., and Dolly, E.D., eds., Mesozoic Paleogeography of west-central United States, Rocky Mountain Section, S.E.P.M., Denver, CO, p. 119-132.

BROWN, R.E., PARKER, H.M., AND SMITH, J.M., 1955, Disposal of liquid wastes to the ground, *in* U. N. Internal Conference on the Peaceful Uses of Atomic Energy 9, United Nations, New York, p. 669-675.

BRYAN, P., AND GORDON, R.G., 1985, Maximum likelihood estimates of the rotation of the Colorado Plateau inferred from paleomagnetic data, *EOS Transactions of AGU*, v. 66, p. 254.

CATER, F.W., AND WELLS, F.G., 1953, Geology and mineral resources of the Gasquet quadrangle, California-Oregon, *U. S. Geological Survey Bulletin 995-C*, p. 79-133.

CHAUDHURI, S. AND CULLERS, R.L., 1979, The distribution of rare earth elements in deeply buried Gulf Coast sediments, *Chemical Geology*, v. 24, p. 327-328.

CLARK, A.M., 1984, Mineralogy of the rare earth elements, *in* Henderson, P., ed., Rare Earth Element Geochemistry, Developments in Geochemistry 2, Elsevier, New York, p. 33-61.

COLLEY, S., THOMSON, J., WILSON, T.R.S., AND HIGGS, N.C., 1984, Post-depositional migration of elements during diagenesis in brown clay and turbidite sequences in the North East Atlantic, *Geochimica et Cosmochimica Acta*, v. 48, p. 1223-1235.

CONEY, P.J., JONES, D.L., AND MONGER, J.W.H., 1980, Cordilleran suspect terranes, *Nature*, v. 288, p. 329-333.

CORDELL, L., 1982, Extension in the Rio Grande rift, *Journal of Geophysical Research*, v. 87, p. 8561-8569.

CULLERS, R., CHAUDHURI, S., KILBANE, N., AND KOCH, R., 1979, Rare-earths in size fractions and sedimentary rocks of Pennsylvanian-Permian age from the mid-continent of the U.S.A., *Geochimica et Cosmochimica Acta*, v. 43, p. 1285-1301.

DAVIS, G.A., MONGER, J.W., AND BURCHFIEL, B.C., 1978, Mesozoic construction of the Cordilleran "collage," central British Columbia to central California, *in* Howell, D.G., and McDougall, K.A., eds., Mesozoic Paleogeography of the western United States, Pacific Coast S.E.P.M., Los Angeles, Calif., p. 1-32.

DAVIS, G.H., 1984, Structural Geology of Rocks and Regions, John Wiley & Sons, New York, 492 p.

DEAN, W.E., LEINEN, M., AND STOW, D.A.V., 1985, Classification of deep-sea, fine-grained sediments, *Journal of Sedimentary Petrology*, v. 55, p. 250-256.

DELANGE, G.J., 1986, Early diagenetic reactions in interbedded pelagic and turbiditic sediments in the Nares Abyssal Plain (western North Atlantic): Consequences for the composition of sediment and interstitial water, *Geochimica et Cosmochimica Acta*, v. 50, p. 2543-2561.

DICK, H.J.B., 1976, The origin and emplacement of the Josephine peridotite of southwestern Oregon, unpublished Ph.D. thesis, Yale University, 409 p.

DILLER, J.S., 1893, Cretaceous and Early Tertiary of Northern California and Oregon, *Geological Society of America Bulletin*, v. 4, p. 205-224.

----- 1902, Topographic development of the Klamath Mountains, Oregon, *U. S. Geological Survey Bulletin*, v. 196, p. 1-69.

----- 1907, The Mesozoic sediments of southwestern Oregon, *American Journal of Science*, v. 23, p. 401-421.

----- 1908, Strata containing the Jurassic flora of Oregon, *Geological Society of America Bulletin*, v. 19, p. 367-402.

----- 1914, Mineral resources of southwestern Oregon, *U. S. Geological Survey Bulletin*, v. 546, p. 1-69, 72-81.

DILLER, J.S., AND KAY, G.F., 1924, Riddle, Oregon, *U. S. Geological Survey Atlas Folio 218*, p. 3-4.

DOLE, H. M., AND BALDWIN, E.M., 1947, A reconnaissance between the Almeda and Silver Peak mines of southwestern Oregon, Oregon Department of Geology and Mineral Industries, *The ORE BIN*, v. 9, p. 95-100.

DZULYNSKI, S., AND WALTON, E.K., 1965, Sedimentary Features of Flysch and Greywackes, Developments in Sedimentology 7, Elsevier, New York, 274 p.

ELDERFIELD, H., AND GREAVES, M.J., 1982, The rare earth elements in seawater, *Nature*, v. 296, p. 214-219.

ELDERFIELD, H. AND SHOLKOVITZ, E.R., 1987, Rare earth elements in the pore waters of reducing nearshore sediments, *Earth and Planetary Science Letters*, v. 82, p. 280-288.

ENGELDER, T., AND GEISER, P., 1979, The relationship between pencil cleavage and lateral shortening within the Devonian section of the Appalachian Plateau, New York, *Geology*, v. 7, p. 460-464.

ETHERIDGE, M.A., 1986, On the reactivation of extensional fault systems, *Philosophical Transactions of the Royal Society of London*, A317, p. 179-194.

EVENSEN, N.M., HAMILTON, P.J., AND O'NIONS, R.K., 1978, Rare-earth abundances in chondritic meteorites, *Geochimica et Cosmochimica Acta*, v. 42, p. 1199-1212.

FABBI, B.P., AND ESPOS, L.F., 1976, X-ray fluorescence analysis of 21 selected major, minor, and trace elements in eight new USGS standard rocks, *in* Flanagan, F.J., ed., Descriptions and Analyses of Eight New USGS Rock Standards, U.S. Geological Survey Professional Paper 840, p. 89-93.

FAGIN, S.W., AND GOSE, W.A., 1983, Paleomagnetic data from the Redding section of the eastern Klamath belt, northern California, *Geology*, v. 11, p. 505-508.

FAHAN, M.R., 1982, Geology and geochronology of a part of the Hayfork terrane, Klamath Mountains, northern California, unpublished master's thesis, University of California at Berkeley, 127 p.

FAHAN, M.R., AND WRIGHT, J.E., 1983, Plutonism, volcanism, folding, regional metamorphism and thrust faulting: Contemporaneous aspects of a major middle Jurassic orogenic event within the Klamath Mountains, North California, *Geological Society of America Abstracts with Programs*, Cordilleran Section, v. 15, p. 272.

FLEET, A.J., 1984, Aqueous and sedimentary geochemistry of the rare earth elements, *in* Henderson, P., ed., Rare Earth Element Geochemistry, Developments in Geochemistry 2, Elsevier, New York, p. 343-373.

FREY, F.A., BRYAN, W.B., AND THOMPSON, G., 1974, Atlantic Ocean floor: Geochemistry and petrology of basalts from Legs 2 and 3 of the Deep-Sea Drilling Project, *Journal of Geophysical Research*, v. 79, p. 5507-5527.

FREY, F.A., HASKIN, M.A., POETZ, J.A., AND HASKIN, L.A., 1968, Rare earth abundances in some basic rocks, *Journal of Geophysical Research*, v. 73, p. 6085-6098.

FREY, R.W., 1975, The realm of ichnology, its strengths and limitations, *in* Frey, R.W., ed., The Study of Trace Fossils: A Synthesis of Principles, Problems, and Procedures in Ichnology, Springer-Verlag, New York, p. 13-38.

GALLOWAY, W.E., 1974, Deposition and diagenetic alteration of sandstone in northeast Pacific arc-related basins: Implications for graywacke genesis, *Geological Society of America Bulletin*, v. 85, p. 379-390.

GARCIA, M.O., 1979, Petrology of the Rogue and Galice Formations, Klamath Mountains, Oregon: Identification of a Jurassic island arc sequence, *Journal of Geology*, v. 87, p. 29-41.

GOLDBERG, E.D., 1958, Determination of opal in marine sediments, *Journal of Marine Research*, v. 17, p. 178-182.

GOLDBERG, E.D., AND ARRHENIUS, G.O.S., 1958, Chemistry of Pacific pelagic sediments, *Geochimica et Cosmochimica Acta*, v. 13, p. 153-212.

GOODGE, J.W., 1986, Relations of Stuart Fork and North Fork terranes in the central Klamath Mountains, Northern California, *Geological Society of America Abstracts with Programs*, Cordilleran Section, v. 18, p. 109.

GORDON, R.G., COX, A., AND O'HARE, S., 1984, Paleomagnetic Euler poles and the apparent polar wander and absolute motion of North America since the Carboniferous, *Tectonics*, v. 3, p. 499-537.

GORSLINE, D.S., 1984, Introduction to a symposium on fine-grained sedimentology, *Geo-Marine Letters*, v. 4, p. 133-138.

GORSLINE, D.S., 1985, Some thoughts on fine-grained sediment transport and deposition, *in* R. Hesse, ed., Sedimentology of Siltstone and Mudstone, *Sedimentary Geology*, v. 41, p. 113-130.

GRAY, D.R., 1979, Microstructure of crenulation cleavages: An indicator of cleavage origin, *American Journal of Science*, v. 279, p. 97-128.

GRAY, G.G., 1983, A kinematic analysis of thrust faulting, west-central Klamath Mountains, California, *Geological Society of America Abstracts with Programs*, Cordilleran Section, v. 15, p. 585.

GRAY, G.G., 1985, Structural, Geochronologic, and Depositional History of the Western Klamath Mountains, California and Oregon: Implications for the Early to Middle Mesozoic Tectonic Evolution of the Western North American Cordillera, unpublished Ph.D. dissertation, University of Texas at Austin, 162 p.

GRAY, G.G., 1986, Native terranes of the Central Klamath Mountains, California, *Tectonics*, v. 5, p. 1043-1054.

HAMILTON, W., 1969, Mesozoic California and underflow of Pacific mantle, *Geological Society of America Bulletin*, v. 80, p. 2409-2430.

HAMILTON, W., 1978, Mesozoic tectonics of the western United States, *in* Howell, D.G., and McDougall, K.A., eds., Mesozoic Paleogeography of the Western United States, Pacific Section, S.E.P.M., Los Angeles, Calif., p. 33-70.

HAMILTON, W., 1981, Plate tectonic mechanism of Laramide deformation, *Contributions to Geology*, v. 19, p. 87-92.

HARDING, D., 1987, Tectonite Structures of the Josephine Peridotite, Oregon: A Record of Plastic Flow in the Mantle During Formation of the Josephine Ophiolite, unpublished Ph.D. thesis, Cornell University, 334 p.

HARPER, G.D., 1980a, Structure and Petrology of the Josephine Ophiolite and Overlying Metasedimentary Rocks, Northwestern California, unpublished Ph.D. thesis, University of California at Berkeley, 259 p.

----- 1980b, The Josephine ophiolite--Remains of a Late Jurassic marginal basin in northwestern California, *Geology*, v. 8, p. 333-337.

----- 1982a, Inferred high primary volatile contents in lavas erupted in an ancient back-arc basin, California, *Journal of Geology*, v. 90, p. 187-194.

----- 1982b, Evidence for large-scale rotations at spreading centers from the Josephine ophiolite, *Tectonophysics*, v. 82, p. 25-44.

----- 1983, A depositional contact between the Galice Formation and a Late Jurassic ophiolite in northwestern California and southwestern Oregon, *Oregon Geology*, v. 45, p. 3-9.

----- 1984, The Josephine ophiolite, northwestern California, *Geological Society of America Bulletin*, v. 95, p. 1009-1026.

HARPER, G.D., AND PARK, R., 1986, Comment on "Paleomagnetism of the Upper Jurassic Galice Formation, southwestern Oregon: Evidence for differential rotation of the eastern and western Klamath Mountains," *Geology*, v. 14, p. 1049-1050.

HARPER, G.D., SALEEBY, J.B., AND NORMAN, E.A.S., 1985, Geometry and tectonic setting of sea-floor spreading for the Josephine ophiolite, and implications for Jurassic accretionary events along the California margin, *in* Howell, D.G., ed., Tectonostratigraphic Terranes of the Circum-Pacific Region, Circum-Pacific Council for Energy and Mineral Resources, Earth Sciences Series No. 1, p. 239-257.

HARPER, G.D., SALEEBY, J.B., CASHMAN, S., AND NORMAN, E., 1986, Isotopic age of the Nevadan Orogeny in the western Klamath Mountains, California-Oregon, *Geological Society of America Abstracts with Programs*, Cordilleran Section, v. 18, p. 114.

HARPER, G.D., SALEEBY, J.B., AND SHARP, W.D., 1983, Late Jurassic transform motion in the western U.S., American Geophysical Union, *EOS*, v. 64, no. 45, p. 846.

HARPER, G.D., AND WRIGHT, J.E., 1984, Middle to Late Jurassic evolution of the Klamath Mountains, California-Oregon, *Tectonics*, v. 3, p. 759-772.

HARRISON, C.G.A., AND LINDH, T., 1982, A polar wandering curve for North America during the Mesozoic and Cenozoic, *Journal of Geophysical Research*, v. 87, B3, p. 1903-1920.

HAQ, B.U., HARDENBOL, J., AND VAIL, P.R., 1987, Chronology of fluctuating sea levels since the Triassic, *Science*, v. 235, p. 1156-1167.

HASKIN, L.A., 1984, Petrogenetic modelling--use of rare earth elements, *in* Henderson, P., ed., Rare Earth Element Geochemistry, Developments in Geochemistry 2, Elsevier, New York, p. 115-152.

HASKIN, L.A., WILDEMAN, T.R., FREY, F.A., COLLINS, K.A., KEEDY, C.R., AND HASKIN, M.A., 1966, Rare earths in sediments, *Journal of Geophysical Research*, v. 71, p. 6091-6105.

HEGGIE, D., KLINKHAMMER, G., AND CULLEN, D., 1987, Manganese and copper fluxes from continental margin sediments, *Geochimica et Cosmochimica Acta*, v. 51, p. 1059-1070.

HELLMAN, P.L., SMITH, R.E., AND HENDERSON, P., 1979, The mobility of the rare earth elements: Evidence and implications from selected terrains affected by burial metamorphism, *Contributions to Mineralogy and Petrology*, v. 71, p. 23-44.

HELPER, M.A., 1983, Deformation-metamorphism relationships in a regional blueschist-greenschist facies terrane, Condrey Mountain Schist, North central Klamath Mountains, N. Calif., *Geological Society of America Abstracts with Programs*, Cordilleran Section, v. 15, p. 427.

HELPER, M.A., 1986, The age and direction of thrusting along the western margin of the Condrey Mountain window, Klamath Mountains, California, *Geological Society of America Abstracts with Programs*, Cordilleran Section, v. 18, p. 116.

HERSHEY, O.H., 1911, Del Norte County (California geology), *Mineral and Science Press*, v. 102, p. 468.

HILL, B., 1983, A preliminary model for crystalline overthrusts and associated deformation in the northern Klamath Mountains, *Geological Society of America Abstracts with Programs*, Cordilleran Section, v. 15, p. 426.

HOBBS, B.E., MEANS, W.D., AND WILLIAMS, P.F., 1976, An Outline of Structural Geology, John Wiley & Sons, New York, 571 p.

HOTZ, P.E., 1971, Geology of lode gold districts in the Klamath Mountains, California and Oregon, *U. S. Geological Survey Bulletin*, 1290, 91 p.

IJIMA, A., MATSUMOTO, R., AND RYUJI, T., 1985, Mechanism of sedimentation of rhythmically bedded chert, *Sedimentary Geology*, v. 41, p. 221-233.

IMLAY, R.W., 1959, Succession and speciation of the pelecypod *Aucella*, *U.S. Geological Survey Professional Paper 314-G*, p. 155-169.

----- 1961, Late Jurassic ammonites from the western Sierra Nevada, California, *U. S. Geological Survey Professional Paper 374-D*, 30 p.

----- 1965, Jurassic marine faunal differentiation in North America, *Journal of Paleontology*, v. 39, p. 1023-1038.

----- 1980, Jurassic paleobiogeography of the conterminous United States in its continental setting, *U. S. Geological Survey Professional Paper 1062*, 134 p.

IMLAY, R.W., DOLE, H.M., WELLS, F.G., AND PECK, D., 1959, Relations of certain Upper Jurassic and Lower Cretaceous formations in southwestern Oregon, *American Association of Petroleum Geologists Bulletin*, v. 43, p. 2770-2785.

IMLAY, R.W., AND JONES, D.L., 1970, Ammonites from the *Buchia* zones in northwestern California and southwestern Oregon, *U. S. Geological Survey Professional Paper 647-B*, 55 p.

IRVING, E., AND IRVING, G.A., 1982, Apparent polar wander paths Carboniferous through Cenozoic and the assembly of Gondwana, *Geophysical Surveys*, v. 5, p. 141-188.

IRWIN, W.P., 1960, Geologic reconnaissance of the northern Coast Ranges and Klamath Mountains, California, *California Division of Mines Bulletin*, v. 179, 80 p.

IRWIN, W.P., 1981, Tectonic accretion of the Klamath Mountains, *in* Ernst, W.G., ed., The Geotectonic Development of California, Prentice-Hall, Englewood Cliffs, New Jersey, p. 29-49.

IRWIN, W.P., JONES, D.L., AND KAPLAN, T.A., 1978, Radiolarians from pre-Nevadan rocks of the Klamath Mountains, California and Oregon, *in* Howell, D.G., and McDougall, K.A., eds., Mesozoic Paleogeography of the Western United States, Pacific Coast Paleogeography Symposium 2, p. 303-310.

JACHENS, R.C., BARNES, C.G., AND DONATO, M.M., 1986, Subsurface configuration of the Orleans fault: Implications for deformation in the western Klamath Mountains, California, *Geological Society of America Bulletin*, v. 97, p. 388-395.

JAYKO, A.S., AND BLAKE, M.C., 1986, Significance of Klamath rocks between the Franciscan complex and Coast Range Ophiolite, Northern California, *Tectonics*, v. 5, p. 1055-1071.

JOHNSTON, D.H., 1987, Physical properties of shale at temperature and pressure, *Geophysics*, v. 52, p. 1391-1401.

JONES, D.L., 1960, Lower Cretaceous (Albian) fossils from southwestern Oregon and their paleogeographic significance, *Journal of Paleontology*, v. 34, p. 152-160.

JONES, D.L., AND MURCHEY, B., 1986, Geologic significance of Paleozoic and Mesozoic radiolarian chert, *Annual Reviews of Earth and Planetary Science*, v. 14, p. 455-492.

KARIG, D.E., 1974, Evolution of arc systems in the western Pacific, *Annual Reviews of Earth and Planetary Science*, v. 2, p. 51-75.

KAYS, M.A., 1967, Tectonic framework of mineralization, Upper Jurassic rocks, southwestern Oregon, *Oregon Department of Geology and Mineral Industries Short Paper 24*, p. 43-53.

KAYS, M.A., 1968, Zones of alpine tectonism and metamorphism Klamath Mountains, southwestern Oregon, *Journal of Geology*, v. 76, p. 17-36.

KAYS, M.A., AND BRUEMMER, J.L., 1964, Gravity field over zones of major tectonism, southwest Oregon, Oregon Department of Geology and Mineral Industries, *The ORE BIN*, v. 26, p. 43-52.

KARIG, D.E., 1974, Evolution of arc systems in the western Pacific, *Annual Reviews of Earth and Planetary Science*, v. 2, p. 51-75.

KLUTH, C.F., BUTLER, R.F., HARDING, L.E., SHAFIQULLAH, M., AND DAMON, P.E., 1982, Paleomagnetism of late Jurassic rocks in the northern Canelo Hills, southeastern Arizona, *Journal of Geophysical Research*, v. 87, p. 7079-7086.

KOCUREK, G., AND DOTT, R.H., 1983, Jurassic paleogeography and paleoclimate of the central and southern Rocky Mountain region, *in* Reynolds, M.W., and Dolly, E.D., eds., Mesozoic Paleogeography of the West-Central United States, p. 101-118.

LANPHERE, M.A., IRWIN, W.P., AND HOTZ, P.E., 1968, Isotopic age of the Nevadan Orogeny and older plutonic and metamorphic events in the Klamath Mountains, California, *Geological Society of America Bulletin*, v. 79, p. 1027-1052.

LAWSON, A.C., 1893, The Cordilleran Mesozoic Revolution, *Journal of Geology*, v. 1, p. 579-586.

LEEDER, M.R., 1982, Sedimentology: Process and Product, George Allen & Unwin, London, 344 p.

LIBBEY, F.W., 1967, The Almeda Mine Josephine County, Oregon, State of Oregon Department of Geology and Mineral Industries, *Short Paper 24*, 53 p.

LINDSLEY-GRIFFIN, N., 1982, Structure, Stratigraphy, Petrology, and Regional Relationships of the Trinity Ophiolite, Eastern Klamath Mountains, California, unpublished Ph.D. dissertation, University of California at Davis, 445 p.

LINDSLEY-GRIFFIN, N., 1983, Lower Paleozoic rocks of the Eastern Klamath Mountains, northern California: constraints on early Paleozoic paleogeography, *Geological Society of America Abstracts with Programs*, v. 15, p. 426-427.

LOUDERBACK, G.D., 1905, The Mesozoic of southwestern Oregon, *Journal of Geology*, v. 13, p. 514-555.

LUNDBERG, N., AND MOORE, J.C., 1986, Macroscopic structural features in Deep Sea Drilling Project cores from forearc regions, *in* Moore, J.C., ed., Structural Fabric in Deep Sea Drilling Project Cores from Forearcs, Geological Society of America Memoir 166, p. 13-44.

MANHEIM, F.T., HATHAWAY, J.C., FLANAGAN, F.J., AND FLETCHER, J.O., 1976, Marine mud, MAG-1, from the Gulf of Maine, *in* Flanagan, F.J., ed., Descriptions and Analyses of Eight New USGS Rock Standards, *U.S. Geological Survey Professional Paper 840*, p. 25-28.

MANKINEN, E.A., 1978, Paleomagnetic evidence for a Late Cretaceous deformation of the Great Valley sequence, Sacramento Valley, California, *Journal of Research of the U.S. Geological Survey*, v. 6, p. 383-390.

MANKINEN, E.A., AND IRWIN, W.P., 1982, Paleomagnetic study of some Cretaceous and Tertiary sedimentary rocks of the Klamath Mountains province, California, *Geology*, v. 10, p. 82-87.

MARTIN, J.M., HOGDAHL, O., AND PHILIPOTT, S.C., 1976, Rare earth element supply to the ocean, *Journal of Geophysical Research*, v. 81, p. 3119-3124.

MAY, S.R., AND BUTLER, R.F., 1986, North American Jurassic apparent polar wander: Implications for plate motion, paleogeography and Cordilleran tectonics, *Journal of Geophysical Research*, v. 91, p. 11519-11544.

MAY, S.R., BUTLER, R.F., SHAFIQULLAH, M., AND DAMON, P.E., 1986, Paleomagnetism of Jurassic volcanic rocks in the Patagonia Mountains, southeastern Arizona: Implications for the North American 170 Ma reference pole, *Journal of Geophysical Research*, v. 91, p. 11545-11555.

MCLENNAN, S.M., AND TAYLOR, S.R., 1980, Geochemical standards for sedimentary rocks: Trace-element data for U.S.G.S. Standards SCo-1, MAG-1, and SGR-1, *Chemical Geology*, v. 29, p. 333-343.

MIALL, A.D., 1986, Eustatic sea level changes interpreted from seismic stratigraphy: A critique of the methodology with particular reference to the North Sea Jurassic record, *American Association of Petroleum Geologists Bulletin*, v. 70, p. 131-137.

MILLER, M.M., 1983, Upper Paleozoic stratigraphy and structure in the eastern Klamath belt, northern California, *Geological Society of America Abstracts with Programs*, Cordilleran Section, v. 15, p. 426.

MILLER, M.M., AND SALEEBY, J.B., 1987, Detrital zircon studies of the Galice Formation: Common provenance of strata overlying the Josephine ophiolite and Rogue island arc--western Klamath Mountains Terrane, *Geological Society of America Abstracts with Programs*, v. 19, p. 772-773.

MITCHELL, H.G., 1970, Facies of an Early Miocene volcanic arc, Malekula Island, New Hebrides, *Sedimentology*, v. 14, p. 187-200.

MOORE, J.C., AND LUNDBERG, N., 1986, Tectonic overview of Deep Sea Drilling Project transects of forearcs, *in* Moore, J.C., ed., Structural Fabric in Deep Sea Drilling Project Cores from Forearcs, Geological Society of America Memoir 166, p. 1-12.

MORAD, S., 1984, Diagenetic matrix in Proterozoic graywackes from Sweden, *Journal of Sedimentary Petrology*, v. 54, p. 1157-1168.

MORTIMER, N., 1986, Late Triassic, arc-related, potassic igneous rocks in the North American Cordillera, *Geology*, v. 14, p. 1035-1038.

MUEKE, G.K., PRIDE, C., AND SARKAR, P., 1979, Rare earth element geochemistry of regional metamorphic rocks, *in* Ahrens, L.H., ed., Origin and Distribution of the Elements 2, Pergamon, Oxford, p. 449-464.

NANCE, W.B., AND TAYLOR, S.R., 1976, Rare earth element patterns and crustal evolution--I. Australian post-Archean sedimentary rocks, *Geochimica et Cosmochimica Acta*, v. 40, p. 1539-1551.

NELSON, C.H., AND NILSEN, T.H., 1974, Depositional trends of modern and ancient deep-sea fans, *in* Modern and Ancient Geosynclinal Sedimentation, S.E.P.M. Special Publcation 19, p. 69-91.

NILSEN, T.H., 1980, Modern and ancient submarine fans: A discussion of papers by R.G. Walker and W.R. Normark, *American Association of Petroleum Geologists Bulletin*, v. 64, p. 1094-1112.

NORMARK, W.R., 1978, Fan valleys, channels, and depositional lobes on modern submarine fans: Characters for recognition of sandy turbidite environments, *American Association of Petroleum Geologists Bulletin*, v. 62, p. 912-931.

O'DRISCOLL, E.S.T., 1986, Observations of the lineament-ore relation, *Philosophical Transactions of the Royal Society of London*, A317, p. 195-218.

PAGE, N.J., BLAIR, W.N., GRAY, F., CANNON, J.K., GRIMES, D.J., AND LEINZ, R.W., 1977, Preliminary reconnaissance geologic map of the Wimer Quadrangle, Oregon, *U.S. Geological Survey Miscellaneous Field Studies MF-848*. Scale 1:62,500.

PARK-JONES, R., 1988, Tectonic setting and deformation of the type Galice Formation, western Klamath Mountains, *Geological Society of America Abstracts with Programs*, Cordilleran Section, v. 20, p. 219-220.

PECK, D.L., IMLAY, R.W., AND POPENOE, W.P., 1956, Upper Cretaceous rocks of parts of southwestern Oregon and northern California, *American Association of Petroleum Geologists Bulletin*, v. 40, p. 1968-1984.

PESSAGNO, E.A., AND BLOME, C.D., *(in press)*, Biostratigraphic, chronostratigraphic, and U/Pb geochronometric data from the Rogue and Galice Formations, Western Klamath terrane (Oregon and California):--Their bearing on the age of the Oxfordian-Kimmeridgian Boundary and the *Mirifusus* first occurrence event, Proceedings of the 2nd International Symposium on Jurassic Stratigraphy, Lisbon, Portugal, 14 p., 2 figs.

PINDELL, J.L., 1985, Alleghenian reconstruction and subsequent evolution of the Gulf of Mexico, Bahamas, and proto-Caribbean, *Tectonics*, v. 4, p. 1-39.

PORTER, J.W., PRICE, R.A., AND MCCROSSAN, R.G., 1982, The western Canada sedimentary basin, *Philosophical Transactions of the Royal Society of London*, A305, p. 169-192.

POWELL, J.W., 1895, Physiographic Regions of the United States, *National Geographic Society Monograph*, p. 96.

PREMOVIC, P.I., PAVLOVIC, M.S., AND PAVLOVIC, N.Z., 1986, Vanadium in ancient sedimentary rocks of marine origin, *Geochimica et Cosmochimica Acta*, v. 50, p. 1923-1931.

PURDOM, W.B., 1977, Guide to the geology and lore of the wild reach of the Rogue River, Oregon, Museum of Natural History, University of Oregon, *Bulletin No. 22*, 67 p.

RAGAN, D.M., 1973, Structural Geology: An Introduction to Geometrical Techniques, John Wiley & Sons, New York, 208 p.

RAMP, L., AND PETERSON, N.V., 1979, Geology and mineral resources of Josephine County, Oregon, *Oregon Department of Geology and Mineral Industries Bulletin 100*, 45 p.

RAMSAY, J.G., 1967, Folding and Fracturing of Rocks, McGraw-Hill, New York, 568 p.

REEVE, S.C., 1975, Paleomagnetic studies of sedimentary rocks of Cambrian and Triassic age, unpublished Ph.D. thesis, University of Texas at Austin.

REKS, I.J., AND GRAY, D.R., 1982, Pencil structure and strain in weakly deformed mudstone and siltstone, *Journal of Structural Geology*, v. 4, p. 161-176.

REKS, I.J., AND GRAY, D.R., 1983, Strain patterns and shortening in a folded thrust sheet: An example from the southern Appalachians, *Tectonophysics*, v. 93, p. 99-128.

RENNE, P.R., CURTIS, G.H., AND SCOTT, G.R., 1986a, Nature and timing of deformation in the Redding section, eastern Klamath Mountains, California, *Geological Society of America Abstracts with Programs*, Cordilleran Section, v. 18, p. 175.

RENNE, P.R., AND SCOTT, G.R., 1986, Comment on "Paleomagnetism of the Upper Jurassic Galice Formation, southwestern Oregon: Evidence for differential rotation of the eastern and western Klamath Mountains," *Geology*, v. 14, p. 1048-1049.

RENNE, P.R., SCOTT, G.R., AND BAZARD, D.R., 1986b, Multicomponent paleomagnetic data from the Redding section, eastern Klamath Mountains: Cratonic Permian directions with secondary Middle Jurassic overprints, *Geological Society of America Abstracts with Programs*, Cordilleran Section, v. 18, p. 175.

RENNE, P.R., SCOTT, G.R., AND BAZARD, D.R., 1988, Multicomponent paleomagnetic data from the Nosoni Formation, Eastern Klamath Mountains, California: Cratonic Permian primary directions with Jurassic overprints, *Journal of Geophysical Research*, v. 93, p. 3387-3400.

RILEY, T.A., 1987, The Petrogenetic Evolution of a Late Jurassic island arc: The Rogue Formation, Klamath Mountains, Oregon, unpublished master's thesis, Stanford University, 40 p.

ROALDSET, E., 1975, Rare earth element distributions in some Precambrian rocks and their phyllosilicates, Numedal, Norway, *Geochimica et Cosmochimica Acta*, v. 39, p. 455-469.

ROALDSET, E., AND ROSENQVIST, I.TH., 1971, Unusual lanthanide distribution, *Nature Physical Science*, v. 231, p. 153-154.

ROSER, B.P., AND KORSCH, R.J., 1985, Plate tectonics and geochemical composition of sandstones: A discussion, *Journal of Geology*, v. 93, p. 81-84.

ROSER, B.P., AND KORSCH, R.J., 1986, Determination of tectonic setting of sandstone-mudstone suites using SiO_2 content and K_2O/Na_2O ratio, *Journal of Geology*, v. 94, p. 635-650.

SALEEBY, J.B., 1981, Ocean floor accretion and volcano-plutonic arc evolution of the Mesozoic Sierra Nevada, *in* Ernst, W.G., ed., The Geotectonic Development of California: Rubey Volume 1, Englewood Cliffs, N.J., Prentice-Hall, p. 132-181.

SALEEBY, J.B., 1984, Pb/U zircon ages from the Rogue River area, western Jurassic belt, Klamath Mountains, Oregon, *Geological Society of America Abstracts with Programs*, Cordilleran Section, v. 16, p. 331.

SALEEBY, J.B., HARPER, G.D., SNOKE, A.W., AND SHARP, W.D., 1982, Time relations and structural-stratigraphic patterns in ophiolite accretion, west central Klamath Mountains, California, *Journal of Geophysical Research*, v. 87, B5, p. 3831-3848.

SCHULTZ, K.L., AND LEVI, S., 1983, Paleomagnetism of Middle Jurassic plutons of the north-central Klamath Mountains, *Geological Society of America Abstracts with Programs*, v. 15, p. 427.

SCHULTZ, L.G., TOURTELOT, H.A., AND FLANAGAN, F.J., 1976, Cody Shale, SCo-1, from Natrona County, Wyoming, *in* Flanagan, F.J., ed., Descriptions and Analyses of Eight New USGS Rock Standards, U.S. Geological Survey Professional Paper 840, p. 21-23.

SCHWEICKERT, R.A., AND COWAN, D.S., 1975, Early Mesozoic tectonic evolution of the western Sierra Nevada, California, *Geological Society of America Bulletin*, v. 86, p. 1329-1336.

SCHWEICKERT, R.A., BOGEN, N.L., GIRTY, G.H., HANSON, R.E., AND MERGUERIAN, C., 1984, Timing and structural expression of the Nevadan orogeny, Sierra Nevada, California, *Geological Society of America Bulletin*, v. 95, p. 967-979.

SEIDERS, V.M., AND BLOME, C.D., 1988, Implications of upper Mesozoic conglomerate for suspect terrane in western California and adjacent areas, *Geological Society of America Bulletin*, v. 100, p. 374-391.

SHANMUGAM, G., 1985, Significance of secondary porosity in interpreting sandstone composition, *American Association of Petroleum Geology Bulletin*, v. 69, p. 378-384.

SHENON, P.J., 1933, Copper deposits in the Squaw Creek and Silver Peak districts and at the Almeda mine, southwestern Oregon, *U. S. Geological Survey Circular 2*, 34 p.

SHILLER, A.M., AND BOYLE, E.A., 1987, Dissolved vanadium in rivers and estuaries, *Earth and Planetary Science Letters*, v. 86, p. 214-224.

SIMPSON, S., 1975, Classification of trace fossils, *in* Frey, R.W., ed., The Study of Trace Fossils: A Synthesis of Principles, Problems, and Procedures in Ichnology, Springer-Verlag, New York, p. 39-54.

SMITH, J.G., PAGE, N.J., JOHNSON, M.G., MORING, B.C., AND GRAY, F., 1982, Preliminary map of the Medford 1^{o} x 2^{o} Quadrangle, *U.S. Geological Survey Open File Report 82-955*. Scale 1:250,000.

SMITH, T.E., AND NOLTIMIER, H.C., 1979, Paleomagnetism of the Newark trend igneous rocks of the north central Appalachians and the opening of the central Atlantic Ocean, *American Journal of Science*, v. 279, p. 778-807.

SNOKE, A.W., 1977, A thrust plate of ophiolitic rocks in the Preston Peak area, Klamath Mountains, California, *Geological Society of America Bulletin*, v. 88, p. 1641-1659.

SORBY, H.C., 1857, On some facts connected with slaty cleavage, British Association for the Advancement of Science, *Report of the Transactions Section*, v. 27, p. 92-93.

STAUDIGEL, H., AND HART, S.R., 1983, Alteration of basaltic glass: Mechanisms and significance for the oceanic crust-seawater budget, *Geochimica et Cosmochimica Acta*, v. 47, p. 337-350.

STEINER, M.B., 1983, Mesozoic apparent polar wandering and plate motions of North America, *in* Reynolds, M.W., and Dolly, E.D., eds., Mesozoic Paleogeography of west-central United States, Rocky Mountain Section, S.E.P.M., Denver, CO, p. 1-12.

STEINER, M.B., AND HELSLEY, C.E., 1975, Reversal pattern and apparent polar wander for the Late Jurassic, *Geological Society of America Bulletin*, v. 86, p. 1537-1543.

STOW, D.A.V., 1985, Fine-grained sediments in deep water: An overview of processes and facies models, *Geo-Marine Letters*, v. 5, p. 17-23.

TALIAFERRO, N.L., 1942, Geologic history and correlation of the Jurassic of southwestern Oregon and California, *Geological Society of America Bulletin*, v. 53, p. 72-112.

TARNEY, J., AND WINDLEY, B.F., 1981, Marginal basins through geological time, *Philosophical Transactions of the Royal Society of London*, A301, p. 217-232.

TAYLOR, S.R., AND MCLENNAN, S.M., 1985, The continental crust: Its composition and evolution: An examination of the geochemical record preserved in sedimentary rocks, Blackwell Scientific Publications, Oxford, 312 p.

THIESSEN, R.L., AND MEANS, W.D., 1980, Classification of fold interference patterns: A reexamination, *Journal of Structural Geology*, v. 2, p. 311-316.

TOBISCH, O.T., SALEEBY, J.B., AND FISKE, R.S., 1986, Structural history of continental volcanic arc rocks, eastern Sierra Nevada, California: A case for extensional tectonics, *Tectonics*, v. 5, p. 65-94.

TULLIS, T.E., 1976, Experiments on the origin of slaty cleavage and schistosity, *Geological Society of America Bulletin*, v. 87, p. 745-753.

TURNER, D.R., DICKSON, A.G., AND WHITFIELD, M., 1980, Water-rock partition coefficients and the composition of natural waters--a reassessment, *Marine Chemistry*, v. 9, p. 211-218.

VAIL, P.R., MICHUM, R.M., AND THOMPSON, S., 1977, Seismic stratigraphy and global changes of sea-level, part 4: Global cycles of relative changes of sea level, *in* Payton, C.E., ed., Seismic Stratigraphy--Applications to Hydrocarbon Exploration, *American Association of Petroleum Geologists Memoir 26*, p. 83-97.

WALLIN, E.T., MATTINSON, J.M., AND POTTER, A.W., 1988, Early Paleozoic magmatic events in the eastern Klamath Mountains, northern California, *Geology*, v. 16, p. 144-148.

WEISS, L.E., AND MCINTYRE, D.B., 1957, Structural geometry of Dalradian rocks of Loch Leven, Scottish Highlands, *Journal of Geology*, v. 65, p. 575-602.

WELLS, F.G., HOTZ, P.E., AND CATER, F.W., 1949, Preliminary description of the geology of the Kerby quadrangle, Oregon, *Oregon Department of Geology and Mineral Industry Bulletin*, v. 40, 23 p.

WELLS, F.G., AND PECK, D.L., 1961, Geologic map of Oregon west of the 121st Meridian, *U. S. Geological Survey Miscellaneous Geological Investigations*, map I-325. Scale 1:500,000.

WELLS, F.G., AND WALKER, G.W., 1953, Geology of the Galice Quadrangle, *U. S. Geological Survey GQ*-25. Scale 1:62,500.

WHETTEN, J.T., AND HAWKINS, J.W., 1970, Diagenetic origin of graywacke matrix minerals, *Sedimentology*, v. 15, p. 347-361.

WHITNEY, J.D., 1879, The auriferous gravels of the Sierra Nevada of California, *Memoir of the Museum of Comparative Zoology*, Harvard, v. 6, no. 1.

WINCHELL, A.N., 1914, Petrology and mineral resources of Jackson and Josephine Counties, Oregon, Oregon Bureau of Mines and Geology, *Mineral Resources of Oregon*, v. 1, 170 p.

WISE, J.P., 1969, Geology and petrology of a portion of the Jurassic Galice Formation, Babyfoot Lake area, S.W. Oregon, unpublished master's thesis, Idaho State University, 108 p.

WOODCOCK, N.H., 1986, The role of strike-slip fault systems of plate boundaries, *Philosophical Transactions of the Royal Society of London*, A317, p. 13-29.

WRIGHT, J.E., AND FAHAN, M.R., (1988), An expanded view of Jurassic orogenesis for the western U. S. Cordillera, Part 1: Middle Jurassic (pre-Nevadan) regional deformation/metamorphism and thrust faulting within an active arc environment, Klamath Mountains, Northern California, *Geological Society of America Bulletin* (*in press*).

WRIGHT, J.E., AND MILLER, E.L., 1986, An expanded view of Jurassic orogenesis for the western U. S. Cordillera, *Geological Society of America Abstracts with Programs*, Cordilleran Section, v. 18, p. 201.